AD_____

Award Number: DAMD17-01-1-0689

TITLE: The BESCT Lung Cancer Program (Biology, Education, Screening, Chemoprevention, and Treatment)

PRINCIPAL INVESTIGATOR: Waun K. Hong, M.D.
Fadlo R. Khuri, M.D.

CONTRACTING ORGANIZATION: The University of Texas
M.D. Anderson Cancer Center
Houston, TX 77030

REPORT DATE: March 2008

TYPE OF REPORT: Final

PREPARED FOR: U.S. Army Medical Research and Materiel Command
Fort Detrick, Maryland 21702-5012

DISTRIBUTION STATEMENT: Approved for Public Release;
Distribution Unlimited

The views, opinions and/or findings contained in this report are those of the author(s) and should not be construed as an official Department of the Army position, policy or decision unless so designated by other documentation.

REPORT DOCUMENTATION PAGE

Form Approved
OMB No. 0704-0188

Public reporting burden for this collection of information is estimated to average 1 hour per response, including the time for reviewing instructions, searching existing data sources, gathering and maintaining the data needed, and completing and reviewing this collection of information. Send comments regarding this burden estimate or any other aspect of this collection of information, including suggestions for reducing this burden to Department of Defense, Washington Headquarters Services, Directorate for Information Operations and Reports (0704-0188), 1215 Jefferson Davis Highway, Suite 1204, Arlington, VA 22202-4302. Respondents should be aware that notwithstanding any other provision of law, no person shall be subject to any penalty for failing to comply with a collection of information if it does not display a currently valid OMB control number. **PLEASE DO NOT RETURN YOUR FORM TO THE ABOVE ADDRESS.**

1. REPORT DATE	2. REPORT TYPE	3. DATES COVERED
01-03-2008	Final	15 Mar 2001– 14 Feb 2008

4. TITLE AND SUBTITLE

The BESCT Lung Cancer Program (Biology, Education, Screening, Chemoprevention, and Treatment)

5a. CONTRACT NUMBER

5b. GRANT NUMBER
DAMD17-01-1-0689

5c. PROGRAM ELEMENT NUMBER

6. AUTHOR(S)

Waun K. Hong, M.D.
Fadlo R. Khuri, M.D.

Email: whong@mdanderson.org

5d. PROJECT NUMBER

5e. TASK NUMBER

5f. WORK UNIT NUMBER

7. PERFORMING ORGANIZATION NAME(S) AND ADDRESS(ES)

The University of Texas
M.D. Anderson Cancer Center
Houston, TX 77030

8. PERFORMING ORGANIZATION REPORT NUMBER

9. SPONSORING / MONITORING AGENCY NAME(S) AND ADDRESS(ES)
U.S. Army Medical Research and Materiel Command
Fort Detrick, Maryland 21702-5012

10. SPONSOR/MONITOR'S ACRONYM(S)

11. SPONSOR/MONITOR'S REPORT NUMBER(S)

12. DISTRIBUTION / AVAILABILITY STATEMENT
Approved for Public Release; Distribution Unlimited

13. SUPPLEMENTARY NOTES

14. ABSTRACT

BESCT program aims to define molecular abnormalities contributing to lung cancer initiation and progression and to develop innovative therapeutic approaches for this cancer. Our specific aims are 1) to understand molecular alterations in lung cancer, 2) to develop chemoprevention strategies for lung cancer, and 3) to implement experimental molecular therapeutic approaches for lung cancer treatment.

15. SUBJECT TERMS
Lung Cancer, genetic alterations, chemoprevention, molecular therapy

16. SECURITY CLASSIFICATION OF:			17. LIMITATION OF ABSTRACT	18. NUMBER OF PAGES	19a. NAME OF RESPONSIBLE PERSON
a. REPORT	b. ABSTRACT	c. THIS PAGE			19b. TELEPHONE NUMBER *(include area code)*
U	U	U	UU	78	USAMRMC

TABLE OF CONTENTS

COVER.....1

SF 298..... 2

INTRODUCTION.....4

PROGRESS REPORT (BODY) 4

Project 1.....4

Project 2.....5

Project 3.....12

Developmental Research Project 16

KEY RESEARCH ACCOMPLISHMENTS.....18

REPORTABLE OUTCOMES 18

CONCLUSIONS.....19

APPENDICES.....20

APPENDIX A - Publications. .....

INTRODUCTION

Lung cancer is a devastating public health hazard worldwide. Advances in surgery, radiation therapy, and chemotherapy of non-small cell lung cancer (NSCLC) have only led to a marginal improvement in five-year survival. To reduce lung cancer incidence and mortality, it is imperative to develop effective therapeutic and preventive strategies targeting lung cancer patients. The BESCT program developed in 2001 aims to define molecular abnormalities contributing to lung cancer initiation and progression and to develop innovative therapeutic approaches for this cancer. Our specific aims are as follows:

- To understand molecular alterations in lung cancer
- To develop chemoprevention strategies for lung cancer
- To implement experimental molecular therapeutic approaches for lung cancer treatment

BESCT is composed of 3 research projects. This report describes the progress for the seventh grant year (March 15, 2007 to March 14, 2008), year 2 of an unfunded extension from the Department of Defense (DoD). This extension was requested due to unforeseen delays opening the BESCT clinical trial to be conducted at Emory University and to complete remaining Specific Aims.

PROGRESS REPORT (Body)

Project 1: Study Mechanisms of Molecular Alterations in Lung Cancer

(PI: Li Mao, M.D.)

Specific Aim 1 ***To determine the mRNA complex responsible for C-CAM1 splicing and identify factor(s) regulating exon 7 splicing.***

This Aim was completed as reported in 2005.

Specific Aim 2 ***To determine function of identified splicing factor(s) in regulation of CEACAM1 and its potential alterations in lung cancer.***

This Aim was summarized and completed in 2005. One publication resulted this year from the this research (Wang et al., 2007).

Specific Aim 3 ***To determine function of DNA methyltransferases and their role in controlling methylation and expression of critical tumor suppressor genes and tumor antigen genes.***

This Aim was completed in 2004.

Specific Aim 4 ***To determine expression and abnormalities of DNMT3B isoforms in lung tumorigenesis and their association with de novo DNA methylation patterns, and clinical applications.***

Update

This aim was completed in 2006.

Specific Aim 5 ***To determine expression of hnRNP-A1 variants in lung cancer cells and their role in the regulation of pre-mRNA splicing.***

Limited progress was made on this aim due to our inability to isolate the protein complex responsible for the splicing abnormality. Thus, this task was terminated and our emphasis was shifted to the extended task, Specific Aim 6, as reported last year.

Specific Aim 6 ***To determine the role of hepatoma-derived growth factor (HDGF) in lung cancer.***

Update

This Aim was completed in 2006.

Key Research Accomplishments

- All Aims were completed and reported last year.

Reportable Outcomes

Publications in peer-reviewed journals

- Wang J, Bhutani M, Pathak AK, Lang W, Ren H, Jelinek J, He R, Shen L, Issa J-P, Mao L. ΔDNMT3B variants regulate DNA methylation in a promoter-specific manner. Cancer Res 67:10647-10652, 2007.

Conclusions

We have concluded this project. The research has demonstrated the importance of ΔDNMT3B, a novel subfamily of DNMT3B discovered in the project, in lung tumorigenesis, the important role in regulation of promoter methylation, and identified HDGF as a key factor in lung cancer progression. These discoveries are progressing to the clinic through continued research and licensing agreements.

Project 2: Develop Novel Strategies for Lung Cancer Chemoprevention

(Project Leader: Fadlo Khuri, M.D.)

Specific Aim 2.1 ***To evaluate the effects of oral bexarotene delivered to former smokers by inhalation alone or in combination with celecoxib.***

(PI: Fadlo Khuri, M.D)

As reported in 2004, we were unable to conduct the clinical trial proposed in the original Specific Aim, "To evaluate the effects of aerosolized 13cRA delivered to former smokers by inhalation alone or in combination with Celecoxib," due to unexpected excessive toxicity with aerosolized delivery. Initial clinical studies have indicated that retinoids decrease the incidence of second primary tumors in patients who have previously undergone resection for NSCLC or head and neck cancer. However, subsequent large-scale chemoprevention trials have demonstrated that retinoids induce substantial toxicity and are of minimal benefit to individuals at high-risk for lung cancer, illustrating the need for more effective lung cancer chemoprevention strategies.

We thus proposed the clinical trial "A Phase I Biologic Study of Bexarotene (Targretin®) and Celecoxib in Patients With Solid Tumors Previously Treated With Standard Chemotherapy." The

objective of this project was to evaluate the chemopreventive potential of bexarotene (Targretin®) and non-steroidal anti-inflammatory agents (NSAIDs) (e.g., celecoxib) in high-risk lung cancer patients.

Update

The protocol was reviewed and approved by Emory Institutional Review Board (IRB) on January 5, 2007. In last year's report, we had an agreement with Eisai Pharmaceuticals regarding the supply of Targretin and expected to have the trial opened quickly. Although, the agreement to supply Targretin was concluded, negotiations with Eisai fell through regarding several other points:

1) Emory requested the ability to terminate the study if needed to protect the health and safety of study subjects.

2) Emory required indemnification from any claims that may come out of the use of results if Eisai wanted the right to use study results for their respective purposes.

3) Eisai asked for outright ownership to inventions from the study but Emory does not feel this is possible given Federal Funding is being utilized for the study.

Emory has been in negotiations with Eisai pharmaceuticals for over one year now. They have been extremely slow in getting back to us at best and non-responsive at times. These issues remain unresolved since Eisai bought Ligand Pharmaceuticals with whom we had negotiated the original agreement for this trial.

We thus explored a similar proposal with AstraZeneca for a clinical trial with celecoxib and ZD1839; however, a publication on celecoxib (Edelman et al., 2008) that came out the day of proposal review dampened their initial enthusiasm. They requested that we review and resubmit in two months.

As a result, we have had discussions with the PI of BESCT, Dr. Hong, and representatives of the DoD, to determine the best course of action to accomplish the original goals of this aim. We were in agreement that, given the considerable time and effort and the outcome, we should not further pursue an agreement and trial with Eisai. Second, given the litigious environment and press surrounding celecoxib, it has also been agreed upon that we should not further pursue the trial with AstraZeneca for this program. Consequently, the strategy to best accomplish our aims in a timely manner under these circumstances is to synergize our program with the BATTLE program, opening the trial at Emory, but with specific correlative research directed towards Aims 2.1 and 3.2. Further details need to be worked out but will be done so in collaboration with Dr. Hong and the DoD and submitted within the next few weeks.

Specific Aim 2.2 ***To evaluate effects of NSAIDs and 4HPR (replace 13cRA) as single agents and in combinations on growth, apoptosis, and carcinogenesis using an in vitro cell system and an animal model.***

(PI: Reuben Lotan, Ph.D.)

Because the retinoid 13cRA shows enhancement of lung cancer among smokers in a clinical trial but has side effects, whereas the synthetic retinoid fenretinide [*N*-(4-hydroxyphenyl) retinamide,

4HPR] is more potent with fewer side effects and has additive effects with celecoxib, we have replaced 13cRA with 4HPR for subsequent *in vitro* and animal experiments.

Update

During the last year, we explored further the mechanisms by which 4HPR induces apoptosis in NSCLC cells and possible nodes for convergence of mechanisms of action of NSAIDs (e.g., celelcoxib) and 4HPR that might explain their additive/synergistic effects. Our previous studies have demonstrated that 4HPR induces apoptosis in lung cancer cells by increasing the generation of reactive oxygen species (ROS). First, we investigated further the mechanism by which 4HPR induces ROS in NSCLC cells by exploring steps that are upstream of ROS generation. One possible source for ROS is NADPH oxidase, a multi-component electron-transfer complex composed of the membrane-bound cytochrome b558 (gp91phox and p22phox) and the cytosolic components (p67phox, p47phox, p40phox and Rac1). Upon activation, the cytosolic components translocate to the plasma membrane where they associate with cytochrome b558, forming an active NADPH oxidase. Because NADPH-mediated generation of ROS is involved in various apoptosis signaling pathways, we hypothesized that it may be a target through which 4HPR induces ROS generation and apoptosis.

Using the bronchioalveolar cancer cell line H522, we found that 4HPR activates the NADPH oxidase regulatory subunit Rac and that this activation is involved in ROS increase and subsequent apoptosis induction. The Rac1 inhibitor NSC-23766 suppressed the increase in ROS in 4HPR-treated cells (Figure 1) indicating that Rac1 is upstream of ROS production.

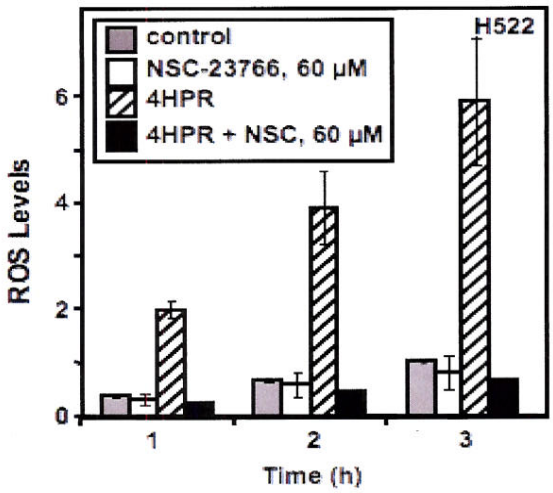


Figure 1. The H522 cells were seeded at a density of 8 x 10^4 cells per well in 24-well plates for 24 hours after which they were switched to serum-free medium alone or containing 60 μM NSC-23766 and incubated overnight prior to treatment with 5 μM of 4HPR for 1, 2, or 3 hours. ROS levels were then assessed using the oxidation-sensitive fluorescent dye DCFH-DA and assessing its conversion to DCF.

Targeting Rac1 expression using small interfering RNA (siRNA), which has been shown to down-regulate Rac1, suppressed the induction of ROS generation by 4HPR in H522 cells by about 50% (Fig. 2). These results indicate that NADPH oxidase may be the source of about 50% of the enhanced ROS production induced by 4HPR with the rest coming presumably from the mitochondria. Our new findings extend the target for 4HPR effects from the mitochondria (our previous findings) to the NADPH oxidase system (this report).

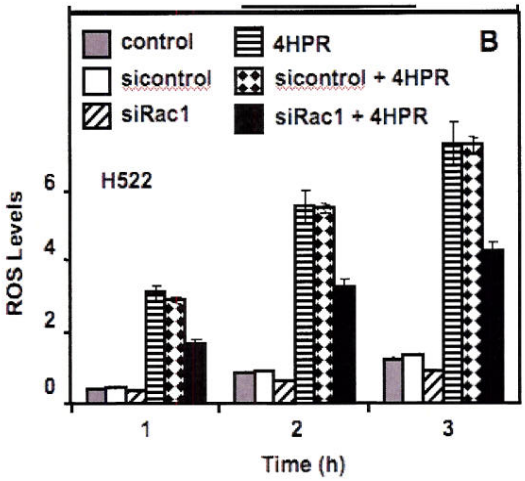


Figure 2. H522 cells were transfected with siCONTROL or Rac1-specific siRNA and then transferred to 24-well plates. The following day cells were switched to serum-free medium in which they were incubated overnight prior to assessment of induction of ROS generation by 4HPR as described in Fig. 1.

Another mechanism that has been proposed to mediate 4HPR-induced apoptosis in other cancer cells (e.g., neuroblastoma) is through an increase in the level of the sphingolipid ceramide. Ceramide is generated from sphingomyelin breakdown through the activation of sphingomyelinase or de novo by ceramide synthase. Ceramide has been shown to activate the major pathways governing cell death such as the endoplasmic reticulum and mitochondria, both of which we had found previously to be modulated by 4HPR. In addition, the NSAID celecoxib has also been reported to increase ceramide level and this increase has been implicated in growth inhibitory effects of celecoxib. Using the H522 lung cancer cells, we first determined the constitutive levels of sphingolipids by employing mass spectrometry techniques. We found that the H522 cells produce the following ceramide species in order of decreasing relative amounts: N-nervonoyl-D-S, N-nervonoyl-D-sphingosine; N-lignoceroyl-DL-DHS, N-lignoceroyl-DL-dihydrosphingosine; N-stearoyl-D-S, N-stearoyl-D-sphingosine; N-palmitoyl-DL-DHS, N-palmitoyl-DL-dihydrosphingosine and N-oleoyl-D-S, N-oleoyl-D-sphingosine (Figure 3).

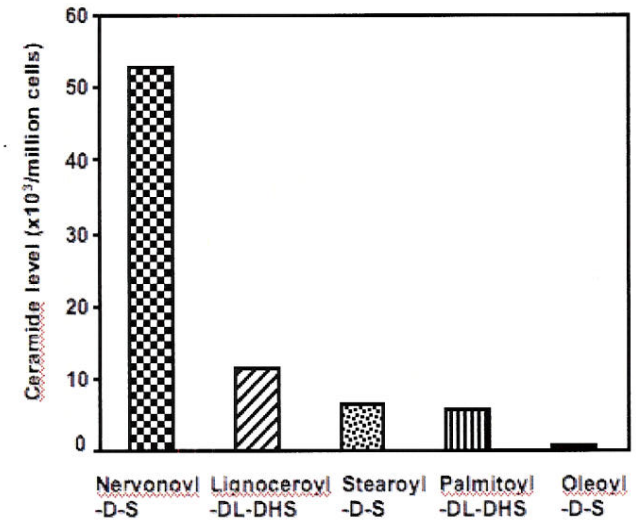


Figure 3. H522 cells were plated in 10 cm diameter dishes and harvested by trypsinization after 24 hours. The cells were then sonicated and ceramides were extracted with chloroform. Extracted samples were analyzed for ceramides using a Quattro Ultima LC/MS/MS (MicroMass Inc., Manchester, UK) coupled to an Agilent 1100 LC system.

We then asked whether 4HPR exerts any effect on the levels of these ceramides. We found that 4HPR increased the levels of several ceramide species compared to controls. An initial increase of 15 to 33 fold was observed in the levels of lignoceroyl-DL-DHS and N-palmitoyl-DL-DHS within 2 hours. The levels of the other ceramides increased by 2 to 4 fold. A second, more dramatic increase was observed between 12 and 24 hours (Fig. 4).

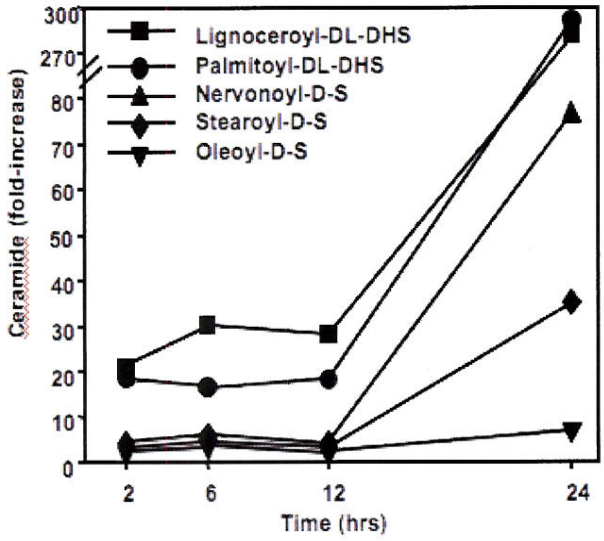


Figure 4. H522 cells were treated with 5 μM 4HPR for the indicated times and then the cells were harvested and extracted for ceramide analysis as in Fig. 3. The levels of ceramides in treated cells were compared to the levels in untreated control cells an expressed as fold increase.

These increases in certain ceramides were much greater than the 3 to 10 fold reported in neuroblastoma cells. Further, we were the first to use mass spectrometry to identify individual ceramide species as previous studies only used thin layer chromatography, a much less sophisticated and quantitative technique. Many of the changes induced by 4HPR including the increase in ROS and activities of mitogen-activated protein kinases (MAPKs) as well as apoptosis were inhibitable by antioxidants such as butylated hydroxyanisole (BHA) because they were upstream of ROS. Rac1 activation described above was the first effect of 4HPR that we had discovered to be an earlier event than ROS generation nad was therefore, not affected by BHA. To determine whether ceramide increase was up- or downstream of ROS, we treated cells with BHA and 4HPR concurrently and analyzed ceramide levels in H522 cells. We found that BHA enhanced ceramide increase in 4HPR-treated cells (Fig. 5, left panel) although it did rescue 75% of the cell population from 4HPR-induced apoptosis (Fig. 5, right panel).

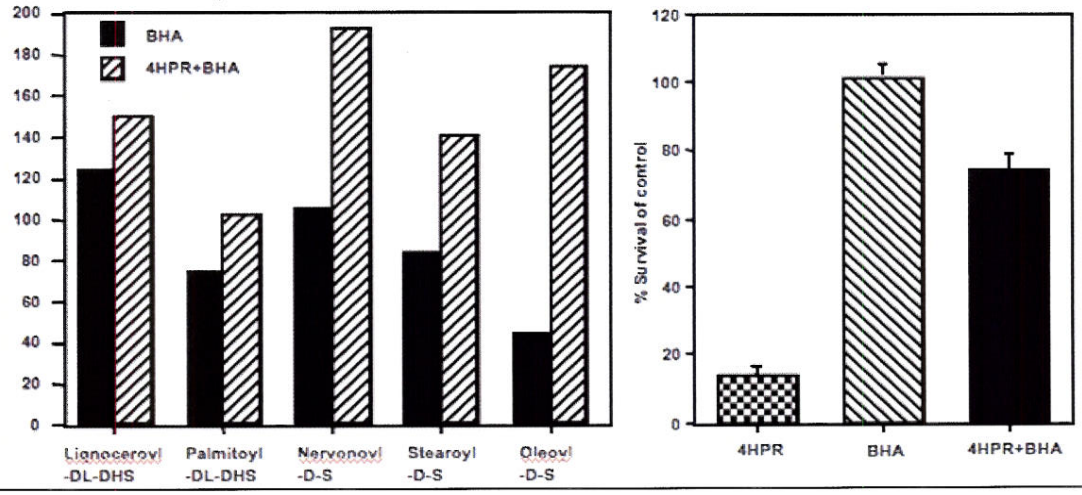


Figure 5. Left panel, H522 cells were plated in 10-cm dishes 24 h before co-treatment with 4HPR (5 μM) and BHA (50 μM) or with each agent alone or none. The ceramide levels were determined later by MS. Change of ceramide level are expressed as % of DMSO-treated control for BHA and of 4HPR-treated cells in 4HPR+BHA. Right panel, the cells were seeded in 96-well plates and trea with the single agents or their combination and cell survival was determined by SRB assay 2 d later.

Since BHA blocks ROS generation, these results indicate that the increases in ceramide levels are independent of the increase in ROS generation induced by 4HPR in the H522 cells. Furthermore, the finding that BHA enhanced the effect of 4HPR on the levels of most ceramide species while suppressing 4HPR-induced cell death raised the question as to whether the increase in ceramide contributes to apoptosis as claimed by others in neuroblastoma cells. To address this issue more directly, we used Fumonisin B1 (FB1) a fungal toxin that can inhibit ceramide synthase. Figure 6 (left panel) shows that FB1 suppressed the increase induced by 4HPR in the levels of all ceramide species except for Oleoyl-D-S, which is the least abundant ceramide in the H522 cells (Fig. 3). Despite the suppression of 4HPR-induced ceramide increase, FB1 failed to decrease growth inhibition or apoptosis induction by 4HPR (Fig. 6 (right panels). These results demonstrate that the increase in ceramide levels by 4HPR is not involved in growth inhibition or apoptosis induction in H522 cells.

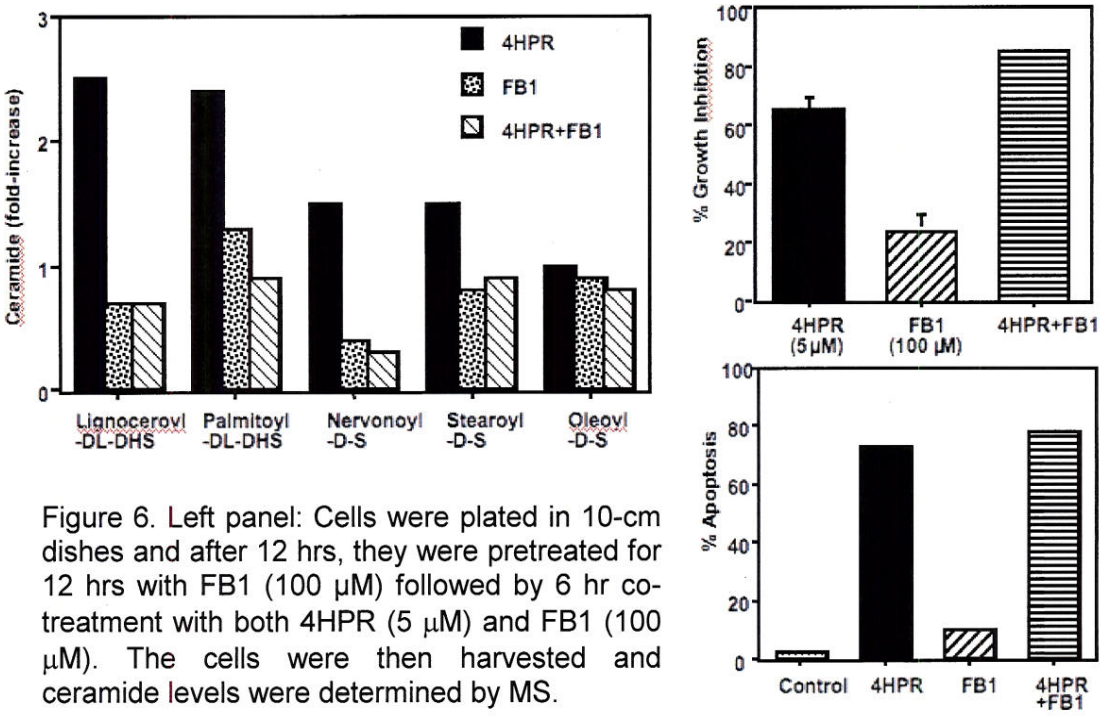


Figure 6. Left panel: Cells were plated in 10-cm dishes and after 12 hrs, they were pretreated for 12 hrs with FB1 (100 μM) followed by 6 hr co-treatment with both 4HPR (5 μM) and FB1 (100 μM). The cells were then harvested and ceramide levels were determined by MS.

Right panels: Cells were seeded in 96-well plates and pretreated with FB1 (100 μM) for 12 h before co-treatment with 4HPR (5 μM) and FB1 (100 μM) for 48 hrs. Growth inhibition and apoptosis were then determined by sulforhodamine B and TUNEL assays, respectively.

Our *in vivo* chemoprevention studies have shown previously that 4HPR used as a single agent was able to suppress lung carcinogenesis induced in Gprc5a knockout mice at a borderline significant rate, whereas celecoxib alone failed to suppress carcinogenesis. During the last year, we examined the effects of the combination of 4HPR and celecoxib and found that the combination of agents had a greater effect than each agent alone. The data have been submitted for statistical analysis to our core. In the near future we will examine tissue specimens from the lungs of these mice to determine the underlying mechanisms for the chemopreventive effects of the combination of the two agents.

Specific Aim 2.3. ***To investigate whether genetic approaches to inhibit PI3K activity decrease lung tumor size and number in k-ras mutant mice.***

(PI: Ho-Young Lee, Ph.D.)

This Aim was discontinued as reported in the 2004 Annual Report due to the variability in the delivery system. A more reliable system was developed and, thus, pursued through our Lung Cancer SPORE grant.

Specific Aim 2.4. ***To analyze differential gene expression between untreated NSCLC cells and celecoxib-treated NSCLC cells using affymetrix oligonucleotide microarrays and characterize genes that may be implicated in mediating apoptosis induction.***

(PI: Reuben Lotan, Ph.D.)

Update

Due to the safety and legal challenges that have persisted with using celcoxib in the clinic, efforts and costs of the gene expression analyses appear futile at this time as we will not have an opportunity to translate any findings to the bedside. Therefore, we put greater efforts in exploring the mechanism of fenretinide action in greater depth because it is likely to lead to clinical trials especially in view of a renewed interest in 4HPR (febretinide) after new intravenous and oral formulations have been developed recently. The NCI has taken a very active interest and role in the development of this agent as seen by this summary of a meeting this past November:

DEPARTMENT OF HEALTH AND HUMAN SERVICES, PUBLIC HEALTH SERVICE, NATIONAL INSTITUTES OF HEALTH NATIONAL CANCER INSTITUTE, 144th NATIONAL CANCER ADVISORY BOARD, Summary of Meeting, November 27, 2007

"Dr. Niederhuber shared an example of the unique role that the NCI plays in the world of drug development. He presented the results of a 26-year-old African-American female patient with cutaneous T-cell lymphoma who was successfully treated at the NIH Clinical Center with fenretinide (4-HPR), a synthetic drug related to vitamin A. Fenretinide was developed initially by Johnson & Johnson in the 1970s as a chemopreventive agent and was brought to the NCI's Rapid Access to Interventions Development (RAID) program by Dr. C. Patrick Reynolds of Children's Hospital in Los Angeles. Dr. Niederhuber said that a trial is underway to develop novel formulations of IV fenretinide. The RAID program is instrumental in bridging the gap between the lead discovery and drug delivery and provides the academic and small business communities with access to preclinical contract research resources."

Key Research Accomplishments

- Discovered that the small GTPase Rac, the regulatory subunit of the NADPH oxidase complex, is the earliest target for 4HPR in the induction of cell death in lung cancer via ROS generation.
- Excluded increase in ceramides as a mechanism for apoptosis induction by 4HPR.

Reportable Outcomes

We have published one manuscript; a second one has been revised and resubmitted to the journal Cancer Research.

Publications in peer-reviewed journals

- Schroeder CP, Yang P, Newman RA, Lotan R. Simultaneous inhibition of COX-2 and 5-LOX activities augments growth arrest and death of premalignant and malignant human lung cell lines. *J. Exptl. Therap. Oncol*, 6: 183-192, 2007.
- Kadara H, Tahara E, Kim HJ, Lotan D, Myers J, Lotan R. Involvement of Rac in 4HPR induced apoptosis. *Cancer Res* 2008, resubmitted.

Conclusions

Our data suggest that 4HPR induces apoptosis by activating Rac1, which then mediates an increase in reactive oxygen species leading to apoptosis. We also ruled out a role for ceramides in this effect, although we found substantial increase in ceramides after 4HPR treatment. Focus has been shifted from celecoxib to 4HPR as a clinical agent.

Project 3: Implement Experimental Molecular Therapeutic Approaches for Lung Cancer
(Project Leader: Fadlo Khuri, M.D.)

Specific Aim 3.1 ***To develop a relatively faithful murine model of lung cancer by crossing the k-ras mutant mouse (T. Jacks) with p53 mutant missense mouse (G. Lozano) and study the evolution of non-small cell lung cancer in primary lung tumor model with metastatic potential and the effectiveness of targeted agents in the model.***

(PI: Guillermina Lozano, Ph.D.)

Update

This Aim was completed. The research was published in *Oncogene* this year, summarizing the details for our K-ras / p53 double-mutant mouse. This model recapitulates lung adenocarcinoma more faithfully demonstrating highly aggressive adenocarcinmoas that metastasize to multiple intrathoracic and extrathoracic sites in a pattern similar to that found in humans. Gender differences were also observed. Thus, this model is thought to be invaluable for future studies relating to metastasis of human lung cancer.

Specific Aim 3.2 ***To evaluate novel signal transduction inhibitors alone, in combination with one another, or with cytotoxic agents in the treatment of the mouse lung cancer and, ultimately, in the treatment of human lung cancers.***

(PI: Fadlo Khuri, M.D.)

Update

We have studied farnesyltransferase inhibitors (FTIs) including lonafarnib in the past five years and found that lonafarnib increased microtubule acetylation and synergy with taxanes in anti-proliferation activity. Detailed findings were published in *Cancer Research* (Marcus et al., 2005). If

indeed synergy between taxanes and lonafarnib is achieved at low doses and is manifested by an increase in microtubule acetylation, this is a hypothesis that needs to be tested prospectively.

We therefore designed a Phase Ib combination trial of lonafarnib and docetaxel in biopsy-accessible solid tumor patients to combine lonafarnib with low doses of docetaxel weekly as an extended study. We plan to continue collaborations with Adam Marcus, PhD, Assistant Professor of Hematology & Oncology, Winship Cancer Institute, and Paraskevi Giannakakou, Ph.D. (now Associate Professor of Medicine and Pharmacology at Cornell University) to further explore the mechanism of this interaction while we initiate this Phase Ib protocol with serial biopsies to assess the efficacy of this combination in various solid tumor patients.

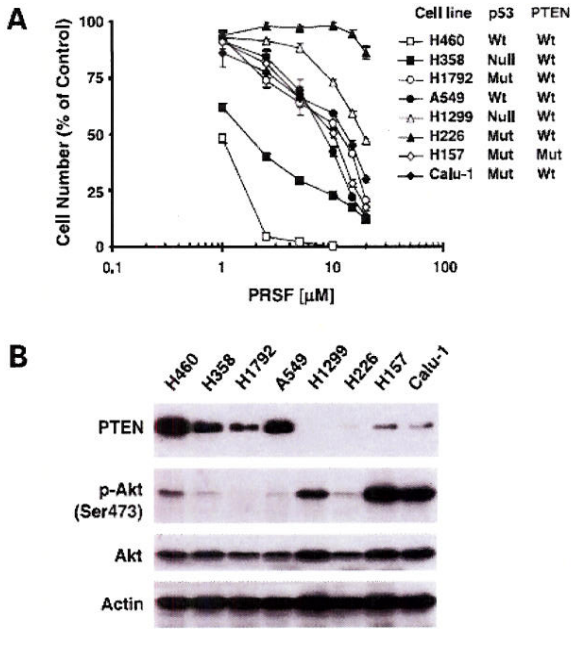


Figure 7. Effects of perifosine on the survival of NSCLC cells (A) and their association with basal levels of p-Akt (B). (A) Cell lines treated with different concentrations of perifosine (PRFS) ranging from 1-20 μM. After 3 days, the cells were subjected to sulforhodamine B assay to determine viable cells. In addition, the p53 and PTEN status of the cell lines is also indicated. (Mean of 4 replicates; error bars, standard deviation. (B) Cells were harvested for whole cell protein lysates and analyzed by western blot.

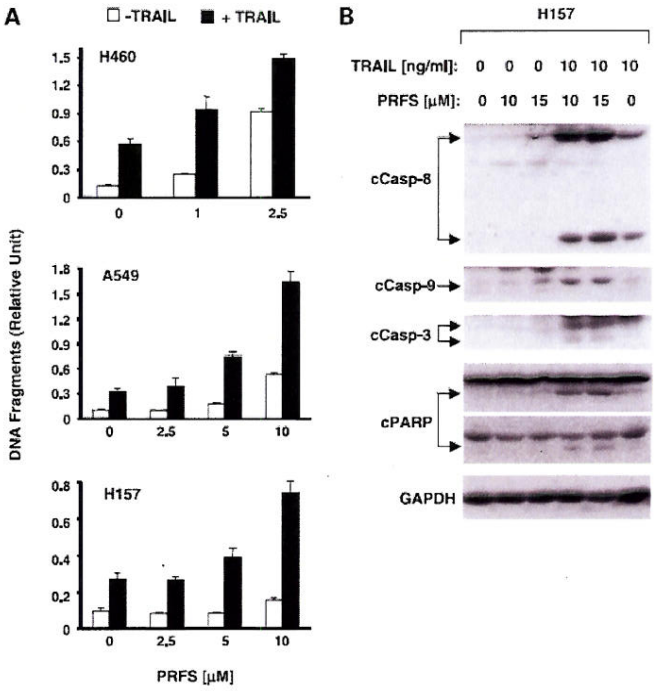


Figure 8. Perifosine cooperates with TRAIL to enhance DNA fragmentation (A) and caspase activation (B) in human NSCLC cells. (A) Cells plated in 96-well plates and treated with the given doses of perifosine (PRFS) alone, 20 ng/ml TAIL alone, or TRAIL + PRFS on the second day. DNA fragmentation assays were performed after 24 hrs. (Mean of triplicates; erro bars, standard deviation) (B) H157 cells were treated with PRFS alone, TRAIL alone, and the combination. Whole cell lysates were prepared after 16 hrs and analyzed by western blots as indicated.

The trial is supported by our NIH/NCI P01 (CA116676-01A1) Program Project grant and Sanofi-Aventis pharmaceuticals, and lonafarnib is provided by Schering Plough. This trial is activated and has 32 of a planned total of 36 patients accrued thus far. Two major responses have been seen, including a complete clinical response in a patient with diffuse dermal metastases from squamous cell skin cancer. The data has been submitted to AACR as a Late Breaking Abstract.

We have also published our results on the Akt inhibitor, perifosine (Elrod et al., 2007). Although perifosine is in clinical trials, the mechanism of action is not well understood. We found that ERK phosphorylation was decreased in all cell lines tested regardless of TRAIL-induced apoptosis.

Consequently, we have concluded that for lung cancer, ERK inhibition is unlikely to be critical for the apoptosis response observed with perifosine. Low levels of phosph-Akt and its further down-regulation were associated with high sensitivity to perifosine-induced apoptosis. We also demonstrated that the combination of perifosine and TRAIL, the ligand for the death receptor 5 (DR5), augmented induction of apoptosis is human NSCLC cell lines (Figure). Thus, we have determined that perifosine, at clinically achievable concentrations, induces apoptosis by inhibiting Akt phosphorylation, reducing total Akt levels. In addition, perifosine induced expression of TRAIL.

Specific Aim 3.3 ***To produce and test a liposomal gene-therapeutic strategy targeted to a novel tumor suppressor gene located on chromosome 3p, both in the mouse model and in human patients with advanced non-small cell lung cancer.***

(PI: Charlie Lu, M.D)

Update

As reported in 2005, we completed the preclinical study and the preclinical data were used to develop the phase I trial of DOTAP:cholesterol-FUS1 liposome complex (Human Gene Transfer Protocol #0201-513). This trial is supported by a different mechanism and is ongoing, currently with 19 patients accrued. An abstract was presented at AACR last year (see Appendix), reporting that the plasmid FUS1 was found to be expressed in 3 out of 3 post-treatment tumor biopsies (3 of 3 pretreatment tumor biopsies were negative). Once data analysis is completed, the manuscript will be prepared and submitted.

Specific Aim 3.4 ***To develop specific vascularly targeted strategies to the vascular endothelium of lung cancer cells to decrease the toxicity to normal cells and enhance the therapeutic index.***

(PI: Ho-Young Lee, Ph.D)

Update

This research was completed last year and summarized in that report.

Specific Aim 3.5 ***To study in vivo and in vitro effects of farnesyl transferase inhibitors and tyrosine kinase inhibitors in mouse models and, ultimately, in humans with lung cancer.***

(PI: Guillermina Lozano, Ph.D.)

Update

Manuscripts are being prepared and we are seeking additional funds from other sources to pursue future studies.

Specific Aim 3.6 ***To measure differences in gene expression between lung tumors that do or do not show metastasis, and in metastatic lesions themselves using the Affymetrix gene chip system.***

(PI: Guillermina Lozano, Ph.D.)

Update

This aim was completed and reported in detail last year. Manuscripts are being prepared.

Specific Aim 3.7 ***To perform array CGH experiments to determine if other genomic changes have occurred.***

Specific Aim 3.8 ***To perform LOH studies at specific loci (if warranted from the data obtained in Specific Aim 3.7).***

(Leader: Guillermina Lozano, Ph.D.)

These studies will not be further pursued here due to lack of funds. Additional sources of the funds will be sought to continue the studies.

Specific Aim 3.9 ***To evaluate GFE-1 peptide effects on blocking lung metastases in a rat model.***

(PI: Yun W Oh, M.D)

This Aim was concluded in 2005; Dr. Yun Oh discontinued participation in the BESCT program as noted in an official letter to Dr. Julie Wilberding at that time.

Key Research Accomplishments

- Determined mechanism for perifosine in lung cancer therapy is related to phospo-Akt levels and apoptosis.
- Determined that a combination of TRAIL ligand and perifosine induces increased levels of apoptosis compared to either agent alone.
- Trial for FUS1-nanoparticles in stage IV lung cancer continues and preliminary report demonstrates gene is expressed in target tissue.
- All aims have been completed.

Reportable Outcomes

Publications in peer-reviewed journals

- Elrod HA, Lin Y-D, Yue P, Wang X, Lonial S, Khuri FR, Sun S-Y. The alkylphospholipid perifosine induces apoptosis of human lung cancer cells requiring inhibition of Akt and activation of the extrinsic apoptotic pathway. *Mol Cancer Ther* 6(7):2029-38; 2007.
- Zheng S, El-Naggar AK, Kim ES, Kurie JM, Lozano G. A Genetic Mouse Model for Metastatic Lung Cancer with Gender Differences in Survival. *Oncogene* 26:6896-6904, 2007.

Abstracts

- Lu C, Sepulveda CA, Ji L, Ramesh R, O'Connor S, Jayachandran G, Hicks ME, Munden RF, Lee JJ, Templeton NS, McMannis JD, Roth JA. Systemic therapy with tumor suppressor FUS1-nanoparticles for stage IV lung cancer. AACR Annual Meeting, 2007, Abstract #LB-348.

Conclusions

The tasks (Aims) of Project 3 have been completed. We have 1) established a faithful mouse model that recapitulates the metastatic nature of human lung cancer that will be invaluable to further probe the molecular basis of metastatic lung cancer and for translational studies; 2) demonstrated the synergistic effect of lonafarnib (SCH66336) with taxanes in anti-proliferation activity; and 3) determined that NSCLC and HNSCC cells develop FTI SCH66336 resistance by inducing survivin expression through an IGF-1R/Akt-dependent pathway. Thus, combining inhibitors of IGF-1R, Akt, or survivin with FTI SCH66336 may be an effective anticancer therapeutic strategy for patients with HNSCC or NSCLC.

We have also identified additional mechanisms to induce apoptosis and cell death in lung cancer cells. Perifosine's activity is closely related to the levels of phospho-Akt. We also determined that this apoptosis can be increased by addition of TRAIL ligand to perifosine therapy.

Finally, we have shown that our nanoparticle system can deliver FUS1 to the target tissue and the trial is ongoing.

Developmental Research Project: A Genetic/Combinatorial Algorithmic Strategy for Anticancer Therapy Development

(PI: Ralph Zinner, M.D)

Targeted therapeutic agents are highly promising in combination because they are both well-tolerated and interact with the targets that cause cancer. However, with new drugs added to the list, the number of possible combinations rises exponentially beyond the capacity of any foreseeable technology to fully screen. In addition, molecular insight often fails to predict clinical performance of single agents, a difficulty that will likely remain as these drugs are combined. We thus proposed a direct functional screen of combinations as a complement to the molecular insight-based approach, MACS (Medicinal Algorithmic Combinatorial Screen), to identify promising combinations that would be otherwise impossible to be found through a simple screen alone. The foundation of MACS is a genetic algorithm. The study adopts a preclinical screen that assesses anticancer efficacies of combinations with cell proliferation assays.

Specific Aim 1 ***To determine feasibility of screening process (robots, cell death assays, combining drugs).***

Update

We have submitted a publication with our results for a screen with 19 different drugs using MACS. Details will be submitted in the next annual or final report, once accepted for publication. Two different algorithms have been used and identified 4HPR, SAHA, and bortezomib to be the "fittest" combinations of all drugs screened. Recent acquisition of funding from The University of Texas Biomedical Engineering Seed Grant "Data Mining Combinations Derived from the Medicinal Algorithmic Combinatorial Screen (MACS)" will enable this project to be continued.

Specific Aim 2 ***To determine the range of outcomes and patterns of cellular response from an initial screening of drug combinations.***

Update

As previously reported, initial analyses of several power sets of 6 drugs in A549 cells showed that 67% of the variance could be explained by linear combinations. We have conducted 4 MAC screens.

More than 500 combinations were studied through the process and were analyzed for linearity. In addition, we will extend Aim 2 by conducting data mining and using pattern recognition analytical tools to make predictions about novel combinations. In a separate but related proposal, we are exploring a complementary method to MACS that will mine many combinations studied using powerful analytical tools to learn whether we can make predictions about combinations not yet studied. This goal will be accomplished through the recent establishment of the collaboration with Dr. Elena Popova of Operations Research and Industrial Engineering at The University of Texas at Austin, and Dr. Paul Damien at the McCombs School of Business, The University of Texas at Austin, and the acquisition of additional funding through The University of Texas Biomedical Engineering Seed Grant. These results are also detailed in the manuscript submitted.

Specific Aim 3 ***To develop genetic algorithm to guide selection and identification of promising combinations of drugs.***

The aim was concluded last year and a manuscript summarizing detailed findings of the study was submitted to *Molecular Cancer Therapeutics* (Zinner et al., 2008), reviewed and editorial comments are being addressed.

Key Research Accomplishments

- MACS screen with 19 different drugs identifying "best fit" drug combination.
- All Aims were completed. The manuscript is currently under review after submission.

Reportable Outcomes

Manuscript, submitted

- Zinner RG, Barrett BL, Popova E, Damien P, Volgin AY, Gelovani JG, Lotan R, Pisano C, Lippman SM, Mills GB, Mao L, Miller JH. Medicinal Algorithmic Combinatorial Screen (MACS) Is a Novel, Rapid, and Efficient Approach to the Identification of Therapeutic Combination Drug Regimens. *Mol Cancer Therap*, 2008 (submitted).

In preparation:

- NCI R01, May 2007. We are proposing to analyze a reverse antibody array data of the triplet, 4SB, across multiple NSCLC cell lines (some data are already generated), and then incorporate molecular insights into a MACS.
- NCI R21; To further develop the triplet, 4SB, in a head and neck mouse model developed by Dr. Reuben Lotan at UT M. D. Anderson Cancer Center.

Conclusions

This study demonstrates the potential feasibility for screening drug combinations of arbitrary size using the Medicinal Algorithmic Combinatorial Screening (MACS) method, which can efficiently identify highly-fit combinations of anticancer agents without prior molecular or functional insight into the interactions of the combined drugs.

KEY RESEARCH ACCOMPLISHMENTS

Project 1: Study Mechanisms of Molecular Alterations in Lung Cancer

- All Aims were completed and reported last year.

Project 2: Develop Novel Strategies for Lung Cancer Chemoprevention

- Discovered that the small GTPase Rac, the regulatory subunit of the NADPH oxidase complex, is the earliest target for 4HPR in the induction of cell death in lung cancer via ROS generation.
- Excluded increase in ceramides as a mechanism for apoptosis induction by 4HPR.

Project 3: Implement Experimental Molecular Therapeutic Approaches for Lung Cancer

- Determined mechanism for perifosine in lung cancer therapy is related to phospo-Akt levels and apoptosis.
- Determined that a combination of TRAIL ligand and perifosine induces increased levels of apoptosis compared to either agent alone.
- Trial for FUS1-nanoparticles in stage IV lung cancer continues and preliminary report demonstrates gene is expressed in target tissue.
- All aims have been completed.

DRP: A Genetic/Combinatorial Algorithmic Strategy for Anticancer Therapy Development

- MACS screen with 19 different drugs identifying "best fit" drug combination.
- All Aims were completed. The manuscript is currently under review after submission.

REPORTABLE OUTCOMES

Manuscripts published in peer-reviewed Journals

- Elrod HA, Lin Y-D, Yue P, Wang X, Lonial S, Khuri FR, Sun S-Y. The alkylphospholipid perifosine induces apoptosis of human lung cancer cells requiring inhibition of Akt and activation of the extrinsic apoptotic pathway. *Mol Cancer Ther* 6(7):2029-38; 2007.
- Schroeder CP, Yang P, Newman RA, Lotan R. Simultaneous inhibition of COX-2 and 5-LOX activities augments growth arrest and death of premalignant and malignant human lung cell lines. *J. Exptl. Therap. Oncol*, 6: 183-192, 2007.
- Wang J, Bhutani M, Pathak AK, Lang W, Ren H, Jelinek J, He R, Shen L, Issa J-P, Mao L. ΔDNMT3B variants regulate DNA methylation in a promoter-specific manner. Cancer Res 67:10647-10652, 2007.
- Zheng S, El-Naggar AK, Kim ES, Kurie JM, Lozano G. A Genetic Mouse Model for Metastatic Lung Cancer with Gender Differences in Survival. *Oncogene* 26:6896-6904, 2007.

Manuscripts, submitted

- Kadara H, Tahara E, Kim HJ, Lotan D, Myers J, Lotan R. Involvement of Rac in 4HPR induced apoptosis. *Cancer Res* 2008, resubmitted.
- Zinner RG, Barrett BL, Popova E, Damien P, Volgin AY, Gelovani JG, Lotan R, Pisano C, Lippman SM, Mills GB, Mao L, Miller JH. Medicinal Algorithmic Combinatorial Screen (MACS) Is a Novel, Rapid, and Efficient Approach to the Identification of Therapeutic Combination Drug Regimens. *Mol Cancer Therap*, 2008 (submitted).

Abstracts

- Lu C, Sepulveda CA, Ji L, Ramesh R, O'Connor S, Jayachandran G, Hicks ME, Munden RF, Lee JJ, Templeton NS, McMannis JD, Roth JA. Systemic therapy with tumor suppressor FUS1-nanoparticles for stage IV lung cancer. AACR Annual Meeting, 2007, Abstract #LB-348.

CONCLUSIONS

In the 7th year grant period, all aims but one (Aim 2.1) have been successfully completed. Due to failed negotiations with Eisai after purchase of the original company, Ligand Pharmaceuticals, the clinical trial of Project 2 (Aim 2.1) has failed to be opened. Our plan is to synergize with the complementary DoD Program BATTLE to both treat patients and to collect specimens to accomplish our original goals.

This year, we have an additional 4 publications and 2 more submitted, including 1 in *Oncogene* and 1 in *Cancer Research*.

Project 1: This project has been completed with important discoveries in promoter methylation of ΔDNMT3B family members and the discovery of HDGF. There findings are being taken to the clinic through additional research and licensing agreements.

Project 2: The original goals of Aim 2.1 will best be served in a timely manner by synergizing with the research in the DoD Program BATTLE. A formal proposal will be submitted for review. The research for Aim 2.2 has been concluded but we have further discovered the convergence of mechanisms and possible nodes for NSAIDs and 4HPr with the small GTPase Rac, which is indicated as the earliest possible target for 4HPR.

Project 3: The tasks (Aims) of Project 3 have been completed. Two additional publications have resulted, concluding this program. These publications described mechanistic research for perifosine, identifying agents which may be synergistic in the clinic and described a novel mouse model which be extremely valuable for future lung cancer metastases studies.

DRP: The study demonstrated the potential feasibility for screening drug combinations of arbitrary size using the Medicinal Algorithmic Combinatorial Screening (MACS) method, which can efficiently identify highly-fit combinations of anticancer agents without prior molecular or functional insight into the interactions of the combined drugs. These findings have been submitted for publication and have resulted in additional peer-reviewed funding for continuation.

APPENDICES

APPENDIX A

Publications

The alkylphospholipid perifosine induces apoptosis of human lung cancer cells requiring inhibition of Akt and activation of the extrinsic apoptotic pathway

Heath A. Elrod, Yi-Dan Lin, Ping Yue, Xuerong Wang, Sagar Lonial, Fadlo R. Khuri, and Shi-Yong Sun

Department of Hematology and Oncology, Winship Cancer Institute, Emory University School of Medicine, Atlanta, Georgia

Abstract

The Akt inhibitor, perifosine, is an alkylphospholipid exhibiting antitumor properties and is currently in phase II clinical trials for various types of cancer. The mechanisms by which perifosine exerts its antitumor effects, including the induction of apoptosis, are not well understood. The current study focused on the effects of perifosine on the induction of apoptosis and its underlying mechanisms in human non–small cell lung cancer (NSCLC) cells. Perifosine, at clinically achievable concentration ranges of 10 to 15 μmol/L, effectively inhibited the growth and induced apoptosis of NSCLC cells. Perifosine inhibited Akt phosphorylation and reduced the levels of total Akt. Importantly, enforced activation of Akt attenuated perifosine-induced apoptosis. These results indicate that Akt inhibition is necessary for perifosine-induced apoptosis. Despite the activation of both caspase-8 and caspase-9, perifosine strikingly induced the expression of the tumor necrosis factor–related apoptosis-inducing ligand (TRAIL) receptor, death receptor 5, and down-regulated cellular FLICE-inhibitory protein (c-FLIP), an endogenous inhibitor of the extrinsic apoptotic pathway, with limited modulatory effects on the expression of other genes including Bcl-2, Bcl-X_L, PUMA, and survivin. Silencing of either caspase-8 or death receptor 5 attenuated perifosine-induced apoptosis. Consistently, further down-regulation of c-FLIP expression with c-FLIP small interfering RNA sensitized cells to perifosine-induced apoptosis, whereas enforced overexpression of ectopic c-FLIP conferred resistance to perifosine. Collectively, these data indicate that activation of the extrinsic apoptotic pathway plays a critical role in perifosine-induced apoptosis. Moreover, perifosine cooperates with TRAIL to enhance the induction of apoptosis in human NSCLC cells, thus warranting future *in vivo* and clinical evaluation of perifosine in combination with TRAIL in the treatment of NSCLC. [Mol Cancer Ther 2007;6(7):2029–38]

Introduction

Alkylphospholipids are a class of antitumor agents which target the cell membrane and induce apoptosis (1, 2). Perifosine, the first orally bioavailable alkylphospholipid, has shown antitumor activity in preclinical models and is currently in phase II clinical trials (1, 3). The mechanisms by which perifosine exerts its antitumor effect remain unclear, although it seems to inhibit Akt (2, 4) and mitogen-activated protein kinase activation (5), whereas inducing c-Jun-NH_2-kinase (JNK) activation (5). Perifosine has also been shown to induce p21 expression leading to cell cycle arrest (6). In addition, perifosine, in combination with other antitumor agents such as the PDK1 inhibitor, UCN-01 (7), histone deacetylase inhibitors (8), and the chemotherapeutic agent etoposide (9), show synergistic antitumor effects.

It is well known that there are two major apoptotic pathways used by mammalian cells to undergo apoptosis. One pathway involves signals transduced through death receptors known as the extrinsic apoptotic pathway; the second pathway relies on signals from the mitochondria called the intrinsic apoptotic pathway. Both pathways involve the activation of a set of caspases, which in turn, cleave cellular substrates and result in the characteristic morphologic and biochemical changes constituting the process of apoptosis (10, 11). The extrinsic pathway is characterized by the oligomerization of cell surface death receptors and activation of caspase-8, whereas the intrinsic pathway involves in the disruption of mitochondrial membranes, the release of cytochrome *c*, and the activation of caspase-9. Through caspase-8–mediated cleavage or truncation of Bid, the extrinsic death receptor apoptotic pathway is linked to the intrinsic mitochondrial apoptotic pathway (10, 11).

Molecules that can block the extrinsic apoptotic pathway include cellular FLICE-inhibitory protein (c-FLIP). c-FLIP prevents caspase-8 activation by death receptors. There are two major isoforms of c-FLIP: $FLIP_L$ consists of two

Received 1/4/07; revised 5/2/07; accepted 5/25/07.

Grant support: The Georgia Cancer Coalition Distinguished Cancer Scholar award (S-Y. Sun), Department of Defense grants W81XWH-04-1-0142-VITAL (S-Y. Sun for Project 4), DAMD17-01-1-0689-BESCT (F.R. Khuri), and an American Cancer Society Fellowship award (H.A. Elrod).

The costs of publication of this article were defrayed in part by the payment of page charges. This article must therefore be hereby marked *advertisement* in accordance with 18 U.S.C. Section 1734 solely to indicate this fact.

Note: H.A. Elrod and Y-D. Lin contributed equally to this work and share equal first authorship. F.R. Khuri and S-Y. Sun are Georgia Cancer Coalition Distinguished Cancer Scholars. H.A. Elrod is a recipient of an American Cancer Society Fellowship.

Requests for reprints: Shi-Yong Sun, Winship Cancer Institute, Emory University School of Medicine, 1365-C Clifton Road Northeast, C3088, Atlanta, GA 30322. Phone: 404-778-2170; Fax: 404-778-5520. E-mail: shi-yong.sun@emoryhealthcare.org

Copyright © 2007 American Association for Cancer Research.

doi:10.1158/1535-7163.MCT-07-0004

NH_2-terminal death effector domains and a COOH-terminal caspase homology domain devoid of enzymatic activity, whereas $FLIP_S$ is only composed of the NH_2-terminal death effector domains and a short COOH-terminal stretch of amino acids not found in $FLIP_L$. It has been shown that c-FLIP expression correlates with resistance against death receptor–induced apoptosis in a variety of cancer cells, and c-FLIP–transfected tumor cell lines develop more aggressive tumors *in vivo* (12, 13). In addition, many studies have shown that down-regulation of c-FLIP is sufficient to confer sensitivity against death receptor–induced apoptosis, whereas c-FLIP expression is associated with chemoresistance and down-regulation of c-FLIP using antisense oligonucleotides or small interfering RNAs (siRNA) sensitizes cells to chemotherapeutic agent–induced apoptosis (12–14).

Akt is known to be critical for tumor cell survival. One of the ways that Akt promotes cell survival is to inhibit apoptosis through its ability to phosphorylate several proapoptotic proteins such as Bad, which are involved in the regulation of the intrinsic apoptotic pathway (15). Moreover, Akt also inhibits the extrinsic death receptor–mediated apoptotic pathway through up-regulation of c-FLIP expression (16, 17). Thus, Akt negatively regulates apoptosis by suppressing both the mitochondria- and death receptor–mediated pathways.

The induction of apoptosis by perifosine has been observed in several cancer cell lines (3, 8, 9, 18). However, this effect has not been determined in non–small cell lung cancer (NSCLC) cells. Moreover, the mechanisms by which perifosine induces apoptosis is generally unknown. In this study, we examined the effects of perifosine on apoptosis in human NSCLC cells and its modulation on different apoptotic molecules in an attempt to understand its mechanisms of action. Our data show that perifosine induces apoptosis, inhibits Akt activation, up-regulates death receptor 5 (DR5) expression, and reduces c-FLIP levels in NSCLC cells. In addition, perifosine in combination with tumor necrosis factor–related apoptosis-inducing ligand (TRAIL) augments the induction of apoptosis.

Materials and Methods

Reagents

Perifosine was supplied by Keryx Biopharmaceuticals, Inc. This agent was dissolved in PBS and stored at −20°C. Stock solution was diluted to the appropriate concentrations with growth medium immediately before use. Human recombinant TRAIL was purchased from PeproTech, Inc.

Cell Lines and Cell Culture

The human NSCLC cell lines used in this study were described previously (19). H157 cell lines that stably express ectopic Lac Z (Lac Z-5) and $FLIP_L$ ($FLIP_L$-6), respectively, and A549 cell lines that stably express ectopic Lac Z (Lac Z-9) and $FLIP_L$ ($FLIP_L$-2), respectively, were described previously (20, 21). These cell lines were grown in a monolayer culture in RPMI 1640 supplemented with glutamine and 5% fetal bovine serum at 37°C in a humidified atmosphere consisting of 5% CO_2 and 95% air.

Cell Growth Assay

Cells were cultured in 96-well cell culture plates and treated the next day with the agents indicated. Viable cell number was estimated using the sulforhodamine B assay, as previously described (19).

Western Blot Analysis

Preparation of whole cell protein lysates and Western blot analysis were described previously (22, 23). Mouse anti–caspase-3 monoclonal antibody was purchased from Imgenex. Rabbit polyclonal antibodies against PTEN, Akt, phospho (p)-Akt (Ser^{473}), phospho (p)-FKHR (Ser^{256}), phospho (p)-GSK3β (Ser^{9}), c-Jun, phospho (p)-c-Jun (Ser^{63}), p44/42, phospho (p)-p44/42 (Thr^{202}/Tyr^{204}), survivin, caspase-8, caspase-9, poly(ADP-ribose) polymerase (PARP) were purchased from Cell Signaling Technology. Rabbit polyclonal anti-DR5 antibody was purchased from ProSci, Inc. Mouse monoclonal anti-FLIP antibody (NF6) was purchased from Alexis Biochemicals. Rabbit anti-G3PDH polyclonal antibody and mouse anti-Bax monoclonal antibody were purchased from Trevigen. Rabbit anti-Puma polyclonal antibody was purchased from EMD Biosciences, Inc. Mouse anti–Bcl-2 and rabbit anti–Bcl-X_L antibodies were purchased from Santa Cruz Biotechnology, Inc. Rabbit anti–β-actin polyclonal antibody was purchased from Sigma Chemicals. Secondary antibodies, goat anti-mouse and goat anti-rabbit horseradish peroxidase conjugates, were purchased from Bio-Rad.

Adenoviral Infection

Adenovirus harboring an empty vector (Ad-CMV) or a constitutively activated form of Akt (myristoylated Akt; Ad-myr-Akt) were provided by Lily Yang (Department of Surgery, Emory University School of Medicine, Atlanta, GA). The procedure for adenoviral infection of cancer cells was described previously (24).

Gene Silencing Using siRNA

Silencing of caspase-8, DR5, c-FLIP, and PTEN were achieved by transfecting siRNA using RNAifect transfection reagent (Qiagen) following the instructions of the manufacturer. Control, caspase-8, and DR5 siRNAs were described previously (22). These siRNAs and c-FLIP siRNA targeting the sequence 5′-AATTCTCCGAACGTGTCACGT-3′ (14) were all synthesized from Qiagen. PTEN siRNA was purchased from Cell Signaling. Cells were plated in 6- or 24-well cell culture plates and transfected with the given siRNAs the next day. After 24 h, the cells were trypsinized and replated in new plates, and on the second day, treated with perifosine as indicated. Gene silencing effects were evaluated by Western blot as described above after the indicated times of treatment.

Apoptosis Assays

Apoptosis was detected either by analysis of caspase activation using Western blot analysis as described above or by Annexin V staining using Annexin V-PE apoptosis detection kit (BD Bioscience) following the instructions of the manufacturer, and analyzed by flow cytometry using FACScan (Becton Dickinson). In addition, we measured

the amounts of cytoplasmic histone-associated DNA fragments (mononucleosome and oligonucleosomes) formed during apoptosis using a Cell Death Detection ELISA^{Plus} kit (Roche Molecular Biochemicals) according to the instructions of the manufacturer.

Results

Effects of Perifosine on Cell Survival and Apoptosis in NSCLC Cells

The effects of perifosine on cell survival were examined in a panel of NSCLC cell lines (Fig. 1A). For the majority of the cell lines tested, there was a dose-dependent decrease in cell survival. The H460 cell line was the most sensitive to perifosine, showing an IC_{50} value of ~1 μmol/L. The H226 cell line was the most resistant to perifosine, in which perifosine at 20 μmol/L decreased cell survival by <20%. Most of the tested cell lines exhibited moderate response to perifosine with IC_{50}s ranging from 8 to 15 μmol/L (Fig. 1A), which are within the clinically achievable and safe peak plasma concentrations of 12 to 15 μmol/L (25, 26). The *p53* and *PTEN* mutation status in the NSCLC cell lines tested did not correlate with sensitivity to perifosine, suggesting that perifosine inhibits cell growth independently of *p53* and *PTEN* mutation status (Fig. 1A). In addition, we examined the protein expression levels of PTEN, total Akt, and p-Akt in the cell lines tested. It seemed that those cell lines (e.g., H460 and H358) with low levels of p-Akt and high levels of PTEN were the most sensitive to perifosine (Fig. 1B).

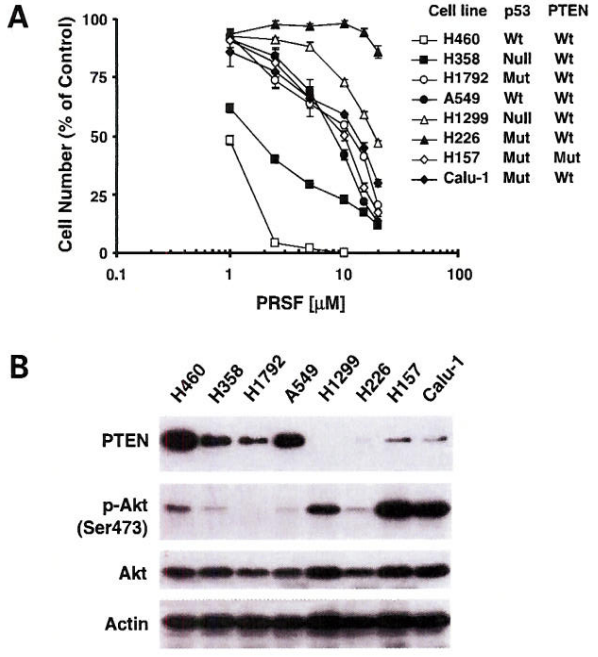


Figure 1. Effects of perifosine on the survival of NSCLC cells (**A**) and their association with basal levels of p-Akt (**B**). **A,** cell lines treated with different concentrations of perifosine (*PRFS*) ranging from 1 to 20 μmol/L. After 3 d, the cells were subjected to sulforhodamine B assay for estimating the viable cells. In addition, the *p53* status and *PTEN* status of the cell lines were also indicated. *Points,* means of four replicate determinations; *bars,* SD. **B,** cell lines with similar cell densities were harvested for the preparation of whole cell protein lysates. The indicated proteins were analyzed by Western blot analysis.

We further examined the effects of perifosine on apoptosis in NSCLC cell lines. As shown in Fig. 2A, perifosine induced apoptosis in H460 and A459 cells as indicated by Annexin V–positive staining. At concentrations of 10 μmol/L, perifosine induced cell death in ~50% of H460 cells, whereas apoptosis was induced in 23% and 33% of the A549 cells after treatment with 10 and 15 μmol/L of perifosine, respectively, suggesting that the H460 cells were more sensitive to perifosine-induced apoptosis. The H157 cells were the least sensitive to perifosine-induced apoptosis with only 10% of H157 cells undergoing apoptosis after treatment with 15 μmol/L of perifosine. We found that perifosine at concentrations ranging from 2.5 to 10 μmol/L induced cleavage of caspase-8, caspase-9, caspase-3, and PARP in H460 cells, whereas it induced partial cleavage of the caspases and PARP only at 10 μmol/L in A549 cells (Fig. 2B). In H157 cells treated with perifosine (up to 10 μmol/L), we failed to detect cleaved bands of the caspases and PARP (Fig. 2B). Because perifosine is effective in decreasing cell number in H157 cells (Fig. 1), we further examined cell cycle alteration in H157 cells after exposure to perifosine and detected 17.9%, 35.8%, and 42.4% G_2-M cells in cells treated with PBS, 10 μmol/L of perifosine, and 15 μmol/L of perifosine, respectively, after a 48 h treatment, indicating that perifosine primarily decreases cell numbers in H157 cells via induction of cell cycle arrest. In the following studies, we focused on revealing the mechanisms underlying perifosine-induced apoptosis.

Effects of Perifosine on the Phosphorylation of Akt, JNK, and ERK

Perifosine has been shown to modulate Akt as well as other signaling pathways (6, 18, 27). We therefore examined whether perifosine modulated similar signal transduction pathways in human NSCLC cells. In examining Akt phosphorylation, we observed that both H460 and A549 cells have very low basal levels of p-Akt, whereas H157 cells have much higher basal levels of p-Akt. When comparing the apoptosis results presented in Fig. 2A, it seems that low basal levels of p-Akt correlated with high sensitivity to perifosine-induced apoptosis. These cell lines exhibited a concentration-dependent decrease in p-Akt levels when exposed to perifosine (p-Akt levels were only detectable in H460 cells after a very long exposure). Interestingly, perifosine also decreased the levels of total Akt in the tested cell lines (Fig. 3A) and the degree of Akt down-regulation also seemed to correlate with cell sensitivity to perifosine-induced apoptosis. In H460 cells, decreases in both Akt and p-Akt levels occurred at 3 h after treatment with perifosine (Fig. 3B), indicating that Akt down-regulation is an early event. In H157 cells, Akt levels were only slightly decreased, whereas p-Akt levels were substantially (by 2.5 μmol/L of perifosine) and rapidly (3 h posttreatment) reduced upon perifosine treatment

(Fig. 3A and B). These results suggest that the perifosine-mediated decrease in p-Akt levels could be due to either Akt protein down-regulation or upstream signaling suppression, depending on the cell lines used. To our knowledge, this is the first demonstration that perifosine down-regulates the levels of total Akt in human cancer cells. We also detected a decrease in the levels of p-FKHR and p-GSK3β, two well-known substrates of Akt (Fig. 3B), furthering the notion that perifosine inhibits Akt signaling in NSCLC cells.

In examining other signal transduction pathways, we observed the basal levels of p-c-Jun were very low in the tested NSCLC cells and were only slightly increased by perifosine in H157 cells, indicating that perifosine-induced JNK activation was a cell line–dependent event. Perifosine did not alter the levels of p42/44, but did decrease the levels of p-p42/44 in all three cell lines tested (Fig. 3A). These data indicate that perifosine down-regulates the ERK (or p42/44) signaling pathway in NSCLC cells.

Enforced Akt Activation Attenuates Perifosine-Induced Apoptosis

To decipher the role of Akt inhibition in perifosine-induced apoptosis, we artificially activated Akt in H460 cells by infecting the cells with adenoviruses carrying a *myr-Akt* gene that codes a constitutively activated form of Akt, and then examined the response of these cells to perifosine treatment. Using Western blot analysis, we detected high levels of myr-Akt, p-Akt, and p-GSK3β in cells infected with Ad-myr-Akt (Fig. 3C). In addition, infection of cells with Ad-myr-Akt also elevated the levels of c-FLIP, which has been shown to be regulated by Akt. (refs. 16, 17; Fig. 3C). In Ad-CMV–infected control cells, treatment with perifosine caused 37% apoptotic cell death (9% in PBS-treated cells) plus 15.2% necrotic cell death. However, we detected only 16% apoptosis (~12% in PBS-treated cells) and <2% necrosis in cells infected with Ad-myr-Akt after treatment with perifosine (Fig. 3D). These results clearly show that enforced Akt activation restores cell resistance to perifosine-induced apoptosis, thus indicating that Akt inhibition is necessary in mediating perifosine-induced apoptosis.

Given that there is an inverse relationship between PTEN expression and p-Akt levels (Fig. 1B), we further determined whether down-regulation of PTEN affects p-Akt levels and cell sensitivity to perifosine. Knockdown of PTEN using PTEN siRNA in H460 cells, which is the most sensitive cell line to perifosine and have the highest levels of PTEN (Fig. 1), increased basal levels of p-Akt. However,

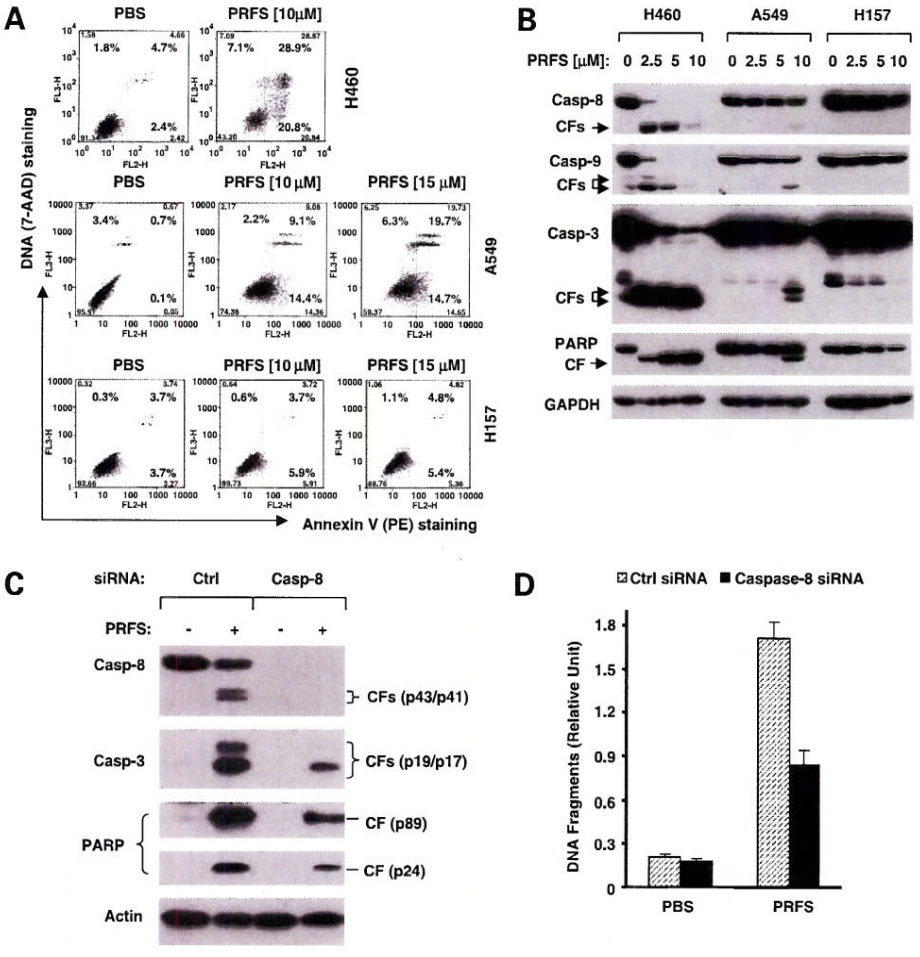


Figure 2. Effects of perifosine on apoptosis induction (**A**) and caspase activation (**B**), and involvement of caspase-8 activation in perifosine-induced apoptosis (**C** and **D**) in NSCLC cells. **A,** cell lines treated with the given concentrations of perifosine (*PRFS*) for 24 h and harvested for the estimation of apoptosis by Annexin V staining. Early apoptotic (*bottom right*), late apoptotic (*top right*), and necrotic (*top left*) cells. **B,** the indicated cell lines were treated with the given concentrations of perifosine for 16 h and harvested for the detection of caspase cleavage by Western analysis. **C** and **D,** H460 cells were seeded in 24-well plates and transfected with control (*Ctrl*) or caspase-8 siRNA the next day. After ~24 h, the cells were trypsinized and replated in new 6-well (**C**) or 96-well (**D**) plates. On the second day, the cells were treated with PBS or 5 μmol/L of perifosine. After 16 h, the cells were subjected to Western blot analysis for the indicated proteins (**C**) or ELISA for measurement of DNA fragments (**D**). *CF,* cleaved form. *Columns,* means of triplicate determinations; *bars,* SD.

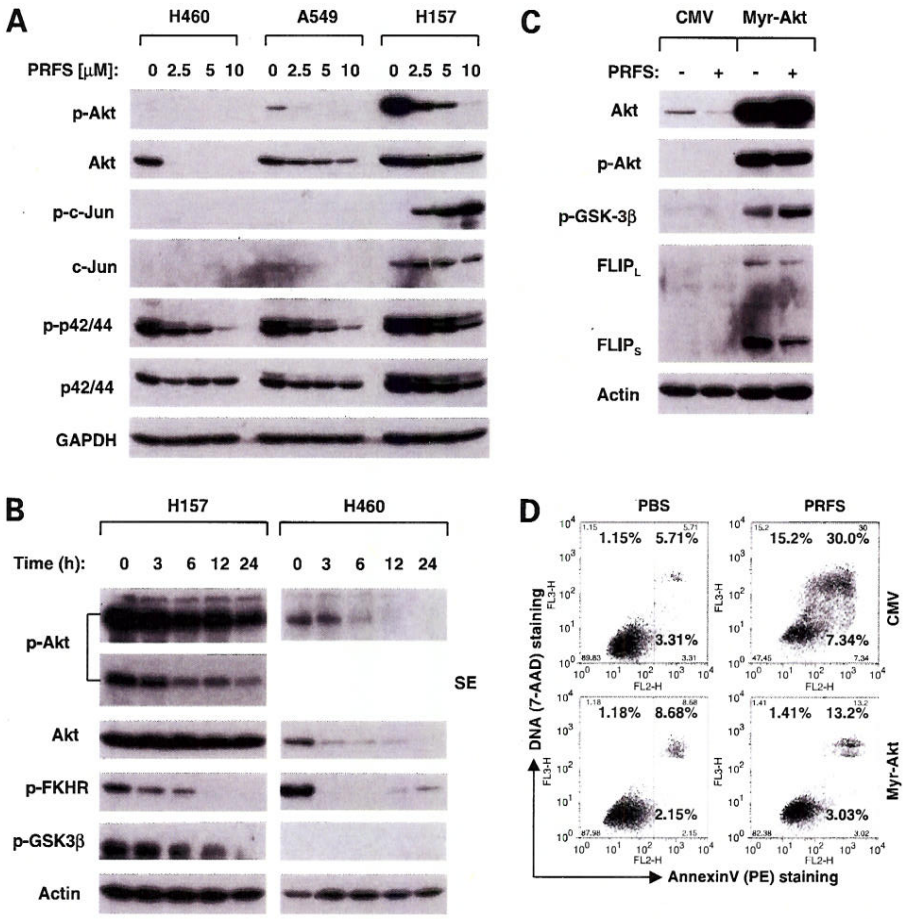


Figure 3. Modulation of Akt, JNK, and ERK signaling pathways by perifosine (**A** and **B**), and involvement of Akt inhibition in perifosine-induced apoptosis (**C** and **D**) in human NSCLC cells. **A** and **B**, NSCLC cell lines treated with the given concentrations of perifosine (*PRFS*) for 16 h (**A**) or with 10 μmol/L (H157) or 5 μmol/L (H460) of perifosine for the indicated times (**B**). The cells were then subjected to a preparation of whole cell protein lysates and subsequent detection of the indicated proteins using Western blot analysis. **C** and **D**, H460 cells were infected with a multiplicity of infection of 200 Ad-CMV or Ad-myr-Akt. Twenty-four hours later, the cells were exposed to 10 μmol/L of perifosine. After 24 h, the cells were harvested for analysis of the given proteins by Western blotting (**C**) and for the detection of apoptosis by Annexin V staining (**D**). *SE*, short exposure.

the p-Akt increase caused by PTEN knockdown could be abrogated by perifosine treatment. Surprisingly, perifosine decreased PTEN levels, which itself did not result in an increase of p-Akt levels, probably because perifosine also inhibits Akt phosphorylation (see Supplemental Fig. S1A).[1] As a result, down-regulation of PTEN by siRNA did not alter cell sensitivity to perifosine as shown by measuring cell number change (Supplemental Fig. S1B),[1] caspase activation (Supplemental Fig. S1A),[1] and apoptotic cells (Supplemental Fig. S1C).[1]

Effects of Perifosine on the Expression of Key Molecules Involved in the Regulation of Apoptosis

To further explore how perifosine induces apoptosis, we next examined the effects of perifosine on the expression of several key genes involved in either the extrinsic apoptotic pathway (e.g., DR5 and c-FLIP) or the intrinsic apoptotic pathway (e.g., Bax, Bcl-2, Bcl-X_L, PUMA, and survivin). Perifosine increased the levels of DR5, particularly in H460 cells (Fig. 4). It seems that DR5 induction is associated with increased sensitivity of cell lines to perifosine. c-FLIP is another key protein that inhibits the extrinsic apoptotic pathway by blocking caspase-8 activation (12). The H460 cells, which are the most sensitive to perifosine, had very low basal levels of c-FLIP, particularly $FLIP_L$, which were further down-regulated by perifosine, whereas the less sensitive A549 and H157 cells have high basal levels of c-FLIP, particularly $FLIP_L$, which were only weakly decreased by perifosine. Perifosine also decreased $FLIP_S$ levels in these cell lines (Fig. 4). It seems that low levels of c-FLIP and their further down-regulation by perifosine were associated with high sensitivity to perifosine-induced apoptosis. Collectively, these results suggest that activation of the DR5-mediated extrinsic apoptotic pathway is important in perifosine-induced apoptosis.

In examining the signaling molecules involved in the intrinsic apoptotic pathway, we found that perifosine did not significantly alter the levels of Bcl-2 in NSCLC cells (Fig. 4). Surprisingly, perifosine decreased Bax levels in all the tested NSCLC cell lines. Perifosine decreased Bcl-X_L levels in H460 cells that were very sensitive to perifosine, but not in A549 and H157 cells that were less sensitive to perifosine (Fig. 4). These data suggest that Bcl-X_L down-regulation may affect cell sensitivity to undergo perifosine-induced apoptosis. H460 cells had low basal levels of survivin, which were further decreased by perifosine,

[1] Supplementary material for this article is available at Molecular Cancer Therapeutics Online (http://mct.aacrjournals.org/).

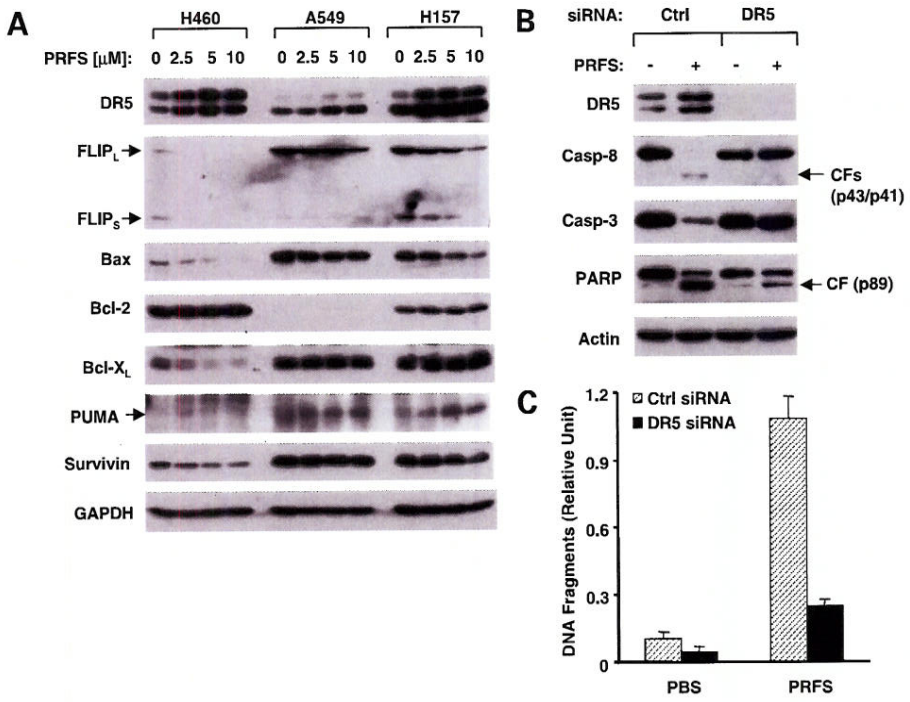


Figure 4. Modulation of apoptosis-related gene expression by perifosine (**A**) and demonstration of the role of DR5 induction in perifosine-induced apoptosis (**B** and **C**) in human NSCLC cells. **A**, NSCLC cell lines treated with the given concentrations of perifosine (*PRFS*) for 16 h. The cells were then subjected to a preparation of whole cell protein lysates and subsequent detection of the indicated proteins using Western blot analysis. **B** and **C**, H460 cells were seeded in six-well plates and transfected with control (*Ctrl*) or DR5 siRNA the next day. After ~20 h, the cells were trypsinized and replated in new 6-well (**B**) or 96-well (**C**) plates. On the second day, the cells were treated with PBS or 7.5 μmol/L of perifosine. After 16 h, the cells were subjected to Western blot analysis for the detection of the indicated proteins (**B**) or ELISA for the measurement of DNA fragments (**C**). *Columns*, means of triplicate determinations; *bars*, SD; *CF*, cleaved form.

whereas H157 and A549 cells had high levels of survivin, which were apparently not altered by perifosine (Fig. 4). Thus, it seems that low basal levels of survivin and its further down-regulation with perifosine are also associated with increased cell sensitivity to perifosine-induced apoptosis. PUMA was slightly increased in A549 and H157 cells, but not in H460 cells, suggesting that PUMA was not important in perifosine-induced apoptosis.

Perifosine Cooperates with TRAIL to Enhance the Induction of Apoptosis

Because perifosine induces DR5 expression and down-regulates c-FLIP levels, we hypothesized that perifosine would cooperate with TRAIL, a DR5 ligand, to enhance the induction of apoptosis. Thus, we examined the effects of perifosine in combination with TRAIL on apoptosis induction in NSCLC cells. As shown in Fig. 5A, perifosine in combination with TRAIL induced higher levels of DNA fragments than did each single agent alone. Moreover, increased amounts of cleaved caspase-8, caspase-9, caspase-3, and PARP were detected in cells treated with the perifosine and TRAIL combination, but were only minimally detected in cells treated with either perifosine or TRAIL alone (Fig. 5B). Thus, we conclude that perifosine cooperates with TRAIL to enhance the induction of apoptosis.

Perifosine Induces Apoptosis Requiring Caspase-8 Activation and DR5 Up-regulation

The data presented above strongly suggest a role for the activation of the extrinsic apoptotic pathway in perifosine-induced apoptosis. Thus, we determined whether perifosine induces apoptosis requiring activation of caspase-8 and up-regulation of DR5. To this end, we silenced the expression of caspase-8 and DR5 using caspase-8 and DR5 siRNAs, respectively, and then examined cell sensitivity to perifosine. By Western blotting, we detected substantially reduced levels of caspase-8 levels including cleaved forms in H460 cells transfected with caspase-8 siRNA compared with those in control siRNA-transfected cells (Fig. 2C), indicating successful caspase-8 knockdown or inhibition of caspase-8 activation. Accordingly, cleavage of caspase-3 and PARP and an increase in DNA fragmentation were also attenuated in caspase-8 siRNA-transfected cells in comparison with control siRNA–transfected cells (Fig. 2C and D). These results indicate that perifosine induces a caspase-8–dependent apoptosis. Similarly, silencing of DR5 expression using DR5 siRNA abrogated DR5 induction (Fig. 4B) and impaired the ability of perifosine to induce cleavage of caspase-8, caspase-3, and PARP (Fig. 4B). In addition, an increase in DNA fragmentation in DR5 siRNA-transfected cells was also reduced compared with control siRNA-transfected cells (Fig. 4C). These data show that DR5 up-regulation is also involved in perifosine-induced apoptosis.

Manipulation of c-FLIP Levels Regulates Cell Sensitivity to Perifosine-Induced Apoptosis and Enhancement of TRAIL-Induced Apoptosis

To further show that the activation of the extrinsic apoptotic pathway participates in perifosine-induced apoptosis, we examined the sensitivity of cell lines that express ectopic FLIP$_L$ to perifosine-induced apoptosis. As presented in Fig. 6A, perifosine increased DNA fragmentation in a dose-dependent fashion in H157-Lac Z-5 cells, but only minimally in H157-FLIP$_L$-6 cells. As a positive control treatment, TRAIL-induced increase in DNA fragmentation

was abolished in H157-$FLIP_L$-6 cells. Similarly, perifosine-induced increase in DNA fragmentation was also abrogated in A549-$FLIP_L$-2 cells in comparison with A549-Lac Z-9 cells (Fig. 6B). Together, these results clearly show that overexpression of ectopic c-FLIP protects cells from perifosine-induced apoptosis.

Because c-FLIP down-regulation was often associated with the enhancement of TRAIL-induced apoptosis (20, 21, 28), we further compared apoptosis induction by the combination of perifosine and TRAIL between A549-Lac Z-9 and A549-$FLIP_L$-2 cell lines. In agreement with the results presented in Fig. 5, the combination of perifosine and TRAIL was much more potent than either perifosine or TRAIL alone in increasing DNA fragmentation in A549-Lac Z-9 cells. However, not only perifosine and TRAIL alone but also their combination exhibited minimal effects on increasing DNA fragmentation in A549-$FLIP_L$-2 cells (Fig. 6B). These results clearly show that overexpression of ectopic c-FLIP confers cell resistance to the combination of perifosine and TRAIL, indicating that c-FLIP down-regulation contributes to perifosine-mediated enhancement of TRAIL-induced apoptosis.

Because the cell lines, A549 and H157, with high basal levels of c-FLIP were relatively less sensitive than H460 cells which have low basal levels of c-FLIP to perifosine-induced apoptosis, we wanted to determine whether down-regulation of c-FLIP sensitized cells to perifosine-induced apoptosis. To this end, we silenced the expression of c-FLIP (both $FLIP_L$ and $FLIP_S$) using siRNA in A549 cells, and then examined their response to perifosine-induced apoptosis. As presented in Fig. 6C, transfection of c-FLIP siRNA reduced the levels of both $FLIP_L$ and $FLIP_S$, which were further reduced after treatment with perifosine. Those cells whose expression of c-FLIP had been reduced with siRNA were more sensitive to caspase-8, caspase-3, and PARP cleavage after perifosine treatment compared with control cells, indicating that c-FLIP levels indeed affect cell sensitivity to perifosine-induced apoptosis.

Discussion

In this study, we have shown that perifosine exerts its growth-inhibitory effects in a panel of NSCLC cell lines, primarily through the induction of apoptosis and/or cell cycle arrest. Importantly, perifosine inhibited the growth of most of the tested NSCLC cell lines with IC_{50}s ranging between 8 and 15 μmol/L (Fig. 1A), which are within the

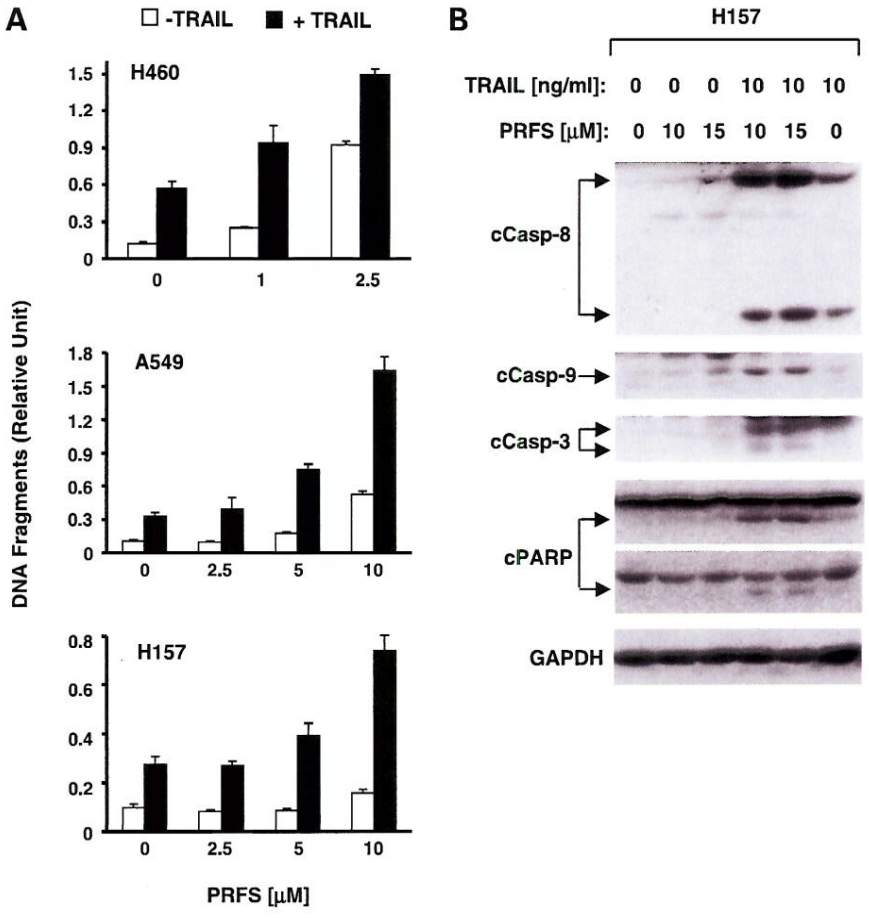


Figure 5. Perifosine cooperates with TRAIL to enhance DNA fragmentation (**A**) and caspase activation (**B**) in human NSCLC cells. **A,** cell lines plated in 96-well plates and treated with the given doses of perifosine (*PRFS*) alone, 20 ng/mL TRAIL alone, or TRAIL plus perifosine on the second day. After 24 h, the cells were subjected to DNA fragmentation using the Cell Death Detection ELISA kit. *Columns,* means of triplicate determinations; *bars,* SD. **B,** H157 cells were treated with perifosine alone, TRAIL alone, and their combinations. After 16 h, the cells were subjected to a preparation of whole cell protein lysates and subsequent detection of the indicated proteins by Western blot analysis. *c,* cleaved.

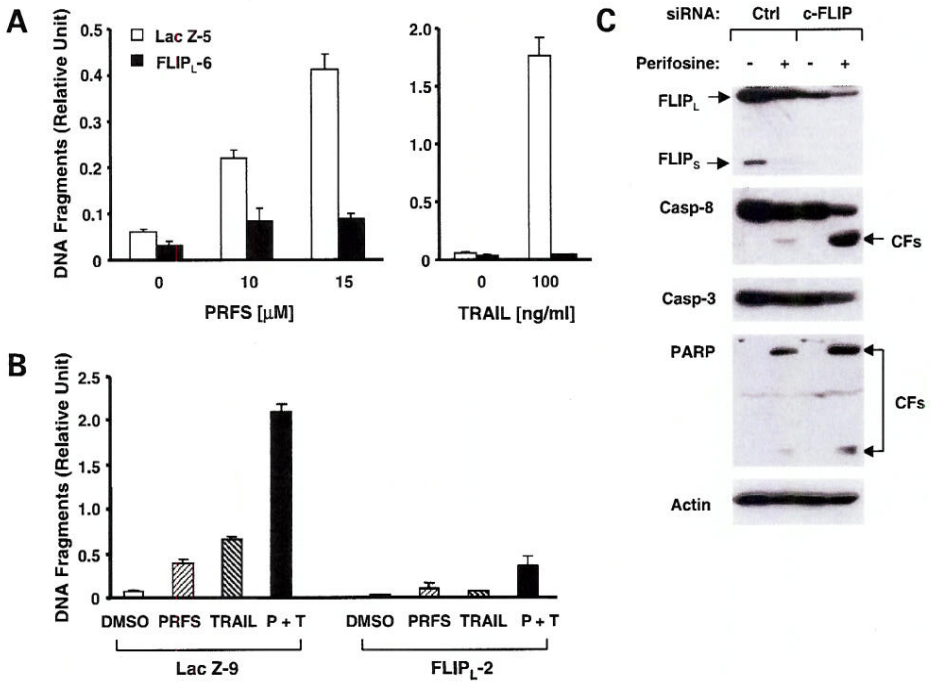


Figure 6. Overexpression of ectopic c-FLIP (**A** and **B**) and silencing of c-FLIP expression (**C**) modulate cell sensitivity to perifosine-induced apoptosis. **A,** H157 cell lines that stably express Lac Z and FLIP$_L$, respectively, were treated with the indicated concentrations of perifosine (*PRFS*) or TRAIL. **B,** A549 cell lines that stably express Lac Z and FLIP$_L$, respectively, were exposed to 10 μmol/L of perifosine, 20 ng/mL of TRAIL, and the combination of perifosine and TRAIL (*P + T*). Twenty-four hours later, after the aforementioned treatment, the cells were subjected to estimation of DNA fragmentation using the Cell Death Detection ELISA kit. *Columns,* mean of triplicate determinations; *bars,* SD. **C,** A549 cells plated in 24-well plates were transfected with control (*Ctrl*) or c-FLIP siRNA. Twenty-four hours later, the cells were exposed to 10 μmol/L of perifosine (*PRFS*). After 24 h, the cells were subjected to a preparation of whole cell protein lysates and subsequent detection of the indicated proteins using Western blot analysis. *CFs,* cleaved fragments.

clinically achievable and safe peak plasma concentration ranges (i.e., 10–15 μmol/L; refs. 25, 26), suggesting the potential of perifosine in the treatment of NSCLCs.

Modulation of Akt, JNK, and ERK signaling pathways and their involvement in perifosine-induced apoptosis has been studied in other types of cancer cells (4, 18, 27). Despite the proapoptotic role of JNK activation in perifosine-induced apoptosis in multiple myeloma (18), we found that perifosine increased p-c-Jun only in one (i.e., H157 cells) of three cell lines tested (Fig. 3A). Given that H157 cells were relatively insensitive to perifosine-induced apoptosis (Fig. 2), we suggest that JNK activation is unlikely to account for the perifosine-induced apoptosis in human NSCLC cells. Perifosine was reported to either decrease or increase ERK phosphorylation depending on cancer cell type (5, 18, 27). In our study, perifosine decreased ERK phosphorylation in all of the three tested cell lines tested, regardless of cell sensitivity to TRAIL-induced apoptosis. Thus, we suggest that ERK inhibition is also unlikely to be critical for perifosine-induced apoptosis in human NSCLC cells.

Although perifosine inhibits Akt activation in different types of cancer cells including the NSCLC cells shown in the current study, enforced activation of Akt through overexpression of the constitutively activated form of Akt, myr-Akt, protects cells from perifosine-induced cell death in one type of cancer cell line (e.g., PC-3 prostate cancer cells; ref. 4) but not in another type of cancer cell (e.g., MM.1S multiple myeloma cells; ref. 18). In our study, we found that the low basal levels of p-Akt (e.g., H460 < A549 < H157) and its further down-regulation were associated with high sensitivity to perifosine-induced apoptosis (H460 > A549 > H157; Figs. 1 and 2). Moreover, overexpression of myr-Akt in H460 cells led to increased levels of p-Akt and resistance to perifosine-induced apoptosis (Fig. 3). Collectively, we conclude that Akt inhibition plays an important role in mediating perifosine-induced apoptosis in human lung cancer cells. We noted that perifosine decreased the levels of total Akt in some NSCLC cells (e.g., H460 and A549), the potency of which is associated with cell sensitivity to perifosine-induced apoptosis, in addition to decreasing Akt phosphorylation. To the best of our knowledge, this is the first demonstration that perifosine decreases the total levels of Akt. Given that Akt reduction is an early event, which occurred at 3 h post–perifosine treatment (Fig. 3B), it is unlikely that Akt reduction occurs secondary to perifosine-induced apoptosis (e.g., cleavage by caspase activation). Nevertheless, ongoing studies are attempting to reveal how perifosine decreases the levels of total Akt.

Perifosine activated both caspase-8 and caspase-9 in human NSCLC cells (Fig. 2B), suggesting that perifosine can induce apoptosis through the extrinsic and/or intrinsic apoptotic pathways. In examining several key proteins involved in the regulation of the extrinsic or intrinsic apoptotic pathways, we found that perifosine strikingly induced DR5 expression and decreased the levels of c-FLIP in all the cells lines tested, whereas having limited or no modulatory effects on the levels of Bcl-2, Bcl-X$_L$, PUMA, and survivin (Fig. 4A). Importantly, the low basal levels of c-FLIP (e.g., FLIP$_L$) and its further down-regulation are associated with increased sensitivity to undergo perifosine-induced apoptosis (e.g., H460 cells). We noted that Bax

levels were lower and Bcl-2 levels were higher in the sensitive H460 cells than in less sensitive A549 and H157 cells (Fig. 4A). Moreover, we found that Bax levels were actually decreased in cells treated with perifosine, although the underlying mechanisms and its effects on perifosine-induced apoptosis are unclear. In fact, our preliminary data show that Bax or PUMA deficiency does not alter cell sensitivity to perifosine-induced apoptosis.[2] Together, we suggest that the activation of the extrinsic apoptotic pathway is important in mediating perifosine-induced apoptosis. This observation is supported by our findings that silencing of caspase-8 or DR5, or overexpression of ectopic c-FLIP protects cells from perifosine-induced apoptosis (Figs. 2, 4, and 6), whereas down-regulation of endogenous c-FLIP using c-FLIP siRNA sensitizes cells to perifosine-induced apoptosis (Fig. 6). In agreement with our findings, a recent study has shown that perifosine induces apoptosis through activation of the Fas-mediated extrinsic apoptotic pathway in human leukemia cells (29). To the best of our knowledge, this is the first study showing that perifosine modulates the expression of DR5 and c-FLIP in human cancer cells.

Some studies have shown that Akt also inhibits the extrinsic apoptotic pathway through the up-regulation of c-FLIP expression (16, 17). In this study, we have shown that perifosine inhibits Akt and reduces c-FLIP levels, both of which are involved in perifosine-induced apoptosis. Indeed, we detected increased levels of c-FLIP in cells infected with Ad-myr-Akt (Fig. 3C), suggesting that Akt activation indeed increases c-FLIP levels in the tested cells. Thus, it is possible that Akt exerts its inhibitory effect on perifosine-induced apoptosis through the up-regulation of c-FLIP. On other hand, perifosine may down-regulate c-FLIP levels through inhibition of Akt; this needs to be investigated in detail in the future.

It is known that TRAIL functions as the DR5 ligand and rapidly induces apoptosis in a wide variety of transformed cells but is not cytotoxic in normal cells *in vitro* and *in vivo* (10, 16, 17). Therefore, TRAIL is considered to be a tumor-selective, apoptosis-inducing cytokine with promising potential for cancer treatment and is currently being tested in phase I clinical trials. In our study, we showed that the combination of perifosine and TRAIL exhibited augmented induction of apoptosis in human NSCLC cells (Fig. 5), which is likely due to the ability of perifosine to induce DR5 expression and down-regulate c-FLIP levels. This finding warrants future *in vivo* animal studies and clinical evaluation of the efficacy of perifosine in combination with TRAIL for the treatment of NSCLC.

Acknowledgments

We are grateful to Zhongmei Zhou for her excellent technical assistance, Dr. Xiangguo Liu for establishment of stable cell lines that overexpress c-FLIP, and Dr. Lily Yang for providing us with Ad-CMV and Ad-myr-Akt.

[2] Unpublished data.

References

1. Hilgard P, Klenner T, Stekar J, et al. D-21266, a new heterocyclic alkylphospholipid with antitumour activity. Eur J Cancer 1997;33:442–6.

2. Ruiter GA, Verheij M, Zerp SF, van Blitterswijk WJ. Alkyl-lysophospholipids as anticancer agents and enhancers of radiation-induced apoptosis. Int J Radiat Oncol Biol Phys 2001;49:415–9.

3. Vink SR, Schellens JH, van Blitterswijk WJ, Verheij M. Tumor and normal tissue pharmacokinetics of perifosine, an oral anti-cancer alkylphospholipid. Invest New Drugs 2005;23:279–86.

4. Kondapaka SB, Singh SS, Dasmahapatra GP, Sausville EA, Roy KK. Perifosine, a novel alkylphospholipid, inhibits protein kinase B activation. Mol Cancer Ther 2003;2:1093–103.

5. Li X, Luwor R, Lu Y, Liang K, Fan Z. Enhancement of antitumor activity of the anti-EGF receptor monoclonal antibody cetuximab/C225 by perifosine in PTEN-deficient cancer cells. Oncogene 2006;25:525–35.

6. Patel V, Lahusen T, Sy T, et al. Perifosine, a novel alkylphospholipid, induces p21(WAF1) expression in squamous carcinoma cells through a p53-independent pathway, leading to loss in cyclin-dependent kinase activity and cell cycle arrest. Cancer Res 2002;62:1401–9.

7. Dasmahapatra GP, Didolkar P, Alley MC, et al. *In vitro* combination treatment with perifosine and UCN-01 demonstrates synergism against prostate (PC-3) and lung (A549) epithelial adenocarcinoma cell lines. Clin Cancer Res 2004;10:5242–52.

8. Rahmani M, Reese E, Dai Y, et al. Coadministration of histone deacetylase inhibitors and perifosine synergistically induces apoptosis in human leukemia cells through Akt and ERK1/2 inactivation and the generation of ceramide and reactive oxygen species. Cancer Res 2005;65:2422–32.

9. Nyakern M, Cappellini A, Mantovani I, Martelli AM. Synergistic induction of apoptosis in human leukemia T cells by the Akt inhibitor perifosine and etoposide through activation of intrinsic and Fas-mediated extrinsic cell death pathways. Mol Cancer Ther 2006;5:1559–70.

10. Ashkenazi A, Dixit VM. Death receptors: signaling and modulation. Science 1998;281:1305–8.

11. Hengartner MO. The biochemistry of apoptosis. Nature 2000;407:770–6.

12. Kataoka T. The caspase-8 modulator c-FLIP. Crit Rev Immunol 2005;25:31–58.

13. Wajant H. Targeting the FLICE inhibitory protein (FLIP) in cancer therapy. Mol Interv 2003;3:124–7.

14. Longley DB, Wilson TR, McEwan M, et al. c-FLIP inhibits chemotherapy-induced colorectal cancer cell death. Oncogene 2006;25:838–48.

15. Cheng JQ, Lindsley CW, Cheng GZ, Yang H, Nicosia SV. The Akt/PKB pathway: molecular target for cancer drug discovery. Oncogene 2005;24:7482–92.

16. Panka DJ, Mano T, Suhara T, Walsh K, Mier JW. Phosphatidylinositol 3-kinase/Akt activity regulates c-FLIP expression in tumor cells. J Biol Chem 2001;276:6893–6.

17. Nam SY, Jung GA, Hur GC, et al. Upregulation of FLIP(S) by Akt, a possible inhibition mechanism of TRAIL-induced apoptosis in human gastric cancers. Cancer Sci 2003;94:1066–73.

18. Richardson PG, Mitsiades C, Hideshima T, Anderson KC. Bortezomib: proteasome inhibition as an effective anticancer therapy. Annu Rev Med 2006;57:33–47.

19. Sun SY, Yue P, Dawson MI, et al. Differential effects of synthetic nuclear retinoid receptor-selective retinoids on the growth of human non-small cell lung carcinoma cells. Cancer Res 1997;57:4931–9.

20. Liu X, Yue P, Schonthal AH, Khuri FR, Sun SY. Cellular FLICE-inhibitory protein down-regulation contributes to celecoxib-induced apoptosis in human lung cancer cells. Cancer Res 2006;66:11115–9.

21. Zou W, Liu X, Yue P, Khuri FR, Sun SY. PPARγ ligands enhance TRAIL-induced apoptosis through DR5 upregulation and c-FLIP down-regulation in human lung cancer cells. Cancer Biol Ther 2007;6:99–106.

22. Liu X, Yue P, Zhou Z, Khuri FR, Sun SY. Death receptor regulation and celecoxib-induced apoptosis in human lung cancer cells. J Natl Cancer Inst 2004;96:1769–80.

23. Sun SY, Yue P, Wu GS, et al. Mechanisms of apoptosis induced by the synthetic retinoid CD437 in human non-small cell lung carcinoma cells. Oncogene 1999;18:2357–65.

24. Jin F, Liu X, Zhou Z, et al. Activation of nuclear factor-κB contributes to induction of death receptors and apoptosis by the synthetic retinoid CD437 in DU145 human prostate cancer cells. Cancer Res 2005;65: 6354 – 63.

25. Crul M, Rosing H, de Klerk GJ, et al. Phase I and pharmacological study of daily oral administration of perifosine (D-21266) in patients with advanced solid tumours. Eur J Cancer 2002;38:1615 – 21.

26. Van Ummersen L, Binger K, Volkman J, et al. A phase I trial of perifosine (NSC 639966) on a loading dose/maintenance dose schedule in patients with advanced cancer. Clin Cancer Res 2004;10:7450 – 6.

27. Momota H, Nerio E, Holland EC. Perifosine inhibits multiple signaling pathways in glial progenitors and cooperates with temozolomide to arrest cell proliferation in gliomas *in vivo*. Cancer Res 2005;65: 7429 – 35.

28. Zhang S, Shen HM, Ong CN. Down-regulation of c-FLIP contributes to the sensitization effect of 3,3′-diindolylmethane on TRAIL-induced apoptosis in cancer cells. Mol Cancer Ther 2005;4:1972 – 81.

29. Gajate C, Mollinedo F. Edelfosine and perifosine induce selective apoptosis in multiple myeloma by recruitment of death receptors and downstream signaling molecules into lipid rafts. Blood 2007;109:711 – 9.

2007 AACR Annual Meeting
April 14-18, 2007
Los Angeles, CA

Print this Page for Your Records Close Window

Abstract Number: LB-348

Presentation Title: **Systemic therapy with tumor suppressor FUS1-nanoparticles for stage IV lung cancer**

Presentation Start/End Time: Tuesday, Apr 17, 2007, 1:00 PM - 5:00 PM

Location: Exhibit Hall, Los Angeles Convention Center

Author Block: *Charles Lu*, *Carmen A. Sepulveda*, *Lin Ji*, *Rajagopal Ramesh*, *Sean O'Connor*, *Gitanjali Jayachandran*, *Marshall E. Hicks*, *Reginald F. Munden*, *J. Jack Lee*, *Nancy S. Templeton*, *John D. McMannis*, *Jack A. Roth*. UT M.D. Anderson Cancer Ctr., Houston, TX, Baylor College of Medicine, Houston, TX

The tumor suppressor gene FUS1 is frequently inactivated early in the development of lung cancer. FUS1 mediates apoptosis in cancer cells but not normal cells through its interaction with Apaf1. We developed a DOTAP:cholesterol nanoparticle encapsulating a FUS1 expression plasmid that showed selective uptake by cancer cells compared to normal cells. In this clinical trial a DOTAP:cholesterol FUS1 nanoparticle was injected intravenously in stage IV lung cancer patients who had progressive disease after cisplatin combination chemotherapy based on preclinical data showing successful treatment of metastatic lung cancer in mouse xenograft models. Nanoparticle-DNA complexes were manufactured in GMP facilities to meet specifications of OD400, size, appearance, and transfection efficiency. Patients received doses ranging from 0.01-0.03mg/kg at 3 week intervals for a maximum of 6 doses. Dexamethasone and diphenhydramine premedications were added and eliminated the only clinically significant toxicity of fever. To date 13 patients have been entered on the study at three different doses (0.1, 0.02, 0.03mg/kg). All patients could be evaluated for the primary endpoint of toxicity, and with pretreatment, there was no significant drug related toxicity. Four patients received only one dose because of rapidly progressing disease at a site requiring local treatment. Eight patients received two or more doses and can be evaluated for response with 3 patients achieving stable disease (3 - 7 months) and 5 patients progressing. Median survival time for all patients is 14.6 months which compares favorably to the published 7 months median survival for second line chemotherapy and 4 months for best supportive care for non-small cell lung cancer. Actuarial survival at 12 months was 55%. A maximum tolerated dose (MTD) has not been reached. Pre and 24 hour posttreatment tumor biopsies were obtained from 3 patients. A quantitative real time reverse transcriptase PCR (RT-PCR) analysis using a plasmid FUS1 sequence-specific probe was performed on samples blinded to time of biopsy. A high level of plasmid FUS1 expression was detected in all 3 posttreatment samples but not in three pretreatment samples and negative controls by RT-PCR. DOTAP:cholesterol FUS1 nanoparticles can be safely administered intravenously in patients with stage IV lung cancer. Gene expression is detected in tumors, and there is an indication of anti-tumor activity.

2007 AACR Annual Meeting
April 14-18, 2007
Los Angeles, CA

Copyright © 2007 American Association for Cancer Research. All rights reserved.
Citation Format: {Authors.} {Abstract Title} [abstract]. In: American Association for Cancer Research Annual Meeting: Proceedings; 2007 Apr 14-18; Los Angeles, CA. Philadelphia (PA): AACR; 2007. Abstract nr {abstract number}

OASIS - Online Abstract Submission and Invitation System™ ©1996-2008, Coe-Truman Technologies, Inc.

Journal of Experimental Therapeutics and Oncology, Vol. 6, pp. 183-192
Reprints available directly from the publisher
Photocopying permitted by license only

© 2007 Old City Publishing, Inc.
Published by license under the OCP Science imprint,
a member of the Old City Publishing Group.

Simultaneous inhibition of COX-2 and 5-LOX activities augments growth arrest and death of premalignant and malignant human lung cell lines

Claudia P. Schroeder[1], Peiying Yang[2], Robert A. Newman[2], Reuben Lotan[1]

[1] Department of Thoracic, Head and Neck Medical Oncology

[2] Department of Experimental Therapeutics; The University of Texas M. D. Anderson Cancer Center
Houston, TX 77030, USA

Correspondence to: Reuben Lotan, Ph.D., MDACC, 1515 Holcombe Boulevard Box 432, Houston, TX 77030 USA
Telephone: +1.713.792.8467. Fax: +1.713.745.5656. E-mail: rlotan@mdanderson.org

(Received November 3, 2006; accepted November 6, 2006; Sponsored by Robert A. Newman)

The arachidonic acid-metabolizing enzymes cyclooxygenase-2 (COX-2) or 5-lipoxygenase (5-LOX) are overexpressed during lung carcinogenesis and their end products (e.g.; PGE_2, 5-HETE, and LTB_4) have been implicated in tumor development. Recently, COX-2 inhibitors (e.g.; celecoxib) and 5-LOX inhibitors (e.g.; MK886 and REV5901) used as single agents have shown promising activities in the treatment and chemoprevention of cancer. However, little is known about the effects of combinations of these inhibitors. We found that simultaneous treatment of premalignant and malignant human lung cell lines with celecoxib, MK886, and REV5901 is more potent in growth suppression and induction of cell death than single or dual combination of these agents. However, their sensitivity to the inhibitors was not directly associated with the expression of COX-2, 5-LOX, or 5-LOX-activating protein (FLAP), but correlated with the production of corresponding metabolites. Furthermore, partial protection of cell death was observed when PGE_2 and/or 5-HETE was added to cell cultures treated with celecoxib, MK886, and REV5901 simultaneously. Our data indicate that a triple drug combination of distinct inhibitors of the eicosanoid metabolism at clinically feasible concentrations were more effective than each agent alone suggesting further investigations.

Key words: COX-2, 5-LOX, MK886, REV5901, celecoxib, human lung cell lines

INTRODUCTION

Lung cancer is the leading cause of cancer-related death in the United States with a less than 15% five-year survival rate, which is only a small improvement over the past several decades[1]. Therefore, the discovery of new strategies and potential agents in order to control the development and progression of human lung cancer is urgently needed.

It has been known that a higher rate of the eicosanoid metabolism, involving the breakdown of arachidonic acid (AA) to multiple endproducts by cyclooxygenases (COXs) and lipoxygenases (LOXs), plays a role in most human epithelial cancers including lung cancer[2-4]. For instance, inducible COX-2 is a known indicator for pathological conditions such as inflammation and cancer, especially those of non-small cell lung cancer histology, which has also been linked to a poorer prognosis[5-7]. Moreover, COX-2 is frequently upregulated in preneoplastic lesions or atypical bronchiolar metaplasia compared with normal lung[8]. As a result, the excessive production of COX-2-derived metabolites, mainly prostaglandin E_2 (PGE_2), stimulates proliferation, reduces apoptosis, and promotes angiogenesis[9,10]. Likewise, abnormalities in the 5-LOX pathway occur frequently during neoplastic transformation of lung tissue involving over-expression of 5-LOX and increased levels of its products, 5-hydroxyeicosatetraenoic acid (5-HETE) and leukotriene B_4 ($LT)B_4$, that have been associated

with proliferative, anti-apoptotic, and angiogenic properties[9,11,12]. Consequently, inhibition of COX-2 and 5-LOX activities suppressed growth and induced apoptosis in a variety of cancer cell lines and preclinical models[13-21]. Moreover, celecoxib and various 5-LOX inhibitors (e.g.; MK886) prevented lung tumorigenesis in carcinogen-induced mouse models[2,15,16]. Interestingly, it has been reported that celecoxib at clinically feasible concentrations not only inhibits the synthesis of PGE_2 but is also capable of modulating various metabolites generated from the LOX pathway, especially 5-HETE and LTB_4 metabolites which derive from the 5-LOX cascade[18,22,23]. Because a dynamic transition between the COX and LOX pathway may play a role in tumor development and progression, it is plausible to target both enzymatic pathways by using COX in combination with LOX inhibitors[20,23,24].

The present study examines the effects of the selective COX-2 inhibitor celecoxib in combination with the selective 5-LOX inhibitor REV5901, and the 5-LOX-activating protein (FLAP) inhibitor MK886 on suppression of cell growth of premalignant and malignant human lung cell lines.

MATERIAL AND METHODS

Reagents and materials

Dulbecco's modified eagle's minimal essential medium (DMEM), keratinocyte serum-free medium (SFM), phosphate-buffered saline (PBS), and trypsin were purchased from Gibco™ Invitrogen Corporation (Carlsbad, CA). Fetal bovine serum (FBS) was from HyClone Laboratories, Inc. (Logan, UT). The COX-2-inhibitor celecoxib (4-[5-(4-methylphenyl)-3-(trifluoromethyl)-1H-pyrazol-1-yl] benzenesulfonamide) was obtained from GD Searle & Co (Chicago, IL), the FLAP-inhibitor MK866 (1-[(4-chlorophenzyl)methyl]-3-[(1,1-dimethylethyl)thio]-α,α-dimethyl-5-(1-methylethyl-1H-indole-2-propanoic acid, sodium salt) was from Biomol Research Laboratories (Plymouth Meeting, PA) and the 5-LOX-inhibitor REV5901 (α-pentyl-3-(2-quinolinylmethoxy)-benzenemethanol) was purchased from Cayman Chemicals Co (Ann Arbor, MI). Bovine serum albumin, dimethyl sulfoxide (DMSO), ethylene diamine tetra acetic acid, and sodium dodecyl sulfate (SDS) were from Sigma Chemical Co. (St. Louis, MO). All culture plastic ware was purchased from BD Bioscience Labware (Bedford, MA). The deuterium-labeled eicosanoids PGE_2, LTB_4, and 5-HETE used as internal standard for ESI-LC/MS/MS analyses were purchased from Cayman Chemical Co. (Ann Arbor, MI).

Cell culture

The cell lines used in this study represent an in vitro model of human lung carcinogenesis including BEAS-2B, bronchial epithelial cells immortalized using SV40/adenovirus-12 hybrid T-antigen, and transformed (1198) or tumorigenic (1170-I) cells derived from BEAS-2B by exposure to cigarette smoke condensate (CSC) in vivo after transplantation into nude mice[25]. Immortalized 1799 cells were derived from BEAS-2B by a similar in vivo transplantation without exposure to CSC[26]. These cell lines were obtained from Dr. Klein-Szanto (Fox Chase Cancer Center, Philadelphia, PA). The non-small cell lung cancer cell lines A549 was purchased from the American Type Cell Culture Collection (ATCC; Rockville, MD). BEAS-2B and 1799 cells were grown in keratinocyte-SFM supplemented with EGF (2.5 µg) and bovine pituitary extract (25 µg) at 37°C in a humidified atmosphere of 95% air and 5% CO_2. The cell lines 1198 and 1170-I were maintained in keratinocyte-SFM containing 3% FBS and bovine pituitary extract (25 µg). A549 cells were cultured in a mixture of DMEM/Ham's F12 medium (1:1, v/v) supplemented with 5% FBS.

Cell growth studies, apoptosis

After trypsinization, 6 x 10^3 cells/well were seeded into 96-well culture plates, allowed to adhere overnight prior to treatment with celecoxib, MK886, REV5901, and their combinations at different concentrations for 72 hrs. Control cultures were grown in medium containing DMSO (0.02%, v/v). Cell number was determined by the sulforhodamine B (SRB) assay using an automated plate reader MR5000 (Dynatech Laboratories Inc., Chantilly, VA)[27]. The inhibition of cell growth was calculated from the equation, % inhibition = (1-OD*t*/OD*c*) x 100%, whereas OD*t* and OD*c* represent optical densities of treated and control cultures, respectively. Concentration response curves were plotted and concentrations of the agents used in this study resulting in 50% growth inhibition (IC_{50}) were calculated by interpolation. The extent of apoptotic and necrotic cells was determined by double staining with Annexin V-FITC and propidium iodide using Annexin-V-FLUOS staining kit from Roche Applied Science (Indianapolis, IN). The cells were seeded into 100 x 20 mm tissue culture dish and allowed to adhere overnight before incubation with the COX and LOX inhibitors. Control cultures were treated with medium containing solvent vehicle only (0.02%, v/v DMSO). After 72 hrs, detached and adherent cells were collected, washed, and stained according to the manufacturer's instructions. Data analysis was performed on a FACSCalibur cytometer utilizing the CellQuest™ software (Becton Dickinson,

San Jose, CA). Three independent experiments were conducted.

Western blot analysis

Samples containing 50 µg of total cellular protein mixed in sample buffer (0.5 M Tris, pH 6.8; 0.3% glycerol; 0.03% β-mercaptoethanol; 10% SDS; 0.001% bromphenolblue) were electrophoretically separated through 10% SDS-polyacrylamide slab gels followed by transfer onto Trans-Blot nitrocellulose membranes (Bio-Rad Laboratories, Hercules, CA). Briefly, cell monolayers were washed twice with ice-cold PBS and collected in lysis buffer containing 150 mM NaCl; 0.02% NaN_3; 2% Igepal CA-630; 0.5% sodium deoxycholate; 0.2% SDS, and 50 mM Tris-HCl, pH 8.0 supplemented with protease inhibitors leupeptin (1 µg/ml), aprotinin (1 µg/ml), pepstatin (0.5 µg/ml), and phenylmethylsulfonyl fluoride (100 µg/ml). Protein concentrations were measured using Bio-Rad protein assay (Bio-Rad Laboratories, Hercules, CA). After blocking with 3% nonfat dry milk solution in 0.1% (w/v) Tween 20 in PBS, the membranes were probed with anti-human antibodies at appropriate dilutions against COX-2 (Oxford Biomedical Research Inc., Oxford, MI), 5-LOX (BD Transduction Lab, Lexington, KY), and FLAP (Santa Cruz Biotechnology Inc., CA). Antibody binding was detected with horseradish peroxidase-linked second antibody and enhanced chemiluminescence (Amersham Biosciences Corp., Piscataway, NJ). Loading and transferring control was confirmed by probing the membranes with anti-β-actin antibody (Sigma Chemical Co, St. Louis, MO).

Measurement of PGE2, 5-HETE, and LTB4

Electrospray ionization liquid chromatography tandem mass spectrometry (ESI-LC/MS/MS) was performed to quantify eicosanoid metabolites as described elsewhere[28,29]. Briefly, an aliquot of 10 µl of 10% BHT and 10 µl of a mixture of internal standards (PGE_2-d_4, 5-HETE-d_8, LTB_4) was added to 1 ml of culture medium. Eicosanoids were eluted with 1 ml of methanol and evaporated under a stream of nitrogen. Samples were reconstituted in 100 µl methanol: 10 mM ammonium acetate buffer (v/v, 70:30, pH 8.5) prior to analysis. ESI-LC/MS/MS was performed using a Quattro Ultima tandem mass spectrometer (Micromass, Beverly, MA) equipped with an Agilent HP1100 binary pump HPLC inlet. Metabolites were separated using a Luna 3 µm phenyl hexyl 2 x 150 mm analytical column (Phenomenex, Torrance, CA). The mobile phase consisted of 10 mM ammonium acetate (pH 8.5) and methanol. The flow rate was 250 µl/min with a column temperature maintained at 50°C and an injection volume of 25 µl. Fragmentation of all compounds was performed using argon as the collision gas at a collision cell pressure of 2.1 x 10^{-3} Torr. The results were expressed as nanograms of each eicosanoid per 10^6 cells. To normalize data, the cell number was measured with an electronic particle counter (Coulter, Hialeah, FL). Results shown represent mean values of at least two independent experiments.

Statistics

The results on growth inhibition induced by combinations of COX-2 and 5-LOX inhibitors represent mean values ± standard deviation (SD) of three independent experiments each performed in quadruplicates. Significance of difference between samples related to control cultures was determined using Student's paired *t*-test with probability (*P*) values less than 0.05 regarded as significant.

RESULTS

Production of PGE2, 5-HETE, and LTB4 and expression of the corresponding AA-metabolizing enzymes in premalignant and malignant human lung cell lines

To determine whether the AA metabolism is altered in cell lines representing an in vitro model of human lung carcinogenesis, we analyzed their production of PGE_2, 5-HETE, and LTB_4 using ESI-LC/MS/MS[28,29]. The endogenous PGE_2 levels in BEAS-2B and 1198 cell lines were very low (0.2 and 0.04 ng/10^6 cells, respectively), whereas A549 cancer cells produced 2.7 ng PGE_2/10^6 cells (Figure 1A). The synthesis of the 5-LOX metabolites 5-HETE and LTB_4 was low in BEAS-2B cells but higher and to a comparable amount in 1198 and A549 cell lines. We then determined the expression levels of COX-2, FLAP, and 5-LOX using immunoblotting. Figure 1B indicates that the enzyme expression showed a correlation with the production of the corresponding COX-2 and 5-LOX metabolites. For example, COX-2 was undetectable in premalignant bronchial epithelial cell lines, however, was strongly expressed in A549 cancer cells. FLAP was detected in all premalignant cell lines with a lower expression in BEAS-2B and a higher level in A549 cells. 5-LOX was expressed in 1198 and A549 cells compared to a faint detection in BEAS-2B, 1799, and 1170-I cell lines.

Effect of celecoxib, MK886, and REV5901 on growth arrest of premalignant and malignant human lung cell lines

Because the production of PGE_2, 5-HETE, and LTB_4 correlated with the expression levels of the

corresponding enzymes, we asked whether the cell lines used in this study exhibit differential sensitivities to the selective COX-2 inhibitor celecoxib, the selective 5-LOX-inhibitor REV5901 and the FLAP-inhibitor MK886 (chemical structures, Figure 2). We found a dose-dependent growth inhibition after 72 hrs of incubation with IC_{50} values ranging from 15.9 to 30.4 μM for celecoxib, 0.3 to 1.7 μM for MK886, and 6.6 to 14.4 μM for REV5901 (Figure 3). Premalignant bronchial epithelial cell lines were more sensitive to the growth-inhibitory effects of celecoxib, MK886, or REV590 than A549 cancer cells as indicative as 1.5 to 2-fold lower IC_{50} values. Furthermore, MK886 that indirectly inhibits 5-LOX activity by blocking FLAP, was approximately 10-fold more potent on a molar basis compared to the selective enzyme inhibitors celecoxib or REV5901.

Simultaneous treatment with celecoxib, MK886, and REV5901 augments growth inhibition compared to treatment with one or two agents

Based on previous studies, which suggest a fine balance between the COX and LOX pathway in tumor cells, we hypothesized that simultaneous inhibition of the AA metabolism by using COX-2 in combination with 5-LOX inhibitors is more effective in suppression of cell growth than each of the inhibitors alone. Therefore, we treated 1198 premalignant and A549 malignant lung cell lines with pharmacologically achievable concentrations of celecoxib (5 μM), MK886 (1 μM), and REV5901 (5 μM) used as single agents and in combinations for 72 hrs before determination of cell numbers by the SRB method. Figure 4 shows that simultaneous treatment of the cells with all three inhibitors was more effective than incubation of the compounds alone or in dual combination. For example, incubation of 1198 and A549 cells with a combination of celecoxib, MK886, and REV5901 suppressed their growth by 58% and 43%, respectively compared to untreated cultures ($P<0.05$). Besides, dual inhibition of COX-2 and 5-LOX enzymes through celecoxib and REV5901 induced a significant growth arrest by 29% and 37% in 1198 and A549 cell lines, respectively ($P<0.05$).

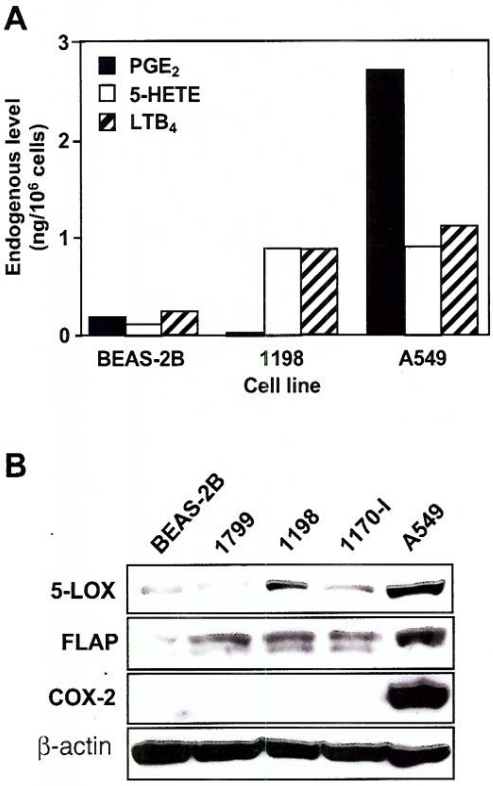
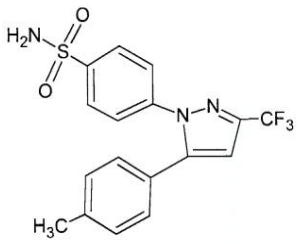


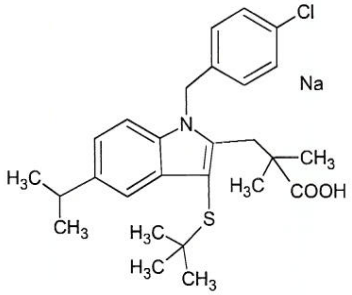
Figure 1. (A) Production of PGE_2, 5-HETE and LTB_4, and (B) expression of 5-LOX, FLAP, and COX-2 in various cell lines representing an in vitro model of human lung carcinogenesis. Cells were treated in standard medium for 72 hrs prior to analysis by ESI-LC/MS/MS or separation of a total of 50 μg of protein per sample using 10% SDS-polyacrylamid gel electrophoresis as described under materials and methods. For the measurement of eicosanoid metabolites, culture medium of three representative cell lines (BEAS-2B, 1198, and A549) was processed. The immunoblot was probed with antibodies specific for COX-2, 5-LOX, and FLAP. β-actin served as loading control.

Cell death is increased by combinations of COX-2 and 5-LOX inhibitors and is partially prevented by PGE2 and 5-HETE

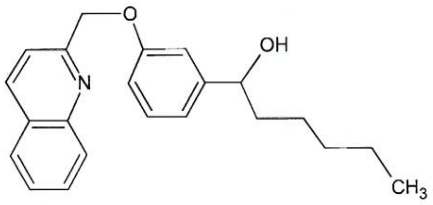
To determine whether induction of apoptosis contributes to the growth-inhibitory activity of COX-2 and 5-LOX inhibitors, we performed double staining of the cells with Annexin V-FITC and propidium iodide followed by flow cytometric analysis. Figure 5 indicates that incubation of 1198 premalignant and A549 malignant cell lines with a triple drug combination of celecoxib (5 μM), MK886 (1 μM), and REV5901 (5 and 7.5 μM, respectively) induced 74.4% and 23.7% cell death, including apoptotic and necrotic cellular fraction, respectively. Addition of exogenous PGE_2 (0.5 μg/ml) and/or 5-HETE (100 nM) to cultures treated with the triple drug combination partially reduced the number of dead cells. For example, 1198



Celecoxib
4-[5-(4-Methylphenyl)-3-(trifluoromethyl)-1H-pyrazol-1-yl] benzenesulfonamide



MK886
1-[(4-Chlorophenzyl)methyl]-3-[(1,1-dimethylethyl)thio]-α,α-dimethyl-5-(1-methylethyl-1H-indole-2-propanoic acid, sodium salt



REV5901
α-Pentyl-3-(2-quinolinylmethoxy)-benzenemethanol

Figure 2. Chemical structure of the selective COX-2 inhibitor celecoxib (4-[5-(4-methylphenyl)-3-(trifluoromethyl)-1H-pyrazol-1-yl]benzenesulfonamide, the FLAP inhibitor **MK886** (1[(4-Chlorophenzyl)methyl]-3-[(1,1-dimethyl)thio]-α,α-dimethyl)-5-(1-methylethyl)-1H-indole-2-propanoic acid, sodium salt), and the selective 5-LOX inhibitor **REV5901** (α-Pentyl-3-(2-quinolinylmethoxy)-benzenemethanol).

cell death induced by a combination of 5 μM celecoxib, 1 μM MK886, and 5 μM REV5901 was partially protected by 56% in the presence of 100 nM 5-HETE (Figure 5A). Moreover, A549 growth arrest was protected by 33% (from 23.7% to 7.9%) when both, PGE_2 and 5-HETE, were added to a combination of 5 μM celecoxib, 1 μM MK886, and 7.5 μM REV5901 (Figure 5B).

DISCUSSION

The deregulation of the AA metabolism in epithelial cancers including lung tumors represents an early sign of malignant transformation[3,9,10]. Hence, its metabolizing enzymes and end products provide promising targets for lung cancer chemoprevention and/or therapy. Indeed, inhibitors of the COX and LOX

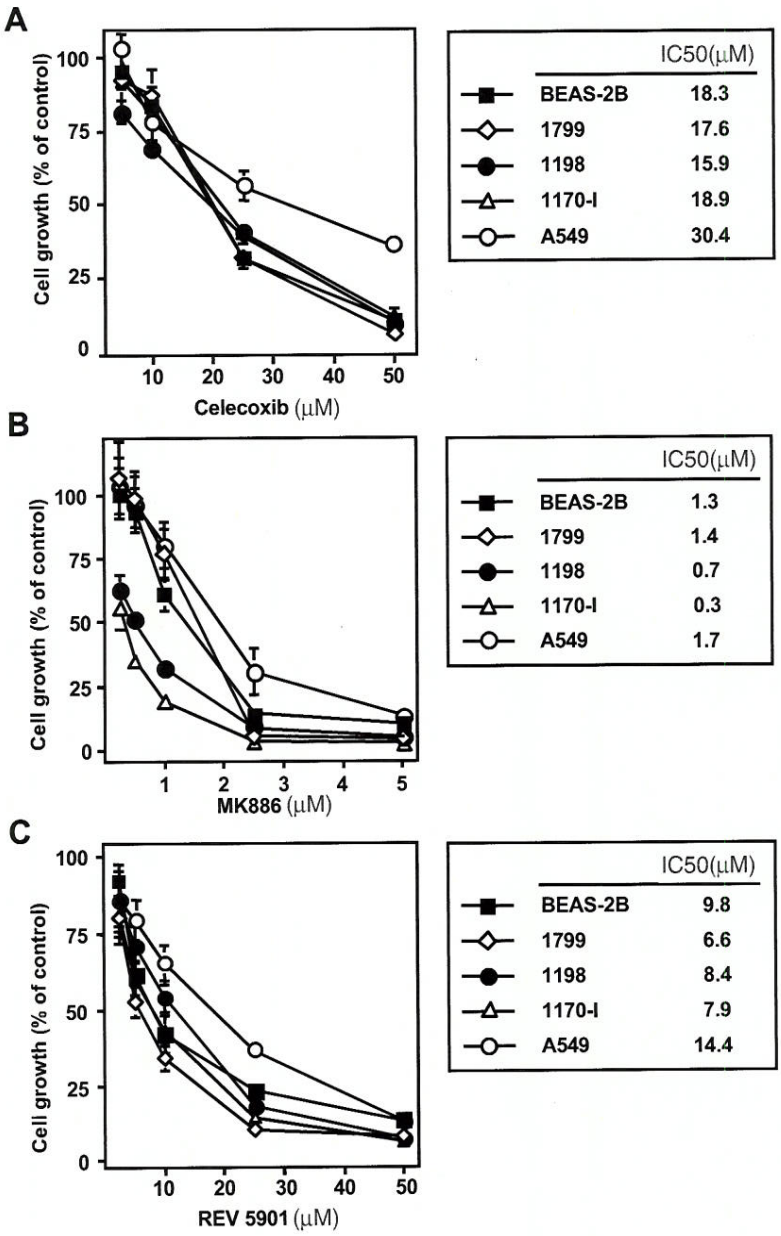


Figure 3. Effects of (A) celecoxib, (B) MK886, or (C) REV5901 on growth suppression of various cell lines representing an in vitro model of human lung carcinogenesis. Cell lines were treated with the inhibitors for 72 hrs before determination of cell number using the SRB assay as described in materials and methods. Concentrations required for the determination of IC50 (μM) values (right panels) were obtained by interpolation of concentration response curves. Results represent mean ± SD of three independent experiments with no drug added serving as control and expressed as 100% cell growth.

pathway have demonstrated anti-tumor and chemopreventive activity in lung cancer cells[13-16,21,22]. However, preclinical and clinical studies that have targeted just one metabolic pathway by using for instance only a COX-2 inhibitor (e.g.; celecoxib) showed modest impact[2,18,30]. It has also been suggested that blocking one metabolic cascade can lead to an enhancement of products generated from another

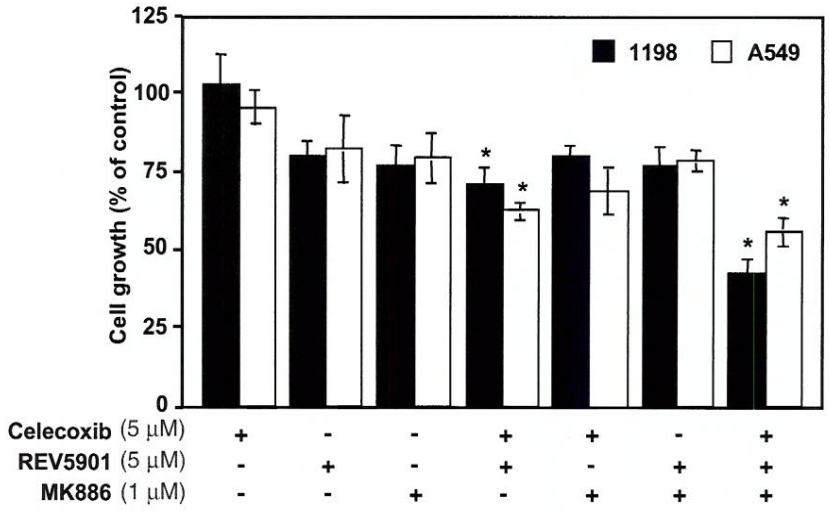


Figure 4. Effects of celecoxib (5 μM), MK886 (1 μM), REV5901 (5 μM), and their combinations on growth of 1198 premalignant (full bars) and A549 malignant (open bars) lung cell lines. The cells were seeded in 96-well culture plates and allowed to adhere overnight before treatment with the inhibitors. Changes in cell growth was determined by the SRB assay after 72 hrs of incubation. Results are expressed as mean ± SD (n=3) with no inhibitor added serving as control and expressed as 100% growth. **P*<0.05, vs untreated cells determined using Student's paired *t*-test.

cascade by re-directing the breakdown of the substrate AA. Specifically, others and we have demonstrated that suppression of PGE_2 by celecoxib at clinically relevant concentrations was accompanied by an increase of multiple 5-LOX metabolites, most significantly 5-HETE or LTB_4[18,22-24]. Therefore, it was of considerable interest to investigate whether a combination of inhibitors of the COX-2 and 5-LOX pathway can suppress growth of human lung cell lines more efficiently than inhibition of either pathway alone.

In this study, we show that a combination of clinically relevant concentrations of the COX-2 inhibitor celecoxib with the 5-LOX inhibitors REV5901, and MK886 was more effective in suppression of growth and induction of death than each of the agents alone or in dual combination. Furthermore, dual inhibition of COX-2 and 5-LOX activities by celecoxib and REV5901 produced a significant greater response than treatment with the individual inhibitors alone. We observed approximately 10-fold greater growth-inhibitory effects on a molar basis with the FLAP inhibitor MK886 than what was achieved with the selective enzyme inhibitors celecoxib or REV5901. MK886 inhibits the translocation of 5-LOX by binding to the active site of FLAP, which is required for the enzymatic activity of 5-LOX[31]. It has also been reported to induce apoptosis independently of both 5-LOX and FLAP[32]. In agreement with previous studies on various type of cancer cell lines, we obtained no direct correlation between the expression status of COX-2, FLAP or 5-LOX and the growth-inhibitory activity of celecoxib, MK886 or REV5901, respectively in premalignant and malignant lung cell lines[17,18,21]. However, the expression levels of COX-2, 5-LOX and FLAP in these cells correlated with the production of their major metabolites PGE_2, 5-HETE, and LTB_4, which increased with the degree of malignancy implicating a role in lung cancer development. Numerous studies have demonstrated that PGE_2 is markedly suppressed by celecoxib at concentrations below 5 μM in cell lines expressing the target enzyme COX-2[18,20,23,24,28]. Likewise, inhibition of 5-LOX activity by MK886 completely blocked the production of 5-HETE in human prostate cancer cells and addition of exogenous 5-HETE protected cells from undergoing apoptosis[14]. On the other hand, COX-2 or 5-LOX inhibitors induce apoptosis in cell lines, which lack the target enzymes, suggesting mechanism(s) unrelated to the suppression of the enzyme activity[18,19,21]. However, our data implicate that suppression of the 5-LOX activity is important for induction of cell death in 1198 and A549 cell lines based on partial protection by exogenous addition of 5-HETE to a triple drug combination of COX-2 and 5-LOX inhibitors compared to cells treated identically

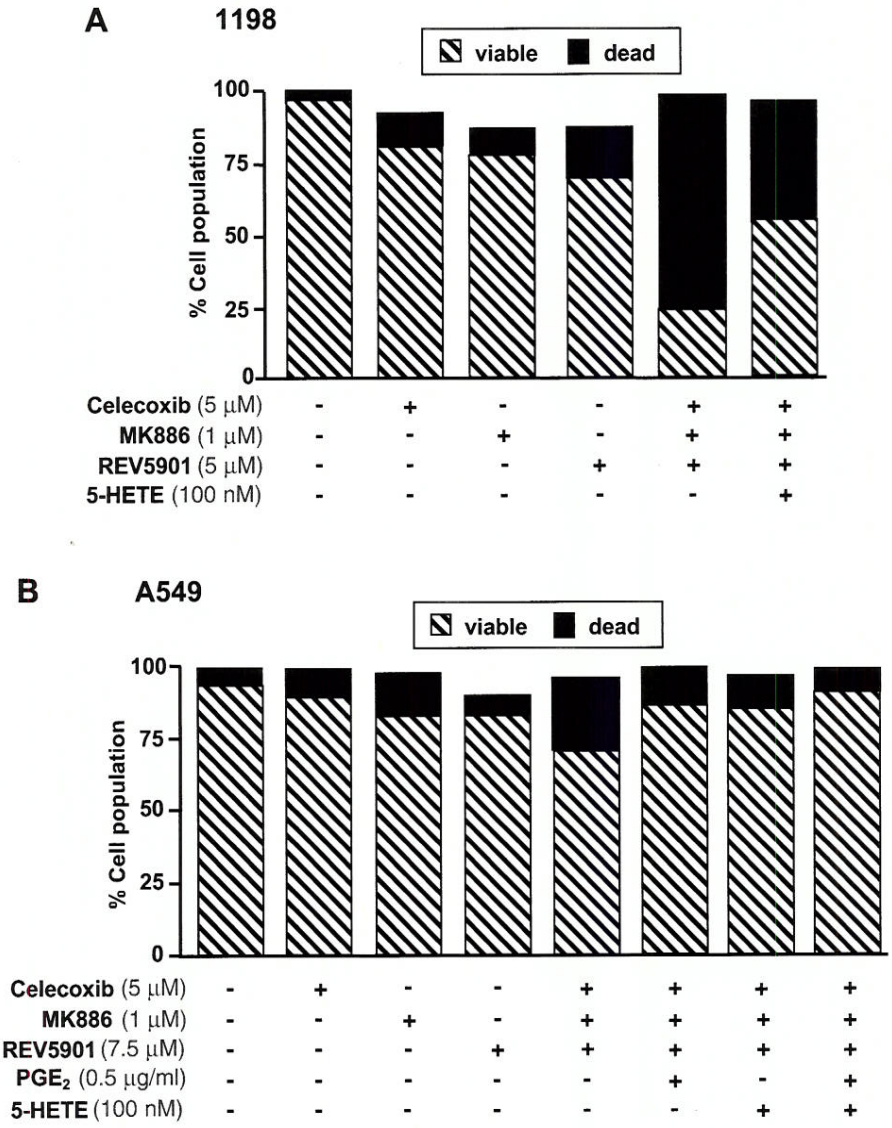


Figure 5. Induction of cell death by celecoxib (5 μM), MK886 (1 μM), REV5901 (5, and 7.5 μM, respectively) alone or in combination and the effects of PGE_2 (0.5 μg/ml), and/or 5-HETE (100 nM) in (A) 1198 and (B) A549 cell lines. The cells were treated with the inhibitors, and/or PGE_2, and 5-HETE for 72 hrs before collection of detached and adherent cells and studied for cell surface Annexin V binding to phosphatidylserin by flow cytometry. Control cultures were treated with medium containing solvent vehicle only (0.02% v/v DMSO). Data shown are representative of three independent experiments.

but without the 5-LOX metabolite. In A549 cells, which express both enzymes COX-2 and 5-LOX, exogenous PGE_2 was also able to rescue some of the cells from death similarly to the effect of 5-HETE while the combination of PGE_2 and 5-HETE in addition to the triple drug treatment was even more effective in preventing cell death than each of the AA metabolites alone. These findings indicate that the COX-2 and 5-LOX inhibitors induced cell death at least in part through suppression of the production of 5-HETE, PGE_2, or both. Moreover, we found that 1198 premalignant cells were more sensitive than A549 malignant cells suggesting that inhibitors of the AA metabolism might be more effective in lung cancer

prevention than in therapy. In fact, Rioux et al. have reported that a combination of the 5-LOX inhibitor A-79175 with the COX inhibitor acetylsalicylic acid reduced tumor multiplicity by 87%, which was the most effective preventive intervention compared to the inhibition of either pathway alone using a mice model of lung carcinogenesis[16].

In conclusion, combinations of low doses of biochemical inhibitors targeting related AA-metabolizing pathways support a rational approach in lung cancer prevention and therapy that warrant further investigations.

ACKNOWLEDGEMENTS

This work was supported by a grant from the National Cancer Institute (PO1 CA98144), and the BESCT Lung Cancer Program from the Department of Defense (DAMD17-01-1-0689-2).

REFERENCES

1. Jemal A, Murray T, Ward E, Samuels A, Tiwari RC, Ghafoor A, et al. Cancer statistics, 2005. *CA Cancer J Clin* 55:10-30, 2005.
2. Bunn PA Jr, Keith RL. The future of cyclooxygenase-2 inhibitors and other inhibitors of the eicosanoid signal pathway in the prevention and therapy of lung cancer. *Clin Lung Cancer* 3:271-277, 2002.
3. Laskin JJ, Sandler AB. The importance of the eicosanoid pathway in lung cancer. *Lung Cancer* 41 Suppl. 1:S73-79, 2003.
4. Sharma S, Yang SC, Zhu L, Reckamp K, Gardner B, Baratelli F, et al. Tumor cyclooxygenase-2/prostaglandin E2-dependent promotion of FOXP3 expression and CD4+ CD25+ T regulatory cell activities in lung cancer. *Cancer Res* 65(12):5211-5220, 2005.
5. Hida T, Yatabe Y, Achiwa H, Muramatsu H, Kozaki K, Nakamura S, et al. Increased expression of cyclooxygenase 2 occurs frequently in human lung cancers, specifically in adenocarcinomas. *Cancer Res* 58:3761-3764, 1998.
6. Wolff H, Saukkonen K, Anttila S, Karjalainen A, Vainio H, Ristimaki A. Expression of cyclooxygenase-2 in human lung carcinoma. *Cancer Res* 58:4997-5001, 1998.
7. Khuri FR, Wu H, Lee JJ, Kemp BL, Lotan R, Lippman SM, et al. Cyclooxygenase-2 overexpression is a marker of poor prognosis in stage I non-small cell lung cancer. *Clin Cancer Res* 7:861-867, 2001.
8. Hosomi Y, Yokose T, Hirose Y, Nakajima R, Nagai K, Nishiwaki Y, et al. Increased cyclooxygenase 2 (COX-2) expression occurs frequently in precursor lesions of human adenocarcinoma of the lung. *Lung Cancer* 30:73-81, 2000.
9. Funk CD. Prostaglandins and leukotriens: advances in eicosanoid biology. *Science* 294:1871-1875, 2001.
10. Wang D, Dubois RN. Prostaglandins and cancer. *Gut* 55:115-122, 2006.
11. Tang DG, Chen YQ, Honn KV. Arachidonate lipoxygenase as essential regulators of cell survival and apoptosis. *Proc Natl Acad Sci USA* 93:5241-5246, 1996.
12. Romano M, Claria J. Cyclooxygenase-2 and 5-lipoxygenase converging functions on cell proliferation and tumor angiogenesis: implications for cancer therapy. *FASEB J* 17:1986-1995, 2003.
13. Avis IM, Jett M, Boyle T, Vos MD, Moody T, Treston AM, et al. Growth control of lung cancer by interruption of 5-lipoxygenase-mediated growth factor signaling. *J Clin Invest* 97:806-813, 1996.
14. Ghosh J, Myers CE. Inhibition of arachidonate 5-lipoxygenase triggers massive apoptosis in human prostate cancer cells. *Proc Natl Acad Sci USA* 95:13182-13187, 1998.
15. Moody TW, Leyton J, Martinez A, Hong S, Malkinson A, Mulshine JL. Lipoxygenase inhibitors prevent lung carcinogenesis and inhibit non-small cell lung cancer growth. *Exp Lung Res* 24:617-628, 1998.
16. Rioux N, Castonguay A. Inhibitors of lipoxygenase: a new class of cancer chemopreventive agents. *Carcinogenesis* 19:1393-1400, 1998.
17. Hong SH, Avis I, Vos MD, Martinez A, Treston AM, Mulshine JL. Relationship of arachidonic acid metabolizing enzyme expression in epithelial cell lines to the growth effects of selective biochemical inhibitors. *Cancer Res* 59:2223-2228, 1999.
18. Schroeder CP, Yang P, Newman RA, Lotan R. Eicosanoid metabolism in squamous cell carcinoma cell lines derived from primary and metastatic head and neck cancer and its modulation by celecoxib. *Cancer Biol Ther* 9:29-34, 2004.
19. Stika J, Vondrácek J, Hofmanová J, Simek V, Kozubík A. MK-886 enhances tumor necrosis factor-α-induced differentiation and apoptosis. *Cancer Lett* 215:129-140, 2004.
20. Gregor JI, Kilian M, Heukamp I, Kiewert C, Kristiansen G, Schimke I, et al. Effects of selective COX-2 and 5-LOX inhibition on prostaglandin and leukotriene synthesis in ductal pancreatic cancer in syrian hamster. *Prostaglandins Leuk Essent Fatty Acids* 73:89-97, 2005.
21. Sun SY, Schroeder CP, Yue P, Lotan D, Hong WK, Lotan R. Enhanced growth inhibition and apoptosis induction in NSCLC cell lines by combination of celecoxib and 4HPR at clinically relevant concentrations. *Cancer Biol Ther* 4:407-413, 2005.
22. Mao JT, Tsu IH, Dubinett SM, Adams B, Sarafian T, Baratelli F, et al. Modulation of pulmonary leukotriene B4 production by cyclooxygenase-2 inhibitors and lipopolysaccharide. *Clin Cancer Res* 10:6872-6878, 2004.
23. Ye YN, Wu WK, Shin VY, Bruce IC, Wong BC, Cho CH. Dual inhibition of 5-LOX and COX-2 suppresses colon cancer formation promoted by cigarette smoke. *Carcinogenesis* 26:827-834, 2005.
24. Li N, Sood S, Wang S, Fang M, Wang P, Sun Z, et al. Overexpression of 5-lipoxygenase and cyclooxygenase 2 in hamster and human oral cancer and chemopreventive effects of zileuton and celecoxib. *Clin Cancer Res* 11:2089-2096, 2005.
25. Klein-Szanto AJ, Iizasa T, Momiki S, Garcia-Palazzo I, Caamano J, Metcalf R, et al. A tobacco-specific N-nitrosamine or cigarette smoke condensate causes neoplastic transformation of xenotransplanted human bronchial epithelial cells. *Proc Natl Acad Sci* USA 89:6693-6697, 1992.
26. Reddel RR, Ke Y, Gerwin BI, McMenamin MG, Lechner JF, Su RT, et al. Transformation of human bronchial epithelial cells by infection with SV40 or adenovirus-12 SV40 hybrid virus, or transfection via strontium phosphate coprecipitation with a plasmid containing SV40 early region genes. *Cancer Res* 48:1904-1909, 1988.

27. Skehan P, Storeng R, Scudiero D, Monks A, McMahon J, Vistica D, et al. New colorimetric cytotoxicity assay for anticancer-drug screening. *J. Natl Cancer Inst* 82: 1107-1112, 1990.

28. Kempen EC, Yang P, Felix E, Madden T, Newman RA. Simultaneous quantification of arachidonic acid metabolites in cultured tumor cells using high performance liquid: chromatography/electrospray ionization tandem mass spectrometry. *Anal Biochem* 297:183-190, 2001.

29. Yang P, Chan D, Felix E, Cartwright C, Menter DG, Madden T, Klein RD, Fischer SM, Newman RA. Formation and antiproliferative effect of prostaglandin E(3) from eicosapentaenoic acid in human lung cancer cells. *J Lipid Res* 45(6):1030-1039, 2004.

30. Lu S, Zhang X, Badawi AF, El-Sohemy A, Archer MC. Cyclooxygenase-2 inhibitor celecoxib inhibits promotion of mammary tumorigenesis in rats fed a high fat diet rich in n-6 polyunsaturated fatty acids. *Cancer Lett* 184:7-12, 2002.

31. Rouzer CA, Ford-Hutchinson AW, Morton HE, Gillard JW. MK886, a potent and specific leukotriene biosynthesis inhibitor blocks and reverses the membrane association of 5-lipoxygenase in ionophore-challenged leukocytes. *J Biol Chem* 265:1436-1442, 1990.

32. Datta K, Biswal SS, Kehrer JP. The 5-lipoxygenase-activating protein (FLAP) inhibitor, MK886, induces apoptosis independently of FLAP. *Biochem J* 340:371-375, 1999.

ΔDNMT3B Variants Regulate DNA Methylation in a Promoter-Specific Manner

Jie Wang,[1,3] Manisha Bhutani,[1] Ashutosh K. Pathak,[1] Wenhua Lang,[1] Hening Ren,[1] Jaroslav Jelinek,[2] Rong He,[2] Lanlan Shen,[2] Jean-Pierre Issa,[2] and Li Mao[1]

Departments of [1]Thoracic/Head and Neck Medical Oncology and [2]Leukemia, The University of Texas M. D. Anderson Cancer Center, Houston, Texas and [3]Department of Oncology, Beijing Cancer Hospital, Beijing University School of Oncology, Beijing, China

Abstract

DNA methyltransferase 3B (DNMT3B) is critical in *de novo* DNA methylation during development and tumorigenesis. We recently reported the identification of a DNMT3B subfamily, ΔDNMT3B, which contains at least seven variants, resulting from alternative pre-mRNA splicing. *ΔDNMT3B*s are the predominant expression forms of *DNMT3B* in human lung cancer. A strong correlation was observed between the promoter methylation of *RASSF1A* gene but not *p16* gene (both frequently inactivated by promoter methylation in lung cancer) and expression of *ΔDNMT3B4* in primary lung cancer, suggesting a role of ΔDNMT3B in regulating promoter-specific methylation of common tumor suppressor genes in tumorigenesis. In this report, we provide first experimental evidence showing a direct involvement of ΔDNMT3B4 in regulating *RASSF1A* promoter methylation in human lung cancer cells. Knockdown of *ΔDNMT3B4* expression by small interfering RNA resulted in a rapid demethylation of *RASSF1A* promoter and reexpression of *RASSF1A* mRNA but had no effect on p16 promoter in the lung cancer cells. Conversely, normal bronchial epithelial cells with stably transfected *ΔDNMT3B4* gained an increased DNA methylation in *RASSF1A* promoter but not *p16* promoter. We conclude that promoter DNA methylation can be differentially regulated and ΔDNMT3Bs are involved in regulation of such promoter-specific *de novo* DNA methylation. [Cancer Res 2007;67(22): 10647–52]

Introduction

DNA methylation plays an essential role in the normal development of the mammalian embryo by regulating gene transcription through genomic imprinting, X chromosome inactivation, and genomic stability (1). It is believed that DNA methylation patterns in somatic cells are established during gametogenesis and early embryonic development via consecutive waves of demethylation and *de novo* methylation (2). The *DNA methyltransferase 3* (*DNMT3*) gene consists of *DNMT3A* and *DNMT3B* and is the major *de novo* DNA methyltransferase that preferentially methylates cytosine in CpG sites (3). Methylation in CpG-rich promoter regions may result in transcriptional silencing of the corresponding genes, which is a major mechanism by which tumor suppressor genes are inactivated in tumorigenesis (4).

DNMT3B contains 24 exons spanning ~47 kb of genomic DNA. Two alternative 5′ exons are used, but the same full-length DNMT3B protein (DNMT3B1 and DNMT3B2) is expected from both transcripts (5). Four additional transcriptional variants (*DNMT3B3, DNMT3B4, DNMT3B5*, and *DNMT3B6*) resulting from alternative pre-mRNA splicing have also been reported (5–7). Some of the variants may compete with each other, thereby resulting in even DNA hypomethylation (7). This possibility suggests a complex biological role of the *DNMT3B* variants. Increased expression of *DNMT3B* has been frequently observed in human cancer cell lines and primary tumors (3). However, an association between the expression level of *DNMT3B* and the promoter methylation status of tumor suppressor genes has not been established (8, 9). These data suggest that the regulation of DNA methylation of these promoters is complex.

ΔDNMT3B, a subfamily of *DNMT3B*, consists of at least seven transcriptional variants by alternative pre-mRNA splicing (10). In non–small cell lung cancer (NSCLC), *ΔDNMT3B* variants are the predominant forms of *DNMT3B* expression (10). We previously observed a strong and independent correlation between *ΔDNMT3B4* expression and DNA methylation of the *RASSF1A* promoter but not the *p16* promoter (11). This finding suggested that *ΔDNMT3B* variants are involved in the regulation of promoter methylation, possibly in a promoter-specific manner.

Materials and Methods

Cell lines. Human NSCLC lines H1299 and H358 were purchased from the American Type Culture Collection. The HBE1 cell line was a gift from Dr. John Minna (The University of Texas Southwest Medical Center, Dallas, TX).

RNA extraction and reverse transcription-PCR. We isolated total RNA from cells by using Tri-Reagent (Molecular Research Center) according to the manufacturer's instruction. The primers used for reverse transcription-PCR (RT-PCR) were described previously (10).

Methylation-specific PCR. One microgram of genomic DNA was used for bisulfite treatment to modify unmethylated cytosine residues, and the modified DNA was used for methylation-specific PCR (MSP) using methylation-specific and unmethylation-specific primers as described previously (10, 11). Unmodified DNA was used to test all the primer sets and we failed to observe any amplified DNA fragment in our experimental conditions.

Small interfering RNA and antisense RNA transfection. Small interfering RNA (siRNA) specifically targeted to the junction of exons 5 and 7 of *ΔDNMT3B* was designed and synthesized chemically (Ambion). Both annealed siRNA and corresponding oligonucleotides of single strands were used. The sequences were 5′-CACGCAACCAGAGAACAAGUU-3′ (sense) and 5′-CUUGUUCUCUGGUUGCGUGUU-3′ (antisense) for the target sequence 5′-AACACGCAACCAGAGAACAAG-3′. siRNA specifically targeting glyceraldehyde-3-phosphate dehydrogenase (*GAPDH*) or scramble siRNA was also obtained from Ambion to serve as controls.

Note: Supplementary data for this article are available at Cancer Research Online (http://cancerres.aacrjournals.org/).

J. Wang, M. Bhutani, and A.K. Pathak contributed equally to this work.

Requests for reprints: Li Mao, Department of Thoracic/Head and Neck Medical Oncology, The University of Texas M. D. Anderson Cancer Center, Box 437, Unit 432, Room FC9.3065, 1515 Holcombe Boulevard, Houston, TX 77030. Phone: 713-792-6363; Fax: 713-792-1220; E-mail: lmao@mdanderson.org.

©2007 American Association for Cancer Research.

doi:10.1158/0008-5472.CAN-07-1337

Bisulfite sequencing of the *RASSF1A* promoter. MSP products were derived from H1299 cells treated with 40 nmol/L siRNA targeting *ΔDNMT3B4/2* or *GAPDH* for 24 h and were recovered by gel purification. The DNA fragments were cloned into a TA cloning vector (Invitrogen) according to the manufacturer's protocol. Plasmid DNA from each clone was then extracted, and inserts in individual clones were sequenced (T3 or T7 primer) using an ABI PRISM 377 DNA sequencer (Perkin-Elmer).

Western blot analysis. Cell lysates were obtained and equal amounts of protein from each sample were diluted with loading buffer, boiled, and loaded onto 7.5% SDS-polyacrylamide gel to be separated by electrophoresis followed by protein transfer to polyvinylidene fluoride membranes (Amersham). Proteins were detected by incubation with corresponding antibodies specific to either DNMT1 or V5 tag (Sigma) followed by blotting with horseradish peroxidase–conjugated secondary antibody (Sigma). The blots were then exposed to chemiluminescent substrate (Amersham) for detection.

Cell growth and cell cycle analyses. The ACEA RT-CES microelectronic cell sensor system (ACEA Biosciences) was used to confirm the number of living cells. The electronic sensors provided a continuous and quantitative measurement of the cell index (which depends on the number of attached

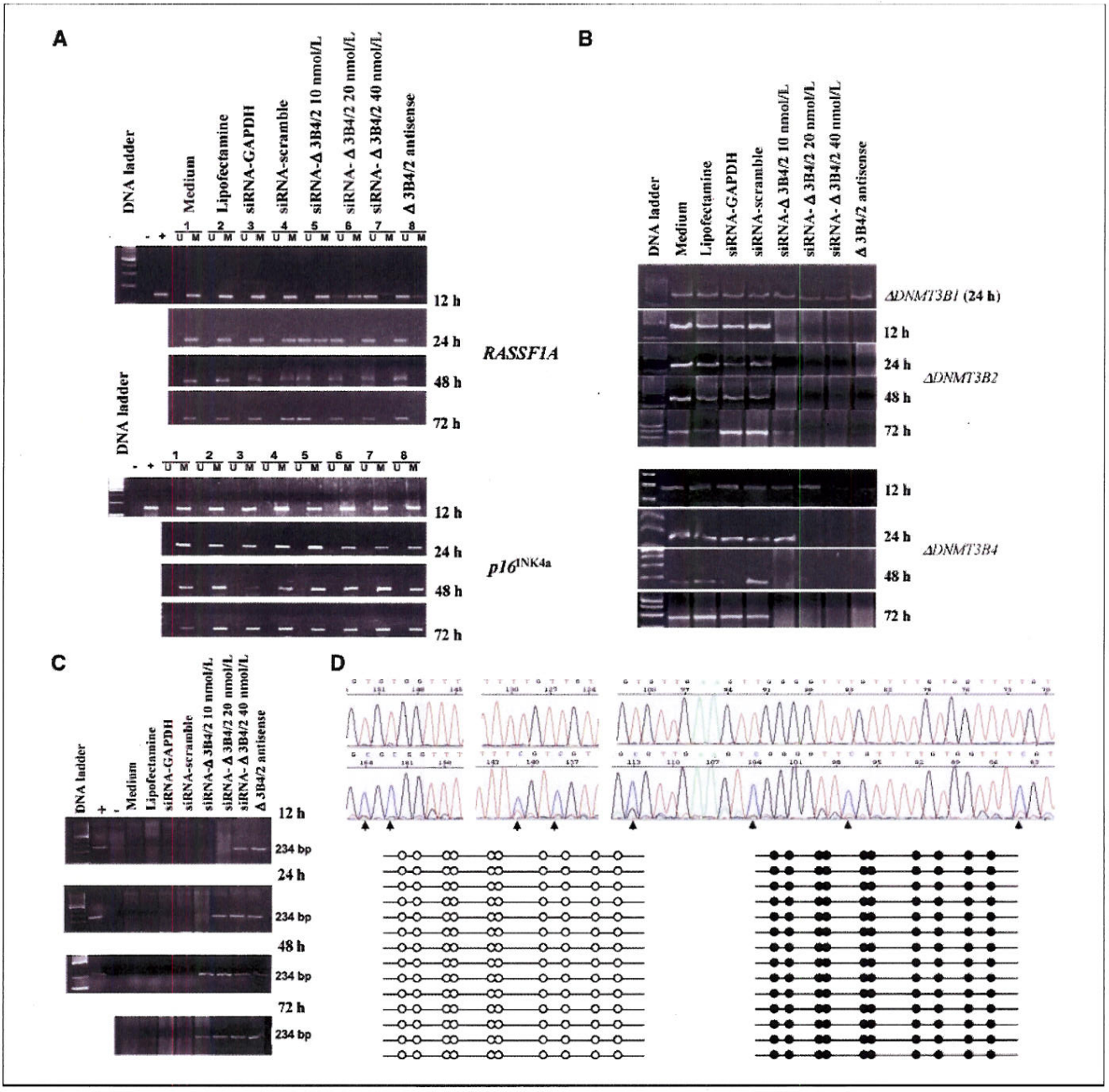


Figure 1. Down-regulation of *ΔDNMT3B4/2* expression and demethylation of *RASSF1A* promoter. *A,* promoter methylation status of *p16* and *RASSF1A* at different time points following treatment as measured by MSP. −, negative control; +, positive control. *U,* unmethylated DNA; *M,* methylated DNA. *B,* expression of *ΔDNMT3Bs* in H1299 cells treated with siRNAs at various time points using RT-PCR. *C,* expression of *RASSF1A* mRNA (234 bp) of the corresponding samples measured by RT-PCR. *D,* methylation status in the *RASS1A* promoter according to bisulfate sequencing analysis. *Arrowheads,* cytosines not converted to thymidines in the CpG sites (*bottom panel of the sequences*) because of the resistance of the methylated cytosines to bisulfate treatment. Line in the figure below the sequences represents a clone. *Open dot,* a CpG site not methylated; *solid dot,* a methylated CpG site. The left set of lines represents clones from cells treated with control, and the right set of lines represents clones from cells treated with siRNA targeting *ΔDNMT3B4/2*.

cells and the shape of the cells) in each well. The cell cycle distribution of the cells was determined using a BD FACSCalibur flow cytometer and CellQuest software (Becton Dickinson).

Stable transfection. pcDNA6/V5-His (Invitrogen) was used to construct plasmids containing full-length *ΔDNMT3B2* or *ΔDNMT3B4*. Empty vector or plasmids containing *ΔDNMT3B2* or *ΔDNMT3B4* were used to transfect HBE1 cells and establish clones with stable expression of the corresponding proteins. Several clones were selected from each transfectant, and passages 5 and 10 were subsequently used for promoter methylation analysis.

Bisulfite pyrosequencing. Pyrosequencing was used to quantitatively measure the levels of cytosine methylation of CpG sites of promoters as described previously (12). The primers used in this study are listed in Supplementary Table S1 and their locations in the CpG islands are presented in Supplementary Fig. S1. Assays were repeated thrice and the means of all experimental results were used with SEs. The quantification of cytosine methylation was performed using Pyro Q-CpG software (Biotage).

Results and Discussion

To test the role of *ΔDNMT3B4* in the promoter-specific methylation of *RASSF1A*, we designed a siRNA that specifically targeted the junction of exons 5 and 7 of *ΔDNMT3B*. Because both *ΔDNMT3B4* and *ΔDNMT3B2* lack exon 6, this siRNA is expected to trigger the degradation of both these transcripts. We used NSCLC cell line H1299 because it carries promoter methylation of both *p16* and *RASSF1A* and expresses a high level of *ΔDNMT3B4* but no detectable *DNMT3B* (10).

We found that down-regulation of *ΔDNMT3B4/2* resulted in *RASSF1A* promoter demethylation in H1299 cells (Fig. 1). In the cells treated with 20 nmol/L or a higher concentration of the siRNA targeting *ΔDNMT3B4/2*, a near complete *RASSF1A* promoter demethylation was observed as early as 12 h after treatment (Fig. 1*A*). This effect was maintained up to 72 h after treatment. The results are consistent with the dose-dependent reduction of *ΔDNMT3B4* expression by the siRNA or antisense treatment (Fig. 1*B*). In contrast, the promoter methylation status of *p16* was not affected (Fig. 1*A*). These results provide the first direct evidence of a causal relationship between ΔDNMT3B4 and the promoter methylation of *RASSF1A* in lung cancer cells.

Consistent with the *RASSF1A* promoter demethylation, *RASSF1A* mRNA expression was restored in the cells also in a dose-dependent manner (Fig. 1*C*). Because MSP is a qualitative assay and cannot reveal the methylation status of each CpG site, we performed bisulfite sequencing of the MSP products from cells with or without *ΔDNMT3B4/2* knockdown. The MSP fragment is a part of the *RASSF1A* promoter and contains 10 CpG sites, excluding the primer sequences. None of the cytosine residues at the 10 CpG sites of the *RASSF1A* promoter fragment were converted to thymidine by bisulfite treatment (an indication of a methylated status) in the 14 individual clones derived from cells without *ΔDNMT3B4/2* knockdown, whereas the cytosine residues at all the 10 CpG sites were converted to thymidine (an indication of an unmethylated status) in all 14 clones derived from cells with *ΔDNMT3B4/2* knockdown (Fig. 1*D*).

In a separate experiment, we used pyrosequencing method to analyze DNA from H1299 cells treated with either 20 nmol/L scramble siRNA control or 20 nmol/L siRNA targeting *ΔDNMT3B4/2* 24 h after treatment. The primers used in this experiment were designed to avoid amplification bias (Supplementary Table S1). We observed that that promoter methylation of *RASSF1A* was decreased from 94% in the control-treated to 33% in the siRNA-treated DNA, whereas no difference was observed in the *p16* promoter between control-treated and the siRNA-treated DNA

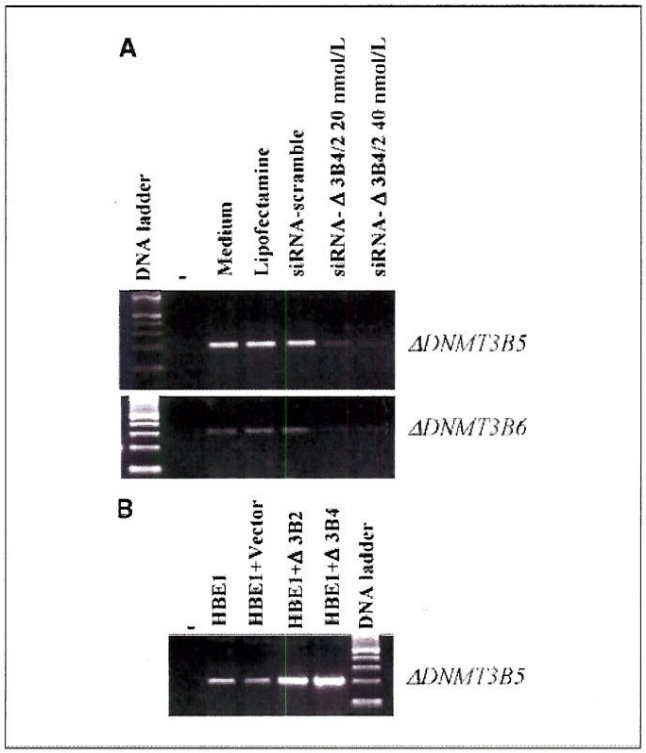


Figure 2. Expression of *ΔDNMT3B5* and *ΔDNMT3B6* following change of *ΔDNMT3B4/2* expression levels. *A*, expression of *ΔDNMT3B5* and *ΔDNMT3B6* in H1299 cells treated with siRNAs measured by RT-PCR. *B*, expression of *ΔDNMT3B5* and *ΔDNMT3B6* in HBE1 cells transfected with *ΔDNMT3B2* or *ΔDNMT3B4*.

(Supplementary Fig. S2). These results indicate that knockdown of *ΔDNMT3B4/2* can reverse the methylated CpG sites in the *RASSF1A* promoter region. Our finding is unlikely due to the inhibition of DNMT1 because the protein expression level was not reduced in the H1299 cells treated with the siRNA (data not shown). To determine whether the *RASSF1A* promoter demethylation due to knockdown of *ΔDNMT3B4/2* is limited to H1299 cells, we performed the same experiments with NSCLC cell line H358. Similar to our results with the H1299 cells, the *RASSF1A* promoter became unmethylated after the siRNA treatment but no effect was observed on the methylated *p16* promoter (data not shown).

To address the issue whether some of the observed results are due to a shift in balance between *ΔDNMT3B4* and other *ΔDNMT3B* isoforms, we also analyzed mRNA expression of *ΔDNMT3B5* and *ΔDNMT3B6* that are expressed in the H1299 cells beside *ΔDNMT3B1* that did not show change in expression levels after siRNA treatment (Fig. 1*A*). Interestingly, the expression of *ΔDNMT3B5* and *ΔDNMT3B6* was reduced in the siRNA-treated samples compared with the controls (Fig. 2*A*). To ensure that the result was not due to nonspecific knockdown by the siRNA, we analyzed the expression of *ΔDNMT3B5* (*ΔDNMT3B6* was not expressed in the cell line) in HBE1 cells transfected with either *ΔDNMT3B2* or *ΔDNMT3B4*. The expression of *ΔDNMT3B5* was increased in the cells transfected with either *ΔDNMT3B2* or *ΔDNMT3B4* compared with controls (Fig. 2*B*). The result indicates that the expression of either *ΔDNMT3B2* or *ΔDNMT3B4* may affect expression levels of *ΔDNMT3B5* and *ΔDNMT3B6*.

We used RT-CES System to determine the dynamic change in cell growth affected by the *ΔDNMT3B4/2* knockout (measured every

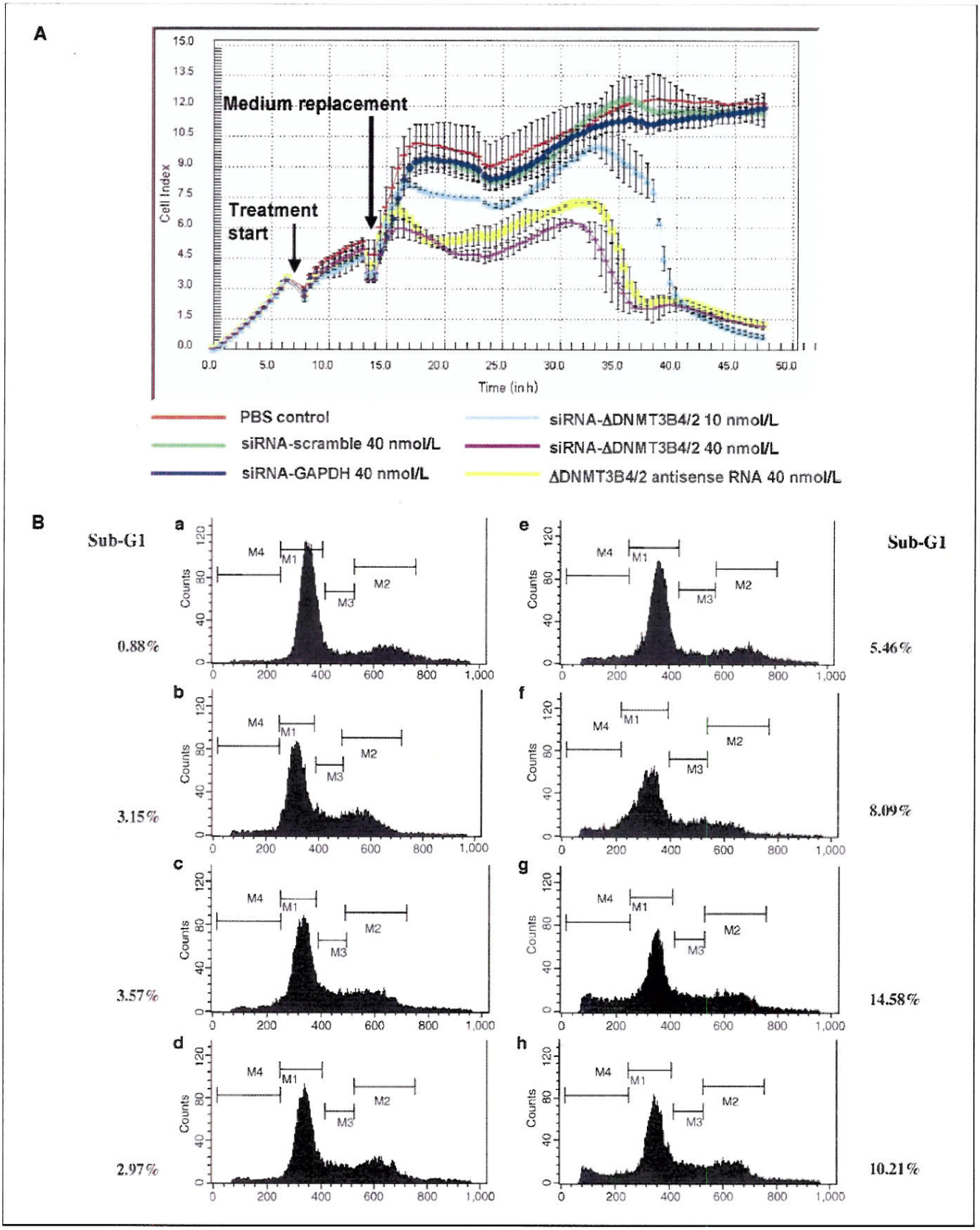
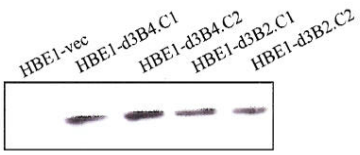


Figure 3. Biological effects of *ΔDNMT3B4/2* down-regulation. *A,* growth of H1299 cells transfected with siRNAs as measured using a microelectronic cell sensor system every 30 min. The representation of individual color lines is indicated and described in the figure. *B,* cell cycle distributions of H1299 cells 24 h after treatment with siRNAs as measured with a flow cytometer (*a*, cells treated with culture medium; *b*, Lipofectamine only; *c*, siRNA targeting *GAPDH; d*, scramble siRNA; *e–g*, 10, 20, and 40 siRNA, respectively; *h*, 40 nmol/L antisense RNA targeting *ΔDNMT3B4/2*). Percentages of sub-G_1 cells were labeled inside each panel.

A



B

Cell Line	Plasmid	Passage	*MGMT*	*GSTP1*	*p16*	*RASSF1A*	*CDH13*	*PR* A	*PR* B	*Line*
HBE1-vec	vector only	5	4	1	4	15	2	8	30	74
HBE1-vec	vector only	10	3	1	4	15	2	9	29	73
HBE1-d3B4.C1	*ΔDNMT3B4*	10	3	1	8	50	2	8	33	64
HBE1-d3B4.C2	*ΔDNMT3B4*	5	4	1	3	45	1	9	33	70
HBE1-d3B4.C3	*ΔDNMT3B4*	5	4	1	3	46	2	8	31	74
HBE1-d3B4.C4	*ΔDNMT3B4*	5	3	1	3	43	2	8	35	64
HBE1-d3B2.C1	*ΔDNMT3B2*	10	5	1	4	16	3	8	33	76
HBE1-d3B2.C2	*ΔDNMT3B2*	5	5	1	2	19	3	8	34	76
HBE1-d3B2.C3	*ΔDNMT3B2*	5	4	1	3	19	2	8	34	74
Normal DNA	NA		2	1	7	9	6	12	10	84
methylated DNA	NA		93	96	94	89	91	91	89	78

Figure 4. Overexpression of *ΔDNMT3B4* resulted in *RASSF1A* promoter hypermethylation. *A*, expression of recombinant ΔDNMT3B4 and ΔDNMT3B2 in HBE1 clones recognized on Western blots using antibody against V5 tag. *HBE1-vec*, vector only–transfected HBE1 cells. *B*, CpG methylation in promoter regions of six genes and in line sequences. Clones d3B4.C1, d3B4.C2, d3B4.C3, and d3B4.C4 expressed ΔDNMT3B4, and clones d3B2.C1, d3B2.C2, and d3B2.C3 expressed ΔDNMT3B2. The values for the genes represent the approximate percentages of the CpG sites that were methylated as measured by pyrosequencing analysis.

30 min). In the H1299 cells, growth was inhibited at ~10 h after treatment with the siRNA-*ΔDNMT3B4/2* in a dose-dependent manner or with the antisense RNA (Fig. 3*A*). Because the RT-CES System works by measuring the electronic impedance of sensor electrodes integrated on the bottom of microtiter E-plates, factors besides cell numbers, such as morphology and tightness of the cells attached to the culture surface, can affect the reading. The major drop observed 36 h after treatment with the siRNA might reflect to a reduced ability of the cells detaching to the plastic surface. To determine the mechanism by which the growth of the *ΔDNMT3B4/2* knockout is inhibited, we used flow cytometry to examine the cell cycle distribution of the H1299 cells 24 h after treatment. We observed an increase in the sub-G_1 fraction of cells treated with the siRNA-*ΔDNMT3B4/2* in a dose-dependent manner or with the antisense RNA (Fig. 3*B*). These results suggest that treatment with siRNA-*ΔDNMT3B4/2* increased apoptosis.

To provide direct evidence to support the possibility that *ΔDNMT3B4* but not *ΔDNMT3B2* contributed to the differential regulation of *RASSF1A* promoter methylation, we constructed mammalian expression plasmids containing *ΔDNMT3B2* or *ΔDNMT3B4* and used HBE1 cells (immortalized, normal-appearing bronchial epithelial cells from a patient with NSCLC; ref. 13). Stable clones expressing *ΔDNMT3B2* or *ΔDNMT3B4* were established (Fig. 4*A*). At passages 5 and 10, we used the quantitative pyrosequencing method to analyze the promoter methylation status of the genes *MGMT, GSTP1, p16, RASSF1A, CDH13*, and *PR* (two regions) in the HBE1 cells transfected with empty vector only, *ΔDNMT3B2*, or *ΔDNMT3B4*. Consistent with our hypothesis that *ΔDNMT3B4* but not *ΔDNMT3B2* contributed to the differential regulation of *RASSF1A* promoter methylation, cells transfected with *ΔDNMT3B4*, but not cells transfected with the empty vector or *ΔDNMT3B2*, showed substantially increased DNA methylation in the *RASSF1A* promoter compared with vector control ($P < 0.001$, Kruskal-Wallis test; Fig. 4*B*). No change in methylation status was observed in any of the other promoters for any of the transfectants (Fig. 4*B*).

Our findings suggest a mechanism for the development of "tissue-specific DNA methylation." This term refers to different promoters being methylated in different cell types or organs during development and tumorigenesis (14). In somatic cells, most of the CpG sites in genomic DNA are methylated except in CpG-enriched promoter regions (CpG islands) of the transcriptionally active genes. The maintenance of established DNA methylation patterns is largely performed by DNMT1, which is constitutively expressed in somatic tissues. The expression of DNMT3B is low or absent in somatic tissues but significantly increased in transformed cancer cells and is thought to be critical to *de novo* promoter methylation (15). During tumorigenesis, *de novo* DNA methylation occurs in the promoters of selected genes and contributes to their functional inactivation by suppressing the expression of those genes. Global analysis of promoter methylation has revealed several abnormally methylated promoters found in tumors but not in normal tissue counterparts (16). However, each tumor exhibits a unique pattern of methylated promoters, although some promoters are commonly methylated in certain tumor types. These observations indicate the presence of cellular mechanisms, which result in differential promoter methylation that is maintainable during tumor development and progression.

In a previous study, we found a statistically significant correlation between *RASSF1A* promoter methylation and *ΔDNMT3B4* expression in a large number of primary NSCLC tumors (11). That result provided *in vivo* evidence of a role for *ΔDNMT3B4* in regulating the methylation of CpG islands in a promoter-specific manner. The results presented in the current report provide enough direct evidence to establish the causal relationship between *ΔDNMT3B4* and *RASSF1A* promoter methylation but not between several other commonly methylated promoters we examined. In the siRNA-based experiment, the down-regulation of *ΔDNMT3B4* resulted in demethylation of the *RASSF1A* promoter but not the *p16* promoter in two NSCLC cell lines. Because the siRNA used also knocked down *ΔDNMT3B2* (because of the shared exon-exon junction between *ΔDNMT3B2* and *ΔDNMT3B4*), a role for *ΔDNMT3B2* in that process cannot be excluded. The experiments using HBE1 cells that express specific *ΔDNMT3B* variants (*ΔDNMT3B2* or *ΔDNMT3B4*) provided conclusive evidence that *ΔDNMT3B4* but not *ΔDNMT3B2* contributes to *RASSF1A*-specific promoter methylation. Although expression levels of *ΔDNMT3B4* may affect expression levels of *ΔDNMT3B5* and *ΔDNMT3B6*, the expression of the later isoforms is unlikely contributed to *RASSF1A* promoter methylation because overexpressing *ΔDNMT3B2* also caused an increased expression of *ΔDNMT3B5* (Fig. 3*B*) but did not affect the methylation status of *RASSF1A* promoter (Fig. 4*B*).

Although our study results firmly establish the importance of ΔDNMT3Bs in promoter-specific methylation, the detailed mechanisms are unknown. DNMT1 is the predominant cellular DNA methyltransferase, but it requires the participation of DNMT3B to achieve promoter methylation (17, 18). Because DNMT3Bs contain a PWWP domain, which has direct DNA-binding capability (19), the fact that there are ΔDNMT3Bs with structural differences at and around the PWWP domain suggests that the ΔDNMT3B variants interact with a class of promoters with a similar consensus sequence and are responsible for the methylation of the promoters. The recent finding that tumor-specific methylated genes have common sequence motifs in their promoters (20) supports this notion. It should be noted that, in our study, overexpression of ΔDNMT3B4 in the HBE1 cells resulted in only partial methylation of the *RASSF1A* promoter; this observation indicates that an additional component or components are needed for the stable and complete methylation of the promoter. Alternatively, the peptide tags fused with ΔDNMT3B4 may cause changes in protein folding and result in reduced efficiency of the protein.

Our findings place ΔDNMT3Bs at the center of *de novo* promoter methylation, particularly in lung tumorigenesis. The promoter-specific demethylation we observed is particularly interesting for cancer therapy because it raises the possibility of inhibiting specific variants of ΔDNMT3B to selectively activate critical tumor suppressor genes whose expression is down-regulated due to promoter methylation. Such an approach may lead to the development of novel therapeutic strategies tailored to individual tumors with particular epigenetic abnormalities. These strategies would cause limited adverse effects because normal tissue would be spared most of the effects of less targeted treatment on the promoters methylated.

Acknowledgments

Received 4/11/2007; revised 8/30/2007; accepted 10/5/2007.

Grant support: Department of Defense grants DAMD17-01-1-01689-1 and W81XWH-05-2-0027.

The costs of publication of this article were defrayed in part by the payment of page charges. This article must therefore be hereby marked *advertisement* in accordance with 18 U.S.C. Section 1734 solely to indicate this fact.

We thank Elizabeth L. Hess for scientific editing of the manuscript.

References

1. Surani MA. Imprinting and the initiation of gene silencing in the germline. Cell 1998;93:309–12.
2. Monk M, Boubelik M, Lehnert S. Temporal and regional changes in DNA methylation in the embryonic, extra-embryonic, and germ cell lineages during mouse embryo development. Development 1987;99:371–82.
3. Okano M, Xie S, Li E. Cloning and characterization of a family of novel mammalian DNA (cytosine-5) methyltransferases. Nat Genet 1998;19:219–20.
4. Jones PA, Baylin SB. The fundamental role of epigenetic events in cancer. Nat Rev Genet 2002;3:415–28.
5. Okano M, Bell DW, Haber DA, Li E. DNA methyltransferases Dnmt3a and Dnmt3b are essential for *de novo* methylation and mammalian development. Cell 1999;99:247–57.
6. Robertson KD, Uzvolgyi E, Liang G, et al. The human DNA methyltransferases (DNMTs) 1, 3a and 3b: coordinate mRNA expression in normal tissues and overexpression in tumors. Nucleic Acids Res 1999;27:2291–8.
7. Saito Y, Kanai Y, Sakamoto M, Saito H, Ishii H, Hirohashi S. Overexpression of a splice variant of DNA methyltransferase 3b, DNMT3b4, associated with DNA hypomethylation on pericentromeric satellite regions during human hepatocarcinogenesis. Proc Natl Acad Sci U S A 2002;99:10060–5.
8. Yakushiji T, Uzawa K, Shibahara T, Noma H, Tanzawa H. Over-expression of DNA methyltransferases and CDKN2A gene methylation status in squamous cell carcinoma of the oral cavity. Int J Oncol 2003;22:1201–7.
9. Sato M, Horio Y, Sekido Y, Minna JD, Shimokata K, Hasegawa Y. The expression of DNA methyltransferases and methyl-CpG-binding proteins is not associated with the methylation status of p14(ARF), p16(INK4a) and RASSF1A in human lung cancer cell lines. Oncogene 2002;21:4822–9.
10. Wang L, Wang J, Sun S, et al. A novel DNMT3B subfamily, ΔDNMT3B, is the predominant form of DNMT3B in non-small cell lung cancer. Int J Oncol 2006;29:201–7.
11. Wang J, Walsh G, Liu DD, Lee JJ, Mao L. Expression of ΔDNMT3B variants and its association with promoter methylation of p16 and RASSF1A in primary non-small cell lung cancer. Cancer Res 2006;66:8361–6.
12. Issa JP, Gharibyan V, Cortes J, et al. Phase II study of low-dose decitabine in patients with chronic myelogenous leukemia resistant to imatinib mesylate. J Clin Oncol 2005;23:3948–56.
13. Ramirez RD, Sheridan S, Girard L, et al. Immortalization of human bronchial epithelial cells in the absence of viral oncoproteins. Cancer Res 2004;64:9027–34.
14. Kitamura E, Igarashi J, Morohashi A, et al. Analysis of tissue-specific differentially methylated regions (TDMs) in humans. Genomics 2006;89:326–37.
15. Liu K, Wang YF, Cantemir C, Muller MT. Endogenous assays of DNA methyltransferases: evidence for differential activities of DNMT1, DNMT2, and DNMT3 in mammalian cells *in vivo*. Mol Cell Biol 2003;23:2709–19.
16. Hatada I, Fukasawa M, Kimura M, et al. Genome-wide profiling of promoter methylation in human. Oncogene 2006;25:3059–64.
17. Rhee I, Bachman KE, Park BH, et al. DNMT1 and DNMT3b cooperate to silence genes in human cancer cells. Nature 2002;416:552–6.
18. Kim GD, Ni J, Kelesoghu N, Roberts RJ, Prodham S. Co-operation and communication between the human maintenance and *de novo* DNA methyltransferases. EMBO J 2002;21:4183–95.
19. Qiu C, Sawada K, Zhang X, Cheng X. The PWWP domain of mammalian DNA methyltransferase Dnmt3b defines a new family of DNA-binding folds. Nat Struct Biol 2002;9:217–24.
20. Keshet I, Schlesinger Y, Farkash S, et al. Evidence for an instructive mechanism of *de novo* methylation in cancer cells. Nat Genet 2006;38:149–53.

Int. J. Cancer: **121,** 2254–2259 (2007)
© 2007 Wiley-Liss, Inc.

ATM sequence variants associate with susceptibility to non-small cell lung cancer

Hushan Yang[1], Margaret R. Spitz[1], David J. Stewart[2], Charles Lu[2], Ivan P. Gorlov[1] and Xifeng Wu[1]*

[1]*Department of Epidemiology, The University of Texas M.D. Anderson Cancer Center, Houston, TX*
[2]*Department of Thoracic/Head and Neck Medical Oncology, The University of Texas M.D. Anderson Cancer Center, Houston, TX*

***ATM* gene mutations have been implicated in many human cancers. However, the role of *ATM* polymorphisms in lung carcinogenesis is largely unexplored. We conducted a case-control analysis of 556 Caucasian non-small-cell lung cancer (NSCLC) patients and 556 controls frequency-matched on age, gender and smoking status. We genotyped 11 single nucleotide polymorphisms of the *ATM* gene and found that compared with the wild-type allele-containing genotypes, the homozygous variant genotypes of *ATM*08 (rs227060) and *ATM*10 (rs170548) were associated with elevated NSCLC risk with ORs of 1.55 (95% CI: 1.02–2.35) and 1.51 (0.99–2.31), respectively. *ATM* haplotypes and diplotypes were inferred using the Expectation-Maximization algorithm. Haplotype H5 was significantly associated with reduced NSCLC risk in former smokers with an OR of 0.47 (0.25–0.96) compared with the common H1 haplotype. Compared with the H1–H2 diplotype, H2–H2 and H3–H4 diplotypes were associated with increased NSCLC risk with ORs of 1.58 (0.99–2.54) and 2.29 (1.05–5.00), respectively. We then evaluated genotype–phenotype correlation in the control group using the comet assay to determine DNA damage and DNA repair capacity. Compared with individuals with at least 1 wild-type allele, the homozygous variant carriers of either *ATM*08 or *ATM*10 exhibited significantly increased DNA damage as evidenced by a higher mean value of the radiation-induced olive tail moment (*ATM*08: 4.86 ± 2.43 *vs.* 3.79 ± 1.51, $p = 0.04$; *ATM*10: 5.14 ± 2.37 *vs.* 3.79 ± 1.54, $p = 0.01$). Our study presents the first epidemiologic evidence that *ATM* genetic variants may affect NSCLC predisposition, and that the risk-conferring variants might act through down-regulating the functions of ATM in DNA repair activity upon genetic insults such as ionizing radiation.**
© *2007 Wiley-Liss, Inc.*

Key words: *ATM*; polymorphism; haplotype; diplotype; NSCLC

Lung cancer accounts for 20% of cancer incidence in the United States and 25% of cancer-related deaths. Approximately 80% of lung cancer cases are non-small cell lung cancer (NSCLC). Deficiencies in DNA repair capacity (DRC), apoptosis control and cell cycle checkpoints have been implicated in the pathogenesis of lung cancer including NSCLC.[1–3] Therefore, the essential role of the ATM protein in double strand break (DSB) DNA damage response and the importance of the DNA repair system in tobacco-related carcinogenesis highlight the potential significance of *ATM* sequence variations on NSCLC risk.

ATM is a tumor suppressor gene frequently mutated in patients with Ataxia Telangiectasia (AT), a rare form of an autosomal recessive malignancy-prone disorder prominently characterized by extremely high sensitivity to ionizing radiation or other DSB-inducing agents.[4] *ATM* encodes a 370-kDa phosphoinositide 3-kinase (PI3K) protein that belongs to the PI3K-like Serine/Threonine protein kinase (PIKK) family. This family functions in DNA damage responses by phosphorylating proteins in various damage-related pathways.[5] ATM exists in an inactive multimer form in the cell nucleus, which dissociates into monomers upon exposure to DSB-inducing genetic insults.[6] The interaction between the MRN (MRE11, RAD50, NBS1) complex and ATM in the presence of damaged DNA yields a more than 80-fold increase in ATM kinase activity, which is capable of relating the signals to a plethora of downstream effectors through phosphorylation of specific serine or threonine amino acid residues.[7] The converging effects of these protein effectors control the outcome of the damaged cells through the regulation of cell cycle arrest, DNA repair and apoptosis.

Aberrations of ATM protein have been implicated in the etiology of many cancers,[8–13] including lung cancer. Through phosphorylating p53 and MDM2 proteins, ATM disrupts the p53-MDM2 interaction and thus, increases the nuclear accumulation of p53.[5] Consistent with this notion, Bartkova *et al.* found that ATM, CHK2, p53 and H2AX were highly expressed and phosphorylated in early precursor lesions of various cancers, suggesting that the ATM-CHK2-p53 axis plays an essential role in the DNA damage-response in the early development stage of these malignancies, including lung cancer.[14] Moreover, Eymin *et al.* reported that the ATM/CHK2 pathway also mediates the $p14^{ARF}$-induced G2 cell cycle checkpoint arrest in response to DNA damaging agents. This pathway is independent of p53 activation and its defects contribute to lung carcinogenesis.[14] Taken together, these observations highlight the pivotal role of ATM in the prevention of lung cancer development through the modulation of multiple pathways. However, most previous studies focused on the carcinogenic effect of *ATM* rare mutations rather than common variants. In a few studies in which *ATM* polymorphisms were investigated, controversial results have been reported in terms of the involvement of *ATM* polymorphisms in the etiology of malignancies such as breast and colorectal cancers.[15–20] There have not been any studies of *ATM* polymorphisms and lung cancer risk in Caucasians. In addition, although *ATM* haplotypes have also been associated with altered cancer risk, most published studies focused on only breast cancer and the haplotypes in these studies were composed of only potential functional SNPs but were not based on haplotype tagging SNPs (htSNP).[15,21–23] Since Bonnen *et al.* reported extensive linkage disequilibrium (LD) across the complete *ATM* locus which suggested that few htSNPs were required to construct complete high-power haplotypes to capture common *ATM* polymorphisms,[24] a comprehensive approach combining the power of htSNPs and functional SNPs may provide more clues to the assessment of *ATM* sequence variants on cancer risk.

To test the hypothesis that common *ATM* sequence variants may modulate NSCLC risk, we assessed the associations of 11 potential *ATM* htSNPs and functional SNPs with NSCLC risk in Caucasians. In addition, we performed a functional assay to evaluate the physiological significance of the observed associations through genotype–phenotype correlation analyses. To the best of our knowledge, this is the first epidemiological study examining the role of *ATM* polymorphisms in NSCLC risk in Caucasians.

Material and methods

Study population

Lung cancer cases were recruited from The University of Texas MD. Anderson Cancer Center. Cases were newly diagnosed and

Grant sponsor: NCI; Grant numbers: CA 111646, CA 55769, CA 70907, DAMD17-02-1-0706; Grant sponsor: Flight Attendant Medical Research Institute.

***Correspondence to:** Department of Epidemiology, Box 1340, The University of Texas M.D. Anderson Cancer Center, 1515 Holcombe Blvd., Houston, TX 77030, USA. Fax: +713-792-4657.
E-mail: xwu@mdanderson.org

Received 15 August 2006; Accepted after revision 18 April 2007
DOI 10.1002/ijc.22918
Published online 20 June 2007 in Wiley InterScience (www.interscience.wiley.com).

histologically confirmed lung cancer patients who had received no previous chemotherapy or radiotherapy. There were no recruitment restrictions on age, gender, ethnicity or cancer-stage. The controls were recruited from the Kelsey-Seybold Clinic, Houston's largest private multispecialty physician group which includes a network of 23 clinics and more than 300 physicians. Potential controls were identified from healthy individuals without a previous diagnosis of cancer except for nonmelanoma skin cancer. We excluded subjects who had recent blood transfusions to control for confounding effects for several functional assays. Potential controls were first surveyed by a short questionnaire for willingness to take part in case-control studies and to provide demographic and smoking status data for matching. Controls were frequency-matched to cases in terms of age (±5 years), gender, ethnicity and smoking status. Definition criteria of smoking status were as previously described.[2] For both cases and controls, after obtaining written informed consent, trained M.D. Anderson staff interviewers administered risk factor questionnaires to study participants. The interview took ~45 min to complete. Data were collected on demographic characteristics (age, gender, ethnicity, *etc.*), work history, tobacco use history and family history of cancer. This case-control study started in 1995 and is currently ongoing. The response rate of participation is ~77.4% for cases and 73.3% for controls. Participants who had blood transfusions within recent 6 months were excluded. At the completion of the interview, 40 ml of blood were drawn from each person and sent to the laboratory for DNA isolation and molecular analysis. Laboratory personnel were blinded to case and control status. Human subject approval was obtained from the institutional review boards of both M.D. Anderson and Kelsey–Seybold. In the current analysis, a total of 556 Caucasian NSCSL patients and 556 cancer-free controls (frequency-matched by age, gender and smoking status) were included.

Selection of ATM *sequence variants*

Eleven potential haplotype-tagging and functional SNPs of the *ATM* gene ranging from 10-kb upstream of the translation initiation site to 5-kb downstream of the translation stop site were chosen based on the data currently available from public SNP databases, including NCBI dbSNP (http://www.ncbi.nlm.nih.gov/projects/SNP), International HapMap Project (http://www.hapmap.org) and Cancer Genome Anatomy Project SNP500Cancer (http://snp500cancer.nci.nih.gov). To choose potential htSNP sets, we used the SNPbrowser 3.5 software (Applied Biosystems, Foster, CA) implementing the pairwise r^2 algorithms. The remaining SNPs with higher than 5% minor allele frequency (MAF) were selected empirically after exhaustively searching the relevant literature to locate potential functional *ATM* SNPs that had been implicated in other cancer association studies.

Probe and primer designs and genotyping

Genotyping was performed using a 5′ nuclease assay-based *TaqMan* assay. Probes and primers for the genotyping were either acquired from the SNP500Cancer database or designed using the PrimerExpress 2.0 software (Applied Biosystems, Foster, CA). The probes were labeled fluorescently with either 6-FAM or VIC on the 5′ end and a nonfluorescent minor groove binder (MGB) quencher on the 3′ end. The genotyping procedure was exactly as described in a previous study.[25] Genomic DNA was extracted from peripheral blood lymphocytes using the Human Whole Blood Genomic DNA Extraction Kit (Qiagen, Valencia, CA). The PCR amplification mix (5 μl) included sample DNA (5 ng), 1 X *TaqMan* buffer A, 200 μM deoxynucleotide triphosphates, 5 mM $MgCl_2$, 0.65 U of AmpliTaq Gold, 900 nM each primer and 200 nM each probe. The PCR condition includes 1 cycle for 10 min at 95°C, 40 cycles for 15 sec at 95°C and 1 min at 60°C. PCR was performed using ABI PRISM® 7900HT sequence detection system (Applied Biosystems) and SDS 2.1 software (Applied Biosystems) was used to analyze the end-point genotyping data. Internal quality controls and negative controls were used to ensure genotyping accuracy and 5% of all samples were randomly selected and genotyped in duplicates with 100% concordance.

Comet assay

Baseline and γ-radiation-induced comet assays were performed in the control group as described previously.[26] The comet assays in this study were performed following exactly the same experimental procedures and using the same software. All reagents were purchased from the same vendor and freshly made. Briefly, fully frosted, agarose-coated slides were covered with a glass coverslip and left at room temperature for 30 min. Blood cultures were either untreated or irradiated with 1.5 Gy using a ^{137}Cs source at room temperature. This dose was reported in our previous studies to be the optimal dose, which is sufficient to induce nuclear DNA damage but is not cytotoxic.[26] The untreated or γ-irradiated blood culture was mixed with low melting point (LMP) agarose (Invitrogen, Carlsbad, CA) in PBS. About 50-μl mixture was immediately spread onto each end of the slide, covered with a fresh coverslip, and left at 4°C for 10 min. The slides were submersed in freshly prepared lysis buffer for 1 hr at 4°C and placed in a horizontal electrophoresis box without power and filled with freshly prepared alkali for 30 min at 4°C. After an electrophoresis at 295–300 mA for 23 min at 4°C, the slides were neutralized in Tris buffer, fixed in 100% methanol for 10 min and stored in the dark at room temperature. Immediately before analysis, slides were hydrated in fresh Tris–HCl and then stained with ethidium bromide. Fifty consecutive cells (25 cells from each end of the slide) were manually selected and quantified with Komet version 4.0.2 (Kinetic Imaging, Bromborough, Wirral, UK) software attached to a fluorescent microscope (Nikon, Melville, NY), which also determined the Olive tail moment parameter [(tail mean − head mean) × (% tail DNA/100)]. The head of the comet represents the cell nucleus and the tail of the comet represents the damaged DNA liberated from the nucleus by electrophoresis. The tail mean is the tail DNA intensity subtracted by background intensity, while the head mean is the head DNA intensity subtracted by background intensity. The percentage of tail DNA is the fraction of DNA that has migrated from the head. The difference between the tail mean and the head mean represents the difference in the distance between the center of gravity of the DNA distribution in the comet head and the center of gravity of the DNA distribution in the comet tail. Since the comet assay was not started from the beginning of the subject recruitment, data was not available for those study subjects who were enrolled before the commencement of the comet assay. In the current analysis, there were 116 controls subjects with baseline comet data. Among them, 112 had γ-radiation-induced comet assay data. There are no significant differences in major host characteristics between the control subjects with comet data and those without comet data (data not shown).

Statistical analysis

Statistical analyses were done using either SAS software (SAS Institute Cary, CA) or Intercooled Stata 8.0 statistical software package (Stata, College Station, TX). χ^2 and Fisher's exact tests were used to assess patient characteristics. The risks were calculated as odds ratios (OR) and 95 percent confidence intervals (95% CI) using unconditional multivariate logistic regression adjusted by age, gender and smoking status (never, former and current smokers). We analyzed the associations between individual SNPs and NSCLC risk by combining the genotypes with at least 1 wild-type allele as the reference group as *ATM* is a tumor suppressor gene that might function in a recessive pattern. Haplotypes and diplotypes were estimated using the Expectation-Maximization (EM) algorithm implemented by the HelixTree program (Golden Helix, Bozeman, MT). Haplotypes with a probability less than 95% were excluded from the final data to ensure analytical reliability.[15] A two sample t test with equal variance was used to determine the genotype–phenotype correlation. $p \leq 0.05$ was considered as the threshold of significance. All statistical analyses were 2-sided.

TABLE I – DISTRIBUTION OF SELECTED HOST CHARACTERISTICS BY CASE-CONTROL STATUS

Variable	Case, *N* (%)	Control, *N* (%)	*p* value[1]
Age (Mean ± SD[2])	60.5 ± 10.6	60.1 ± (10.3)	0.48
Gender			
Male	309 (55.6)	309 (55.6)	
Female	247 (44.4)	247 (44.4)	1.00
Smoking status			
Never	94 (16.9)	106 (19.1)	
Former	219 (39.4)	236 (42.4)	
Current	243 (43.7)	214 (38.5)	0.20[3]
Ever	462 (83.1)	450 (80.9)	0.35[4]
Pack-years (Mean ± SD)	50.6 ± 29.1	47.3 ± 32.1	0.11

[1]*p* values were derived from the χ^2 test for categorical variables (gender and smoking status) and *t* test for continuous variables (age and pack-years).–[2]SD, standard deviation.–[3]Among never, former and current smokers.–[4]Ever smokers compared with never smokers.

Results

Individual ATM *polymorphisms and NSCLC risk*

Table I lists the selected characteristics of the study population and illustrates that the case patients and control subjects were well matched on age, gender and smoking status. The average genotyping call rate for all SNPs is 97.4 % (95.8–98.9%) and there are no significant call rate differences between cases and controls (the average call rate is 97.6 and 97.3% for cases and controls, respectively).

Table II summarizes the name, reference number, gene position and genotypic distributions of each SNP and their associations with NSCLC risk. Two highly linked intronic SNPs, *ATM*08 and *ATM*10, exhibited significant and borderline significant associations with NSCLC risk, respectively, when their homozygous wild-type plus heterozygous genotypes were used as the reference group. For the *ATM*08 polymorphism, when compared to the wild-type CC genotype, carriers of 1 variant allele (CT) showed a nonsignificant protective effect (OR = 0.79 (0.61–1.02)) whereas the homozygous variant genotype (TT) exhibited a nonsignificant association with an increased NSCLC risk (OR = 1.38 (0.89–2.13)) (data not shown). However, when the genotypes of at least 1 wild-type allele were combined together as the reference group (CC + CT), the TT genotype demonstrated a significant association with an increased NSCLC risk (OR = 1.55 (1.02–2.35)). Similarly, when the group with at least 1 wild-type allele of *ATM*10 was used as a reference (AA + AC), the CC genotype showed a borderline statistically significant association with an elevated risk (OR = 1.51 (0.99–2.31)).

The manifested risk of both SNPs were more evident in males, in young people (≤61 years old), and in former smokers with ORs of 1.87 (1.08–3.26) 2.32 (1.26–4.27) and 2.01 (1.05–3.84) for *ATM*08 respectively, and ORs of 1.84 (1.04–3.24), 2.09 (1.13–3.88) and 2.07 (1.08–3.94) for *ATM*10 respectively (Table III). The double-variant genotypes of other SNPs including *ATM*01, *ATM*02, *ATM*05, *ATM*06 *ATM*07, *ATM*09 and *ATM*11 did not exhibit apparent alterations in ORs. The small sample size of the homozygous-variant genotypes of *ATM*03 and *ATM*04 limited their further analysis (Table II).

Associations of ATM *haplotypes with NSCLC risk*

Eight haplotypes with frequency greater than 1% in both cases and controls were identified. Six common haplotypes accounted for 98% of the total haplotypes. Other software implemented with Bayesian algorithm[27] produced very similar results (data now shown). The most common haplotype H1 (TTCCGTCCGAT) (in the order from *ATM*01 to *ATM*11) showed a frequency of 36% in both cases and controls. There was no overall association between haplotypes and NSCLC risk using the most common H1 haplotype as the reference group (Table IV). However, on stratified analysis, the H5 haplotype (TTCTGTCCGAT) was significantly associated with a decreased risk in former smokers (OR = 0.47 (0.25–0.96)) (Table IV).

Associations of ATM *diplotypes with NSCLC risk*

Diplotypes were reconstructed using the estimated haplotypes with probability greater than 95% (Table V). The 10 highest diplotypes constituted more than 86% of the cases and 86% of the controls. Compared to the most common diplotype (H1–H2), H2–H2 manifested a borderline significant association with increased NSCLC risk (OR = 1.58 (0.99–2.54)). The effect was more prominent in young people with an OR of 2.26 (1.13–4.52) and in former smokers with an OR of 2.22 (1.06–4.65) (data not shown). The increased risk associated with H2–H2 was in line with the result of the individual significant SNPs since H2–H2 was the only diplotype containing homozygous variant alleles of both *ATM*08 and *ATM*10. The H3–H4 diplotype also exhibited a significant risk effect (OR = 2.29 (1.05–5.00)), which was higher in females (OR = 8.17 (1.69–39.33)) (data not shown). The H2–H4 diplotype did not demonstrate overall significance; however, it showed a significant effect within the strata of females (OR = 2.85 (1.03–7.79)) and never smokers (OR = 3.94 (1.04–14.93)) (data not shown).

Genotype–phenotype correlations in controls

To validate the biological implication of the demonstrated associations between increased NSCLC risk and *ATM*08/*ATM*10, we performed genotype–phenotype correlation analyses in 116 control subjects with available comet data. The baseline comet assay showed no noteworthy distinctions between the reference group and the homozygous variants (Table VI). However, individuals with homozygous variant genotypes demonstrated significantly elevated γ-radiation-induced DNA damage, as represented by higher levels of olive tail moment, compared to carriers of at least 1 wild-type allele in either *ATM*08 or *ATM*10 (*ATM*08, TT *vs.* CC+CT: 4.86 ± 2.43 *vs.* 3.79 ± 1.51, $p = 0.04$; *ATM*10, CC *vs.* AA + AC: 5.14 ± 2.37 *vs.* 3.79 ± 1.54, $p = 0.01$) (Table VI). The average interassay coefficient variation for the γ-radiation comet assay was 9.8% (data not shown), which is modest compared with the variation resulting from genotype differences of *ATM*08 and *ATM*10.

Discussion

The main finding of this report is that two-linked intronic SNPs of *ATM* exhibited a similar recessive pattern of association with increased NSCLC risk, which is strongly supported by the comet assay indicating that the variants might function through influencing the DNA damage/repair pathway of the host cell. No literature has investigated the associations of these 2 SNPs with any form of cancer or other diseases. The close proximity of the 2 SNPs (in introns 61 and 62) to the *ATM* PI3 kinase domain (exons 60 and 61) lends support to the hypothesis that these 2 SNPs might regulate ATM PI3 kinase activity by affecting either the kinase domain or FAT domain immediately before the kinase motif.

All SNPs conformed to Hardy–Weinberg Equilibrium (HWE) in both case patients and control subjects, except for *ATM*08 and *ATM*10, which showed significant deviation in controls (Table II, 0.02 and 0.04, respectively). However, the divergence from HWE is not likely the result of genotyping errors since we observed complete concordance from genotyping quality controls. Moreover, neither of the 2 SNPs were still out of HWE when the Bonferroni-corrected significance threshold was applied to test the null hypothesis of HWE to detect genotyping errors.[28] Similar results were obtained when we used the less conservative Benjamini–Hochberg step-up procedure to control for false discovery rate (FDR) of HWE at the 5% level (data not shown). More importantly, the results of our comet functional assays measuring the DNA damage/DRC indicated that the homozygous variant genotype of these 2 SNPs were associated with significantly higher lev-

TABLE II – CASE-CONTROL DISTRIBUTION OF GENOTYPES OF 11 POTENTIAL *ATM* SEQUENCE VARIANTS

	Reference	Position	Genotypes	Cases, *N* (%)	Controls, *N* (%)	OR[1] (95% CI[1])[2]	HWE[3] *p* (controls)
*ATM*01	rs228589	5′ region	AA + AT	434 (80.7)	433 (80.8)	1.00 (reference)	0.31
			TT	104 (19.3)	103 (19.2)	1.01 (0.74–1.37)	
*ATM*02	rs664677	Intron	TT + TC	445 (81.4)	441 (81.7)	1.00 (reference)	0.34
			CC	102 (18.6)	99 (18.3)	1.03 (0.81–1.14)	
*ATM*03	rs1800058	Exon, nsSNP[4]	CC + CT	549 (99.8)	550 (100)	1.00 (reference)	0.60
			TT	1 (0.2)	0 (0)	N/A[5]	
*ATM*04	rs1800889	Exon, sSNP[4]	CC + CT	548 (100)	550 (99.8)	1.00 (reference)	0.80
			TT	0 (0)	1 (0.2)	N/A	
*ATM*05	rs1801516	Exon, nsSNP	GG + GA	537 (98.7)	536 (98.2)	1.00 (reference)	0.59
			AA	7 (1.3)	10 (1.8)	0.70 (0.26–1.85)	
*ATM*06	rs611646	Intron	TT + TA	445 (81.4)	458 (85.0)	1.00 (reference)	0.18
			AA	102 (18.6)	81 (15.0)	1.30 (0.95–1.80)	
*ATM*07	rs609429	Intron	GG + GC	436 (80.9)	438 (81.4)	1.00 (reference)	0.25
			CC	103 (19.1)	100 (18.6)	1.04 (0.76–1.41)	
*ATM*08	rs227060	Intron	CC + CT	469 (88.7)	495 (92.4)	1.00 (reference)	0.02
			TT	60 (11.3)	41 (7.6)	**1.55 (1.02–2.35)**	
*ATM*09	rs664143	Intron	GG + GA	433 (80.6)	441 (82.3)	1.00 (reference)	0.16
			AA	104 (19.4)	95 (17.7)	1.12 (0.82–1.52)	
*ATM*10	rs170548	Intron	AA + AC	483 (89.3)	500 (92.6)	1.00 (reference)	0.04
			CC	58 (10.7)	40 (7.4)	**1.51 (0.99–2.31)**	
*ATM*11	rs4585	3′ region	TT + TG	442 (80.8)	440 (81.5)	1.00 (reference)	0.14
			GG	105 (19.2)	100 (18.5)	1.05 (0.77–1.42)	

The bold type face indicates a significant results.
[1]OR, odds ratio; CI, confidence interval.–[2]Adjusted for age, gender and smoking status.–[3]HWE, Hardy–Weinberg equilibrium.–[4]nsSNP, non-synonymous SNP; sSNP, synonymous SNP.–[5]N/A, not available.

TABLE III – CASE-CONTROL DISTRIBUTIONS OF *ATM*08 AND *ATM*10 STRATIFIED BY SELECT VARIABLES

	*ATM*08				*ATM*10		
	Cases, *N* (%)	Controls, *N* (%)	Adjusted, OR (95% CI)[1]		Cases, *N* (%)	Controls, *N* (%)	Adjusted, OR (95% CI)
Age							
<61[2]							
CC + CT	233 (83.8)	231 (81.1)	1.00 (reference)	AA + AC	242 (88.3)	265 (94.0)	1.00 (reference)
TT	45 (16.2)	54 (18.9)	**2.32 (1.26–4.27)**	CC	32 (11.7)	17 (6.0)	**2.09 (1.13–3.88)**
>61							
CC + CT	236 (90.1)	228 (90.5)	1.00 (reference)	AA + AC	241 (90.3)	235 (91.1)	1.00 (reference)
TT	26 (9.9)	24 (9.5)	1.05 (0.59–1.89)	CC	26 (9.7)	23 (8.9)	1.12 (0.62–2.02)
Sex							
Male							
CC + CT	256 (87.1)	275 (92.6)	1.00 (reference)	AA + AC	265 (88.0)	246 (92.1)	1.00 (reference)
TT	38 (12.9)	22 (7.4)	**1.87 (1.08-3.26)**	CC	36 (12.0)	21 (7.9)	**1.84 (1.04–3.24)**
Female							
CC + CT	213 (90.6)	220 (92.1)	1.00 (reference)	AA + AC	218 (90.8)	221 (92.1)	1.00 (reference)
TT	22 (9.4)	19 (7.9)	1.17 (0.61–2.23)	CC	22 (9.2)	19 (7.9)	1.16 (0.61–2.21)
Smoking status							
Never smoker							
CC + CT	84 (92.3)	97 (91.5)	1.00 (reference)	AA + AC	96 (93.2)	94 (91.3)	1.00 (reference)
TT	7 (7.7)	9 (8.5)	0.89 (0.32–2.49)	CC	7 (6.8)	9 (8.7)	0.85 (0.30–2.38)
Former smoker							
CC + CT	182 (86.7)	207 (92.8)	1.00 (reference)	AA + AC	184 (86.8)	215 (93.1)	1.00 (reference)
TT	28 (13.3)	16 (7.2)	**2.01 (1.05–3.84)**	CC	28 (13.2)	16 (6.9)	**2.07 (1.08–3.94)**
Current smoker							
CC + CT	203 (89.0)	191 (92.3)	1.00 (reference)	AA + AC	213 (90.3)	191 (92.7)	1.00 (reference)
TT	25 (11.0)	16 (7.7)	1.46 (0.75–2.82)	CC	23 (9.7)	15 (7.3)	1.36 (0.69–2.69)

[1]Adjusted for age, gender and smoking status.–[2]61 is the mean age of control subjects.

els of gamma-radiation-induced DNA damage, strongly suggesting that the elevated risk associated with them are biologically plausible rather than being attained by population selection bias.

Validation through functional assays lends supports to the conclusions drawn from genotyping data. However, such assays are scarce in most published cancer association studies. In the present report, we performed the comet assay, a single cell gel electrophoresis-based laboratory test frequently used to evaluate DNA damage/repair and genotoxicity,[29] to assess the correlation of *ATM* genotypes with the host DNA damage/repair capacity in the control group. We discovered that radiation-induced-, but not baseline-, DNA damage was significantly higher in the homozygous variant genotypes of both *ATM*08 and *ATM*10, when compared to genotypes with at least 1 wild-type allele. This was strongly consistent with the role played by ATM in monitoring radiation-induced DSB DNA damage and initiating the corresponding repair process.[30] The delicate structure of the ATM protein has remained elusive, which has limited in-depth investigation of the interactions between ATM and relevant signal effectors implicated in DSB repair. It is clear that one of the converging effects of the ATM-mediated signal pathways is to induce cell cycle arrest and allow the cell to repair the damage. Therefore, the hypothesis that *ATM* functional variants influence the function of the ATM protein on DNA repair coincide with the phenotypic assay results that the samples with homozygous variants of either *ATM*08 or *ATM*10 showed a significant increase in DNA damage as well as increased NSCLC risk. This finding was further supported by the data showing the associations of diplotype H2–H2,

TABLE IV – DISTRIBUTION OF *ATM* HAPLOTYPES AND NSCLC RISK IN CASE PATIENTS AND CONTROL SUBJECTS BY SMOKING STATUS

Haplotypes sequence	Overall			Never smoker			Former smoker			Current smoker		
	Cases, *N* (%)	Controls, *N* (%)	OR (95% CI)[1]	Cases, *N* (%)	Controls, *N* (%)	OR (95% CI)	Cases, *N* (%)	Controls, *N* (%)	OR (95% CI)	Cases, *N* (%)	Controls, *N* (%)	OR (95% CI)
H1 TTCCGTCCGAT	388 (36.3)	397 (36.6)	1.00 (reference)	63 (34.6)	92 (43.8)	1.00 (reference)	157 (36.9)	154 (33.3)	1.00 (reference)	168 (36.4)	151 (36.7)	1.00 (reference)
H2 ACCCGAGTACG	334 (31.2)	338 (31.2)	1.01 (0.82–1.24)	55 (30.2)	67 (31.9)	1.17 (0.72–1.90)	133 (31.2)	144 (31.2)	0.91 (0.66–1.27)	146 (31.6)	127 (30.8)	1.03 (0.74–1.42)
H3 ACCCATGCAAG	160 (15.0)	156 (14.4)	1.04 (0.80–1.35)	27 (14.8)	22 (10.5)	1.81 (0.95–3.48)	66 (15.5)	69 (14.9)	0.96 (0.64–1.44)	67 (14.5)	65 (15.8)	0.93 (0.62–1.40)
H4 ACCCGAGCAAG	102 (9.5)	99 (9.1)	1.06 (0.78–1.45)	20 (11.0)	16 (7.6)	1.93 (0.91–4.05)	38 (8.9)	49 (10.6)	0.77 (0.48–1.25)	44 (9.5)	34 (8.3)	1.15 (0.70–1.90)
H5 TTCTGTCCGAT	40 (3.7)	53 (4.9)	0.76 (0.49–1.18)	10 (5.5)	6 (2.9)	2.24 (0.75–6.60)	13 (3.1)	27 (5.8)	**0.47 (0.25–0.96)**	17 (3.7)	20 (4.9)	0.79 (0.40–1.57)
H6 TTTCGTCCGAT	33 (3.1)	24 (2.2)	1.47 (0.85–2.54)	5 (2.7)	6 (2.9)	1.38 (0.39–4.84)	13 (3.1)	11 (2.4)	1.23 (0.53–2.85)	15 (3.2)	7 (1.7)	2.00 (0.79–5.06)
Others[2]	13 (1.2)	17 (1.6)	0.76 (0.36–1.59)	2 (1.1)	1 (0.5)	2.18 (0.19–25.5)	6 (1.4)	8 (1.7)	0.72 (0.24–2.13)	5 (1.1)	8 (1.9)	0.59 (0.19–1.85)

[1]Adjusted for age, gender and smoking status.–[2]This category combined all other haplotypes.

TABLE V – *ATM* DIPLOTYPES AND NSCLC RISK

Diplotype	Cases *N* (%)	Controls *N* (%)	OR (95% CI)[1]
H1–H2	120 (22.4)	137 (25.3)	1.00 (reference)
H1–H1	72 (13.5)	68 (12.5)	1.21 (0.80–1.83)
H1–H3	61 (11.4)	56 (10.3)	1.23 (0.79–1.91)
H2–H2	58 (10.8)	41 (7.6)	**1.58 (0.99–2.54)**
H2–H3	46 (8.6)	55 (10.1)	0.92 (0.58–1.47)
H1–H4	32 (6.0)	34 (6.3)	1.05 (0.61–1.81)
H2–H4	30 (5.6)	34 (6.3)	1.02 (0.58–1.77)
H3–H4	21 (3.9)	11 (2.0)	**2.29 (1.05–5.00)**
H2–H5	14 (2.6)	17 (3.1)	0.90 (0.42–1.93)
H1–H5	13 (2.4)	16 (3.0)	0.94 (0.43–2.05)
Others[2]	68 (12.7)	73 (13.5)	1.08 (0.71–1.63)

[1]Adjusted for age, gender and smoking status.–[2]This category combines all other diplotypes.

TABLE VI – ASSOCIATIONS OF GENOTYPES OF *ATM*08 AND *ATM*10 WITH DNA DAMAGE/REPAIR ASSESSED BY COMET ASSAY IN CONTROL SUBJECTS

	Baseline			γ-radiation-induced		
	N	Mean ± SD[1]	*p* value[2]	*N*	Mean ± SD	*p* value
ATM08						
CC + CT	103	1.38 ± 0.70		99	3.79 ± 1.51	
TT	11	1.39 ± 0.79	0.96	11	4.86 ± 2.43	**0.04**
ATM10						
AA + AC	101	1.39 ± 0.72		97	3.79 ± 1.54	
CC	10	1.43 ± 0.80	0.85	10	5.14 ± 2.37	**0.01**

[1]SD, standard deviation.–[2]*p* value for *t* test.

the only analyzed diplotype containing the homozygous variants of both *ATM*08 and *ATM*10, with elevated NSCLC risk. Previous reports have suggested that most mutations/variations in *ATM* region exert aberrant functions by influencing ATM activity instead of its protein expression.[31,32] Analysis of kinase activity of Ser^{1981}-phosphorylated ATM,[6] as well as the expression profile of the total ATM level using peripheral blood cells derived from subjects with different *ATM*08/*ATM*10 genotypes will cast more light on this hypothesis.

No significant gene-dose effect was identified for either *ATM*08 or *ATM*10. This may be because *ATM* is a tumor suppressor gene and, thereby, 2 copies of the gene need to be inactivated before carcinogenesis ensues. This recessive functional fashion is a common theme of many tumor suppressor genes and the "two-hit" hypothesis of carcinogenesis is the most convincing explanation for its working mechanism.[33] We also noticed that the elevated risks for *ATM*08 and *ATM*10 were higher in former smokers than in current smokers. An unambiguous hypothesis regarding interaction between smoking and *ATM* genetic variants has yet to be developed. The genetic effects of *ATM* variants observed in this study may have been overwhelmed by the strong smoking exposure in current smokers. Moreover, as the results of the stratified analyses were based on relatively small sample size, this result needs to be interpreted with caution and requires validation in larger studies. Among the 6 intronic SNPs analyzed, *ATM*02, *ATM*07 and *ATM*09 have been associated with risk of breast cancer[15,16]; however, our data did not suggest that any of these was related to NSCLC risk. *ATM*05, the only nsSNP currently identified as having an MAF $\geq$ 10%, has been implicated in various types of cancer[18–20] but showed no effect in this study. Furthermore, haplotypes constructed using only potential functional SNPs (nsSNPs and regulatory SNPs, including *ATM*01, *ATM*03, *ATM*05 and *ATM*11) did not reveal any association with NSCLC risk (data not shown).

In a recent case-control study, Kim *et al.* described the association of rs664143 (*ATM*09) with increased lung cancer risk in a Korean population.[22] This SNP did not show an evident link with NSCLC risk in our study, possibly due to the remarkable difference in the allelic frequency between these 2

populations.[22] In addition, we restricted our case patients to NSCLC, whereas Kim *et al.* investigated all lung cancer subtypes.

In summary, our study presents the first epidemiological data describing the associations of 2 common *ATM* polymorphisms (*ATM*08 and *ATM*10) and elevated NSCLC risk. The hypothesis that these 2 SNPs function through influencing ATM kinase activity was underscored by the independent phenotypic assay analyzing DNA repair profiles. Nevertheless, we cannot rule out the possibility that other rare *ATM* polymorphisms in LD with these 2 SNPs are the real causative agents. Further investigations exploring the molecular mechanism of the proposed *ATM* functional variations as well as the downstream signal transducers mediating the observed effects are warranted to provide a new dimension to our current understanding of the significance of *ATM* sequence variants in a more inclusive picture of lung carcinogenesis.

References

1. Breuer RH, Postmus PE, Smit EF. Molecular pathology of non-small-cell lung cancer. Respiration 2005;72:313–30.
2. Wu X, Roth JA, Zhao H, Luo S, Zheng YL, Chiang S, Spitz MR. Cell cycle checkpoints, DNA damage/repair, and lung cancer risk. Cancer Res 2005;65:349–57.
3. Zhao H, Spitz MR, Tomlinson GE, Zhang H, Minna JD, Wu X. Gamma-radiation-induced G2 delay, apoptosis, and p53 response as potential susceptibility markers for lung cancer. Cancer Res 2001;61:7819–24.
4. Taylor AM, Byrd PJ. Molecular pathology of ataxia telangiectasia. J Clin Pathol 2005;58:1009–15.
5. Shiloh Y. ATM and related protein kinases: safeguarding genome integrity. Nat Rev Cancer 2003;3:155–68.
6. Bakkenist CJ, Kastan MB. DNA damage activates ATM through intermolecular autophosphorylation and dimer dissociation. Nature 2003;421:499–506.
7. Lee JH, Paull TT. ATM activation by DNA double-strand breaks through the Mre11-Rad50-Nbs1 complex. Science 2005;308:551–4.
8. Thorstenson YR, Roxas A, Kroiss R, Jenkins MA, Yu KM, Bachrich T, Muhr D, Wayne TL, Chu G, Davis RW, Wagner TM, Oefner PJ. Contributions of ATM mutations to familial breast and ovarian cancer. Cancer Res 2003;63:3325–33.
9. Fan R, Kumaravel TS, Jalali F, Marrano P, Squire JA, Bristow RG. Defective DNA strand break repair after DNA damage in prostate cancer cells: implications for genetic instability and prostate cancer progression. Cancer Res 2004;64:8526–33.
10. Thompson D, Duedal S, Kirner J, McGuffog L, Last J, Reiman A, Byrd P, Taylor M, Easton DF. Cancer risks and mortality in heterozygous ATM mutation carriers. J Natl Cancer Inst 2005;97:813–22.
11. Zhang L, Jia G, Li WM, Guo RF, Cui JT, Yang L, Lu YY. Alteration of the ATM gene occurs in gastric cancer cell lines and primary tumors associated with cellular response to DNA damage. Mutat Res 2004;557:41–51.
12. Jones JS, Gu X, Lynch PM, Rodriguez-Bigas M, Amos CI, Frazier ML. ATM polymorphism and hereditary nonpolyposis colorectal cancer (HNPCC) age of onset (United States). Cancer Causes Control 2005;16:749–53.
13. Monni O, Knuutila S. 11q deletions in hematological malignancies. Leuk Lymphoma 2001;40:259–66.
14. Eymin B, Claverie P, Salon C, Leduc C, Col E, Brambilla E, Khochbin S, Gazzeri S. p14ARF activates a Tip60-dependent and p53-independent ATM/ATR/CHK pathway in response to genotoxic stress. Mol Cell Biol 2006;26:4339–50.
15. Lee KM, Choi JY, Park SK, Chung HW, Ahn B, Yoo KY, Han W, Noh DY, Ahn SH, Kim H, Wei Q, Kang D. Genetic polymorphisms of ataxia telangiectasia mutated and breast cancer risk. Cancer Epidemiol Biomarkers Prev 2005;14:821–5.
16. Angele S, Romestaing P, Moullan N, Vuillaume M, Chapot B, Friesen M, Jongmans W, Cox DG, Pisani P, Gerard JP, Hall J. ATM haplotypes and cellular response to DNA damage: association with breast cancer risk and clinical radiosensitivity. Cancer Res 2003;63:8717–25.
17. Tamimi RM, Hankinson SE, Spiegelman D, Kraft P, Colditz GA, Hunter DJ. Common ataxia telangiectasia mutated haplotypes and risk of breast cancer: a nested case-control study. Breast Cancer Res 2004;6:R416–R22.
18. Gutierrez-Enriquez S, Fernet M, Dork T, Bremer M, Lauge A, Stoppa-Lyonnet D, Moullan N, Angele S, Hall J. Functional consequences of ATM sequence variants for chromosomal radiosensitivity. Genes Chromosomes Cancer 2004;40:109–19.
19. Maillet P, Chappuis PO, Vaudan G, Dobbie Z, Muller H, Hutter P, Sappino AP. A polymorphism in the ATM gene modulates the penetrance of hereditary non-polyposis colorectal cancer. Int J Cancer 2000;88:928–31.
20. Heikkinen K, Rapakko K, Karppinen SM, Erkko H, Nieminen P, Winqvist R. Association of common ATM polymorphism with bilateral breast cancer. Int J Cancer 2005;116:69–72.
21. Koren M, Kimmel G, Ben-Asher E, Gal I, Papa MZ, Beckmann JS, Lancet D, Shamir R, Friedman E. ATM haplotypes and breast cancer risk in Jewish high-risk women. Br J Cancer 2006;94:1537–43.
22. Kim JH, Kim H, Lee KY, Choe KH, Ryu JS, Yoon HI, Sung SW, Yoo KY, Hong YC. Genetic polymorphisms of ataxia telangiectasia mutated affect lung cancer risk. Hum Mol Genet 2006;15:1181–6.
23. Langholz B, Bernstein JL, Bernstein L, Olsen JH, Borresen-Dale AL, Rosenstein BS, Gatti RA, Concannon P. On the proposed association of the ATM variants 5557G>A and IVS38-8T>C and bilateral breast cancer. Int J Cancer 2006;119:724–5.
24. Bonnen PE, Story MD, Ashorn CL, Buchholz TA, Weil MM, Nelson DL. Haplotypes at ATM identify coding-sequence variation and indicate a region of extensive linkage disequilibrium. Am J Hum Genet 2000;67:1437–51.
25. Gu J, Zhao H, Dinney CP, Zhu Y, Leibovici D, Bermejo CE, Grossman HB, Wu X. Nucleotide excision repair gene polymorphisms and recurrence after treatment for superficial bladder cancer. Clin Cancer Res 2005;11:1408–15.
26. Schabath MB, Spitz MR, Grossman HB, Zhang K, Dinney CP, Zheng PJ, Wu X. Genetic instability in bladder cancer assessed by the comet assay. J Natl Cancer Inst 2003;95:540–7.
27. Stephens M, Donnelly P. A comparison of bayesian methods for haplotype reconstruction from population genotype data. Am J Hum Genet 2003;73:1162–9.
28. Chen YC, Giovannucci E, Lazarus R, Kraft P, Ketkar S, Hunter DJ. Sequence variants of Toll-like receptor 4 and susceptibility to prostate cancer. Cancer Res 2005;65:11771–8.
29. Tice RR, Agurell E, Anderson D, Burlinson B, Hartmann A, Kobayashi H, Miyamae Y, Rojas E, Ryu JC, Sasaki YF. Single cell gel/comet assay: guidelines for in vitro and in vivo genetic toxicology testing. Environ Mol Mutagen 2000;35:206–21.
30. Kurz EU, Lees-Miller SP. DNA damage-induced activation of ATM and ATM-dependent signaling pathways. DNA Repair (Amst) 2004;3:889–900.
31. Banin S, Moyal L, Shieh S, Taya Y, Anderson CW, Chessa L, Smorodinsky NI, Prives C, Reiss Y, Shiloh Y, Ziv Y. Enhanced phosphorylation of p53 by ATM in response to DNA damage. Science 1998;281:1674–7.
32. Canman CE, Lim DS, Cimprich KA, Taya Y, Tamai K, Sakaguchi K, Appella E, Kastan MB, Siliciano JD. Activation of the ATM kinase by ionizing radiation and phosphorylation of p53. Science 1998;281:1677–9.
33. Knudson A. Alfred Knudson and his two-hit hypothesis. (Interview by Ezzie Hutchinson). Lancet Oncol 2001;2:642–5.

Supplemental data

Figure S1. CpG islands of the genes analyzed. Exons of individual genes are depicted as empty boxes and transcription starting sites at exon 1 are marked with arrows. Vertical bars show individual CpG sites. Black boxes and lines flanked with arrow heads indicate areas studied for DNA methylation by pyrosequencing and methylation specific PCR, respectively.

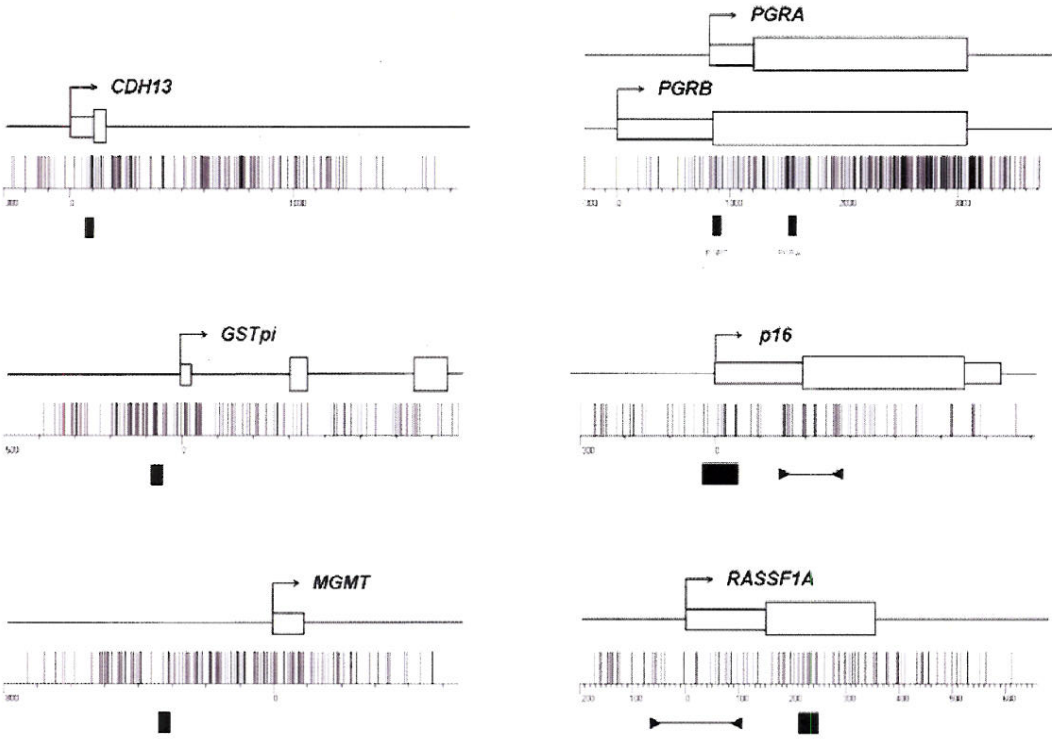
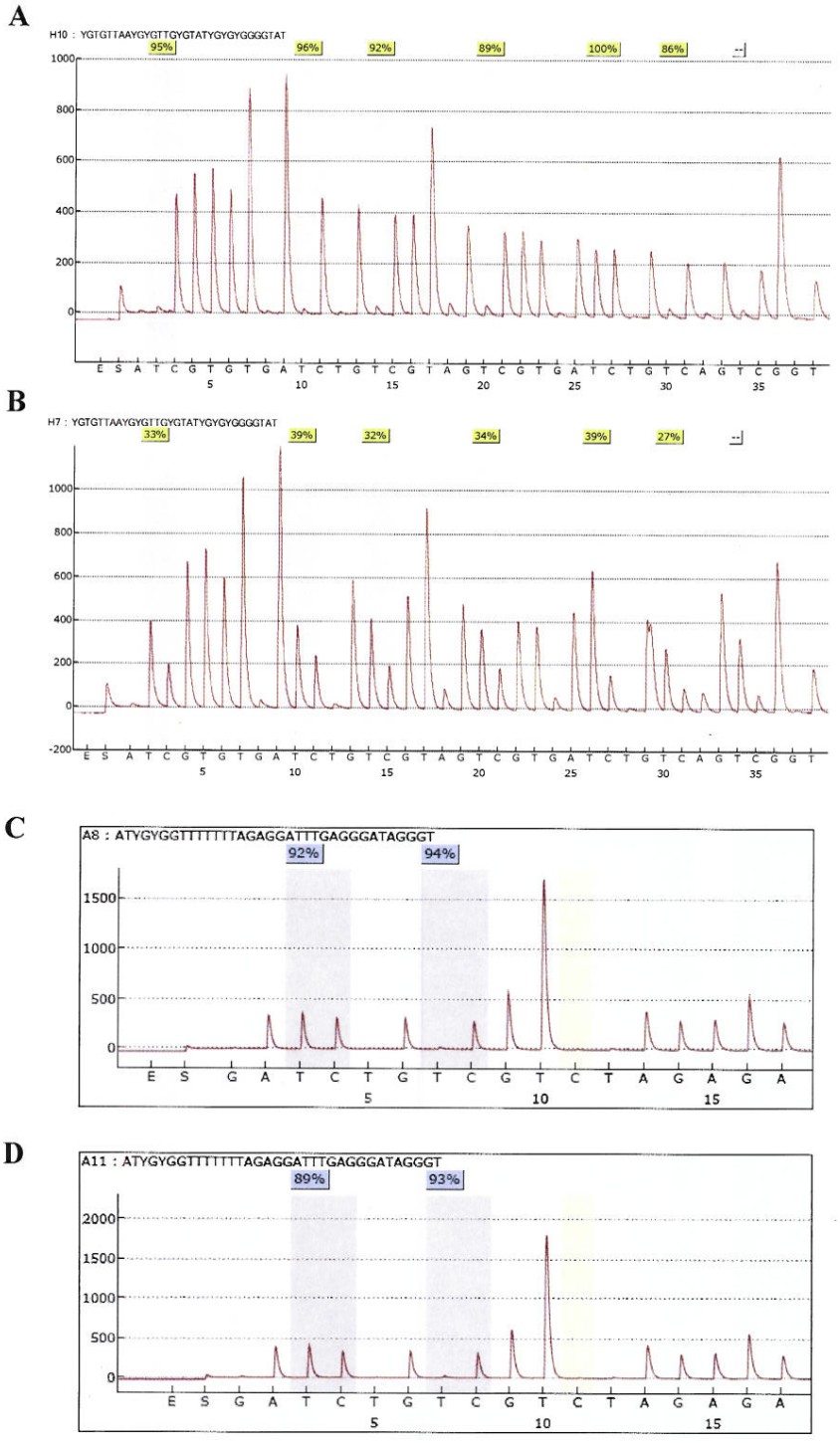


Figure S2. Representative graphs showing demethylation of *RASS F1A* promoter but not *p16* promoter by ΔDNMT3B2/4 siRNA treatment in H1299 cells measured by pyrosequencing. *RASSF1A* promoter methylation status in cells treated with control siRNA (A) or ΔDNMT3B2/4 siRNA (B). *p16* promoter methylation status in cells treated with control siRNA (C) or ΔDNMT3B2/4 siRNA (D).



Oncogene (2007) 26, 6896–6904
© 2007 Nature Publishing Group All rights reserved 0950-9232/07 $30.00
www.nature.com/onc

ORIGINAL ARTICLE

A genetic mouse model for metastatic lung cancer with gender differences in survival

S Zheng[1,4], AK El-Naggar[2], ES Kim[3], JM Kurie[3] and G Lozano[1,4]

[1]*Department of Cancer Genetics, The University of Texas MD Anderson Cancer Center, Houston, TX, USA;* [2]*Department of Pathology, The University of Texas MD Anderson Cancer Center, Houston, TX, USA;* [3]*Department of Thoracic/Head and Neck Medical Oncology, The University of Texas MD Anderson Cancer Center, Houston, TX, USA and* [4]*Program in Genes and Development, The University of Texas Graduate School of Biomedical Sciences, Houston, TX, USA*

Lung cancer is a devastating disease with poor prognosis. The design of better therapies for lung cancer patients would be greatly aided by good mouse models that closely resemble the human disease. Unfortunately, current models for lung adenocarcinoma are inadequate due to the absence of metastases. In this study, we incorporated both *K-ras* and *p53* missense mutations into the mouse genome and established a more faithful genetic model for human lung adenocarcinoma, the most common type of lung cancer. Mice with both mutations developed advanced lung adenocarcinomas that were highly aggressive and metastasized to multiple intrathoracic and extrathoracic sites in a pattern similar to that of human lung cancer. These mice also showed a gender difference in cancer-related death. Additionally, the presence of both mutations induced pleural mesotheliomas in 23% of these mice. This mouse model recapitulates the metastatic nature of human lung cancer and will be invaluable to further probe the molecular basis of metastatic lung cancer and for translational studies.
Oncogene (2007) **26,** 6896–6904; doi:10.1038/sj.onc.1210493; published online 7 May 2007

Keywords: *p53*; *K-ras*; mesotheliomas

Introduction

Lung cancer is the leading cause of cancer-related deaths. Although considerable effort has provided insight into the molecular events leading to the progression and metastasis of lung cancer, little improvement in treatment outcome has been achieved.

Many mouse models have been developed for lung cancer to test new treatment options. Xenograft models, in which human tumor cells are grafted into immune compromised mice, have been extensively used for preclinical testing. However, these models have intrinsic flaws, generally resulting in poor predicative power of the clinical efficacy of anticancer agents (Becher and Holland, 2006; Sausville and Burger, 2006). Susceptible mouse strains, including A/J and SWR, spontaneously develop lung tumors, with the sensitivity strongly associated with a polymorphism in intron 2 of the *K-ras* gene (You *et al.*, 1992; Malkinson and You, 1994). These strains are also highly sensitive to the induction of lung tumors by chemical carcinogens. For example, a single dose of 4-(methylnitrosamino)-1-(3-pyridyl)-1-butanone (NNK) in A/J mice induces alveolar hyperplasias, lung adenomas, and adenocarcinomas 42 weeks after carcinogen treatment (Belinsky *et al.*, 1993). Increased tumor induction by vinyl carbamate was demonstrated in transgenic mice carrying a mutant *p53* with an Ala-to-Val mutation at codon 135 and a deletion of a *K-ras* allele (Wang *et al.*, 2006a, b). These and many other studies illustrate that the A/J model is a useful one to evaluate chemointerventive agents of lung tumors (Castonguay *et al.*, 1991; Hecht *et al.*, 1991). Unfortunately, lung tumors in A/J mice treated with carcinogens are generally not aggressive and do not metastasize.

To overcome these deficiencies, investigators have attempted to establish models that mimic the genetic signature of lung cancer. Two of the most common molecular changes identified in human lung cancer are mutations of the *p53* and *K-ras* genes (Mitsudomi *et al.*, 1992; Salgia and Skarin, 1998). Missense mutations in the *p53* gene are found in more than 50% of human lung cancers, while *p53* deletions are rare (Takahashi *et al.*, 1989; Chiba *et al.*, 1990; Greenblatt *et al.*, 1994). The hot spot p53 mutations in lung cancer occur at amino acids 157, 158, 175, 245, 248, 249 and 273 (Toyooka *et al.*, 2003; Vahakangas *et al.*, 2001). Constitutive activation of the *K-ras* gene through mutations occurs in 30% of lung cancers, about 80% of which occur at codon 12 (Rodenhuis *et al.*, 1988; Rodenhuis and Slebos, 1992).

Current genetic models of human lung adenocarcinoma are also limited by the absence or rare occurrence of metastasis (Meuwissen and Berns, 2005). In one model, mice inherit a latent mutant *K-ras* allele at the endogenous locus (*K-ras*^{LA1}), which is spontaneously

Correspondence: Professor G Lozano, Department of Cancer Genetics, The University of Texas MD Anderson Cancer Center, 1515 Holcombe Blvd., Unit 1010, Houston, TX, USA.
E-mail: gglozano@mdanderson.org
Received 23 September 2006; revised 31 January 2007; accepted 9 March 2007; published online 7 May 2007

activated *in vivo* (Johnson *et al.*, 2001). The activated *K-ras*^{LA1} allele expresses mutant K-ras with an aspartic acid at codon 12, inducing multifocal lung adenocarcinomas in heterozygous mice (*K-ras*$^{LA1/+}$). The advantage of this model is that somatic activation of the *K-ras* proto-oncogene in mouse lung mimics mutational activation of the *K-ras* gene occurring in human lung cancer. The disadvantage, however, is that lung adenocarcinomas in this model, and in one with an accompanying deletion of *p53*, rarely metastasize.

Likewise, mouse models with *p53* mutations have recently been described. One particular mutation generated at the endogenous *p53* allele contains an arginine-to-histidine substitution at codon 172, which corresponds to the hot spot mutation at 175 in human *p53* (Liu *et al.*, 2000; Lang *et al.*, 2004; Olive *et al.*, 2004). The first mouse model with this mutation expresses low levels of mutant p53 because of an intronic deletion of a single nucleotide (p53$^{R172H\Delta g}$) (Liu *et al.*, 2000). Strikingly, however, *p53*$^{R172H\Delta g/+}$ mice develop osteosarcomas and carcinomas that metastasize at a frequency of 69 and 40%, respectively, a phenotype not observed in *p53*$^{+/-}$ mice. This metastatic phenotype was confirmed in the latest models expressing mutant p53 at appropriate levels (Lang *et al.*, 2004; Olive *et al.*, 2004). These models demonstrate that mutant p53 has a gain of function in addition to loss of function *in vivo*, and reproduce the metastatic nature of human cancers. Unfortunately, however, mice expressing mutant p53 rarely develop lung adenocarcinomas.

Since mice inheriting a *p53* missense mutation develop a wide range of tumors that metastasize, we postulated that *K-ras* mutation could initiate lung adenocarcinoma, while *p53* mutation could exacerbate the phenotype by promoting dissemination of cancer cells. In an effort to develop a more faithful mouse model, one with similar molecular changes and metastatic behavior to human lung cancer, we generated mice with both *p53* and *K-ras* missense mutations. We found that the combination of these mutations resulted in lung adenocarcinomas with a high incidence of metastases and gender differences in cancer-related death. This new mouse model thus most closely simulates human metastatic lung cancer and provides an immunocompetent system to test novel therapeutic agents *in vivo*.

Results

Lung cancer in p53$^{R172H\Delta g/+}$ K-ras$^{LA1/+}$ *mice*

The *p53*$^{R172H\Delta g/+}$ mice carrying a missense mutation in one *p53* allele (Liu *et al.*, 2000) were crossed with *K-ras*$^{LA1/+}$ mice carrying a latent mutant *K-ras* allele (Johnson *et al.*, 2001) to generate *K-ras*$^{LA1/+}$, *p53*$^{R172H\Delta g/+}$ and *p53*$^{R172H\Delta g/+}$ *K-ras*$^{LA1/+}$ mice. All genotypes produced from the above cross were included in the cohort study and were in a 129Sv background. The *p53*$^{R172H\Delta g/+}$ *K-ras*$^{LA1/+}$ mice are sometimes referred to as double mutant mice for simplicity. For comparison, *p53*$^{+/-}$ *K-ras*$^{LA1/+}$ mice were also generated and included in this study.

At necropsy, *p53*$^{R172H\Delta g/+}$ *K-ras*$^{LA1/+}$ mice had substantial lung tumor burden (Figure 1Aa). Histologically, the lesions were atypical adenomatous hyperplasia (AAH), adenomas and adenocarcinomas. AAH, the precursor lesion of human lung adenocarcinoma (Kitamura *et al.*, 1999), was identified in multifocal and diffuse patterns contiguous with well-defined or ill-defined adenomas and adenocarcinomas (Figure 1Ba). Lung adenomas and adenocarcinomas were frequently juxtaposed and merging (Figure 1Bb). The majority of double mutant mice had multiple large or diffuse adenocarcinomas, which had papillary/glandular phenotypes or were poorly differentiated (Figure 1Aa and Bc, d). Lung adenocarcinoma cells usually had enlarged vesicular nuclei with prominent nucleoli, similar to human lung adenocarcinoma cells. Surfactant protein C (SPC), which is frequently expressed in human lung adenocarcinoma, was detected in murine lung adenocarcinomas by immunohistochemistry (Figure 1Be). Papillary hyperplasia of bronchial epithelial cells was also observed in double mutant mice (Figure 1Bf). These hyperplastic cells are positive for CC10, a Clara cell marker, suggesting an alternative origin of lung adenocarcinoma in this model (Figure 1Bg).

Strikingly, lung adenocarcinomas in this model were highly invasive and metastatic (Figure 1Ab–e and Bh, i). Metastatic lesions in the lymph node and liver stained positive for SPC (Figure 1Bh and i, respectively).

Pleural mesothelioma, which originates from mesothelial cells of the pleura, was also observed in *p53*$^{R172H\Delta g/+}$ *K-ras*$^{LA1/+}$ mice. Grossly, multiple lesions appeared on the pleura and multiple enlarged lymph nodes were observed in the mediastinum (Figure 2A). Microscopically, mesothelial cells were observed proliferating in a papillary pattern into pleural space (Figure 2Ba). Early-stage pleural mesotheliomas were localized and clearly identified on top of hyperplastic lung tissue and adenoma (Figure 2Bb and c). Late-stage pleural mesotheliomas invaded lung parenchyma (Figure 2Bd). The majority of pleural mesotheliomas in this model were biphasic, composed of both epithelioid and sarcomatoid cancer cells with pronounced pleomorphism and marked nuclear atypia. Sarcomatoid lesions were associated with spindle cell fibrous components, resembling human fibrous mesothelioma (Figure 2Be). Highly aggressive mesotheliomas extended into surrounding tissues and metastasized to mediastinal lymph nodes, liver, pancreas, ovary, and other sites (Figure 2Bf and data not shown). Pleural mesotheliomas in this model were positive for at least one marker, Calretinin or Cytokeratin 6 (Figure 2Bg, h and Table 1), and negative for SPC (Figure 1Be) and for periodic acid-Schiff (PAS) staining (data not shown). These data further verified the histological diagnosis of mesothelioma. There are no reports of pleural mesothelioma in previously published *K-ras*$^{LA1/+}$ mice probably due to the low frequency of this tumor type (Johnson *et al.*, 2001). We also did not observe mesotheliomas in *p53*$^{R172H\Delta g/+}$ or *p53*$^{R172H/+}$ mice (Liu *et al.*, 2000; Lang *et al.*, 2004).

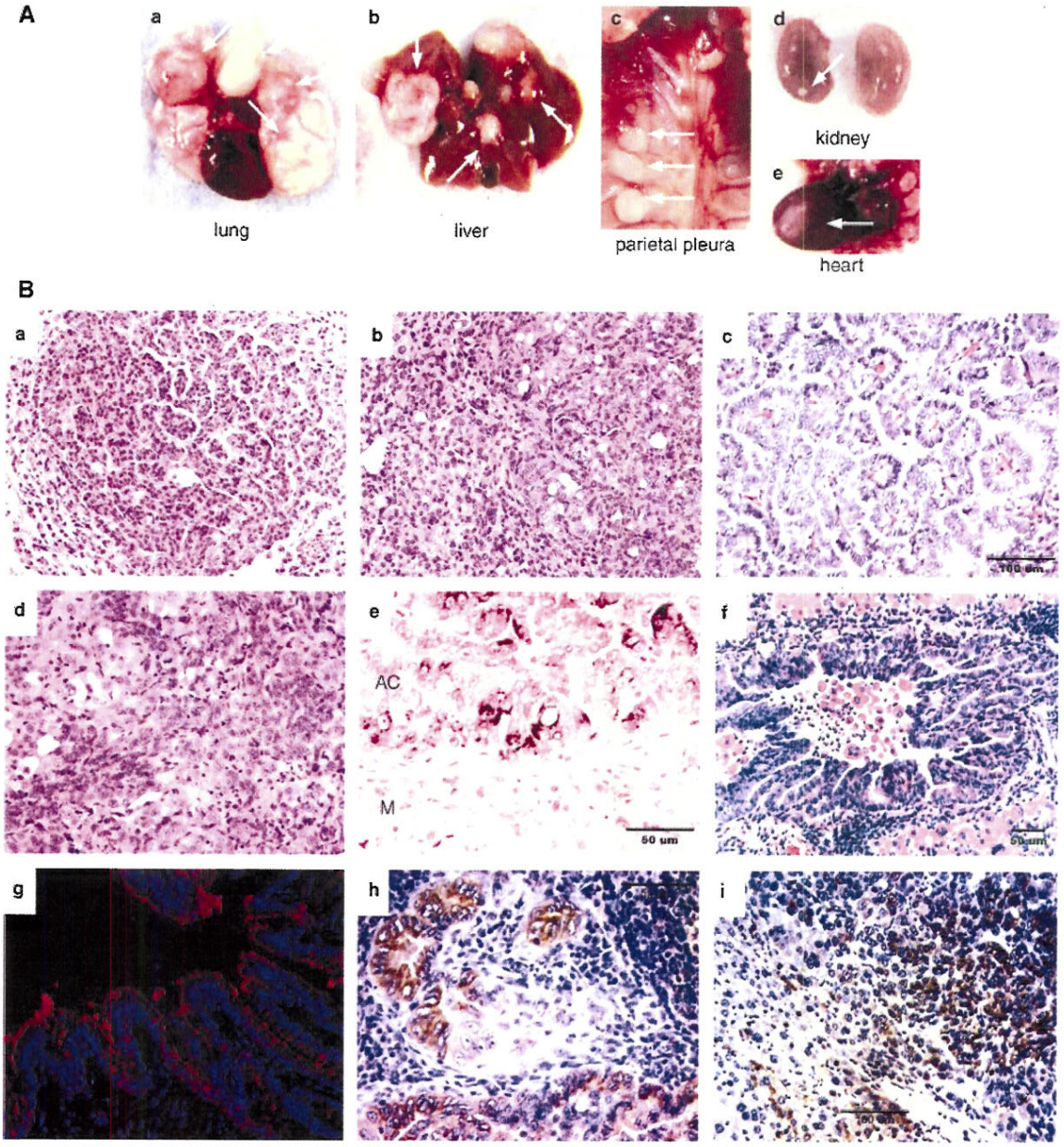


Figure 1 $p53^{R172H\Delta g/+}$ $K\text{-}ras^{LA1/+}$ mice developed highly aggressive lung adenocarcinomas with metastases to multiple sites. (**A**) Photographs of lung tissue with high tumor burden, adenocarcinomas (a), metastatic lesions to the liver (b), parietal pleura (c), kidney (d), and heart (e). Representative tumors are marked by arrows. (**B**) Photomicrographs of adenomatous alveolar hyperplasia (a), merged adenoma and adenocarcinoma (b), lung adenocarcinoma with a papillary growth pattern (c), poorly differentiated lung adenocarcinoma (d). Immunohistochemistry to detect SPC staining in lung adenocarcinoma (AC) and adjacent pleural mesothelioma (M) (e). A bronchial hyperplasia of epithelial cells (f) was stained for CC10 by immunofluorescence (red) and nuclei are stained with Topro 3 (blue) (g). SPC staining of lung adenocarcinoma metastases to the lymph node (h) and liver (i). Tumor sections in (a–d) and (f) were stained by H&E.

Tumor spectrum in $p53^{R172H\Delta g/+}$ $K\text{-}ras^{LA1/+}$ *mice*

All $p53^{R172H\Delta g/+}$ $K\text{-}ras^{LA1/+}$ mice developed lung tumors. The major type of malignancy was lung adenocarcinoma, which developed in 52 of 56 double mutant mice (Table 2). Pleural mesothelioma was identified in 13 of these 56 mice. Six out of these 13 mice also had peritoneal mesotheliomas. Grossly, anatomical extension of thoracic lesions into the abdominal cavity through the diaphragm was noted in three of the six mice with peritoneal mesotheliomas. In addition to lung tumors, lymphoma infiltration in lung appeared in 6/56 (10.7%) of double mutant mice. Mice with both lung adenocarcinomas and lung lymphomas did not develop any metastases, probably because they died at a younger age than mice with only lung adenocarcinomas (median survival of 256 days compared to 317 days for those without lymphomas; $P = 0.0053$).

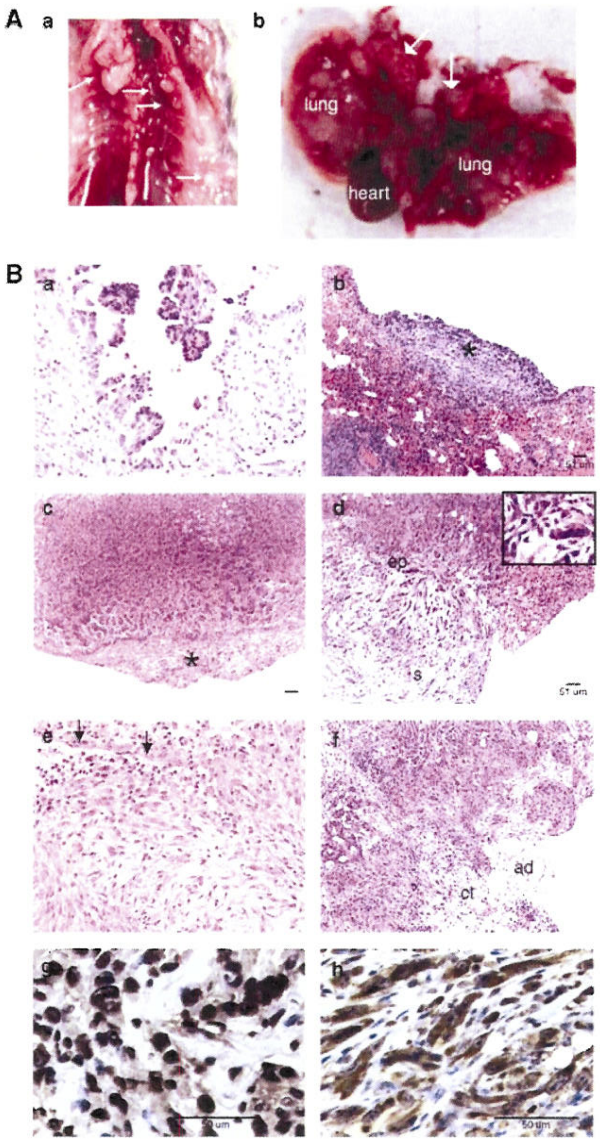


Figure 2 $p53^{R172H\Delta g/+}$ $K\text{-}ras^{LA1/+}$ mice also developed highly aggressive pleural mesotheliomas. (**A**) Photographs of multiple lesions of mesothelioma (diagnosed microscopically) on parietal pleura (a, arrows) and metastases in mediastinum (b, arrows). (**B**) Photomicrographs of bland papillary proliferation of mesothelial cells arising from the pleural lining (a) nodular pleural mesothelioma (*) on top of lung parenchyma (b) localized pleural mesothelioma (*) clearly distinguished from the underlying adenoma with glandular differentiation (c) biphasic pleural mesothelioma having both epithelial (ep) and sarcomatoid (s) components encroached into lung parenchyma (d), inset shows pleomorphism and nuclear atypia in mesotheliomas (d), a fibrous mesothelioma growing exophytically (e, arrows mark the visceral pleura), pleural mesothelioma spread to extrapleural connective (ct) and adipose (ad) tissues (f) positive Calretinin staining (g) and positive staining for Cytokeratin 6 (h) in mesotheliomas by immunohistochemistry. Tumor sections in (a–f) were stained by H&E.

For comparison, 48 $K\text{-}ras^{LA1/+}$ mice were also analysed. They developed a tumor spectrum similar to that of double mutant mice (Table 2). Pleural mesotheliomas were identified in 4/48 $K\text{-}ras^{LA1/+}$ mice, but no mesotheliomas were identified in the peritoneum. The incidence of pleural mesotheliomas in $K\text{-}ras^{LA1/+}$ mice was lower than that in double mutant mice (χ^2, $P<0.05$). As previously reported, $p53^{R172H\Delta g/+}$ mice develop lymphomas, sarcomas, and carcinomas, a few of which are lung adenocarcinomas (Liu *et al.*, 2000) (Table 2).

Table 1 Calretinin and Cytokeratin 6 immunostaining in mesothelioma

Mesothelioma	*Calretinin*	*Cytokeratin 6*
1	+	–
2	NS[a]	+
3	+	+
4	+	–
5	–	+
6	–	+
7	+	–
8	+	–
9	+	NS
10	+	–
11[b]	+	–

[a]NS: not stained due to small size. [b]A putative metastasis.

High metastatic potential of lung adenocarcinoma in $p53^{R172H\Delta g/+}$ $K\text{-}ras^{LA1/+}$ *mice*

Lung adenocarcinomas in $p53^{R172H\Delta g/+}$ $K\text{-}ras^{LA1/+}$ mice were much more aggressive and metastatic than those in $K\text{-}ras^{LA1/+}$ mice. At 3–4 months of age, double mutant mice developed AAH, lung adenomas, and small, focal adenocarcinomas with no metastasis (data not shown). Metastases were identified at 7–14 months of age in dissected double mutant mice. Histologically, metastases were found in 19 of 52 $p53^{R172H\Delta g/+}$ $K\text{-}ras^{LA1/+}$ mice that had developed lung adenocarcinomas (36.5%), while metastases were found in the two of 44 $K\text{-}ras^{LA1/+}$ mice that had developed lung adenocarcinomas (4.5%), which was significantly different (χ^2, $P<0.001$). Lung adenocarcinomas were widely disseminated to multiple intrathoracic and extrathoracic sites in double mutant mice (Table 3). Seeding was restricted to the mediastinum in the two $K\text{-}ras^{LA1/+}$ mice with metastases (Table 3). The average number of sites of metastases was 2.3 per $p53^{R172H\Delta g/+}$ $K\text{-}ras^{LA1/+}$ mouse. Mediastinal structures were the major metastatic sites (mediastinal lymph nodes/adipose tissue and heart). Extrathoracic sites of metastases included liver, adrenal glands, body wall, kidneys, and mesentery/lymph nodes. Previously published data show that $p53^{+/-}$ $K\text{-}ras^{LA1/+}$ mice develop lung adenocarcinomas with more malignant features, but no metastasis (Johnson *et al.*, 2001). We also analyzed five $p53^{+/-}$ $K\text{-}ras^{LA1/+}$ mice and found that they developed lung tumors but no metastasis, as reported previously (data not shown). Thus, the metastatic burden was the most remarkable difference among $p53^{R172H\Delta g/+}$ $K\text{-}ras^{LA1/+}$, $p53^{+/-}$ $K\text{-}ras^{LA1/+}$ and $K\text{-}ras^{LA1/+}$ mice. Notably, not all enlarged nodules seen in the mediastinum at necropsy were metastases. These were reactive lymph nodes, an observation consistent with that in human lung cancer (Kerr*et al.*, 1992).

Table 2 Tumor spectra of $p53^{R172H\Delta g/+}$ $K\text{-}ras^{LA1/+}$, $K\text{-}ras^{LA1/+}$, and $p53^{R172H\Delta g/+}$ mice

Tumor types	*$p53^{R172HAg/+}$ $K\text{-}ras^{LA1/+}$ # of mice (%)*[a]	*$K\text{-}ras^{LA1/+}$ # of mice (%)*[b]	*$p53^{R172HAg/+}$ # of mice (%)*[c]
Lung/pleura			
Adenocarcinoma	35 (62.5)	34 (70.8)	3 (13)
Adenocarcinoma + mesothelioma	13 (23.2)[d]	4 (8.3)[d]	0
Adenocarcinoma + lymphoma	4 (7.1)	6 (12.5)	1 (4.3)
Adenoma[e] ± lymphoma	4 (7.1)	4 (8.3)	1 (4.3)
Sarcoma			
Osteosarcoma	0	0	8 (34.8)
Angiosarcoma	4 (7.1)	4 (8.3)	0
Fibrosarcoma	3 (5.4)	1 (2.1)	0
Unclassified	2 (3.6)	0	3 (13)
Lymphoma	6 (10.7)	12 (25)	8 (34.8)
Carcinomas (other)			
Pancreatic carcinoma	2 (3.6)	0	0
Squamous carcinoma	1 (1.8)	1 (2.1)	5 (21.7)
Rectal mucinous adenocarcinoma	0	2 (4.2)	0
Melanoma	0	1 (2.1)	0
Papilloma	9 (16.1)	13 (27.1)	0

[a]Total 56 $p53^{R172HAg/+}$ $K\text{-}ras^{LA1/+}$ mice were analysed. [b]Total 48 $K\text{-}ras^{LA1/+}$ mice were analysed. [c]Total 23 $p53^{R172HAg/+}$ mice were analysed. [d]χ^2, $P<0.05$. [e]Mice in this category did not have overt adenocarcinomas.

Table 3 Site and frequency of metastases from primary lung adenocarcinomas

Sites of metastases	*$p53^{R172HAg/+}$ $K\text{-}ras^{LA1/+}$ #/total with metastases (%)*[a]	*$K\text{-}ras^{LA1/+}$ #/total with metastases (%)*[b]	*$p53^{R172HAg/-}$ #/total with metastases (%)*[c]
Intrathoracic sites			
Mediastinal lymph node	13/19 (68.4)	2/2 (100)	1/1 (100)
Heart	4/19 (21.1)	0/2	1/1 (100)
Parietal pleura	3/19 (15.8)	0/2	0/1
Diaphragm	3/19 (15.8)	0/2	0/1
Extrathoracic sites			
Liver	3/19 (15.8)	0/2	1/1 (100)
Adrenal gland	4/19 (21.1)	0/2	0/1
Kidney	2/19 (10.5)	0/2	0/1
Mesentery/lymph node	2/19 (10.5)	0/2	0/1
Pancreas	1/19 (5.3)	0/2	0/1
Eye tissue	1/19 (5.3)	0/2	0/1
Body wall[d]	6/19 (31.6)	0/2	1/1 (100)
Mammary	1/19 (5.3)	0/2	0/1

[a]Total 52 $p53^{R172HAg/+}$ $K\text{-}ras^{LA1/+}$ mice with lung adenocarcinomas were analysed for metastases. [b]Total 44 $K\text{-}ras^{LA1/+}$ mice with lung adenocarcinomas were analysed for metastases. [c]Total 4 $p53^{R172HAg/+}$ mice with lung adenocarcinomas were analysed for metastases. [d]Including skeletal muscle on trunk and subcutaneous tissue/lymph node. Lesions that did not penetrate parietal pleura were considered as metastases.

The status of the wild-type *p53* allele was examined in lung adenocarcinomas and metastases of $p53^{R172H\Delta g/+}$ $K\text{-}ras^{LA1/+}$ mice by quantitative real-time PCR using specific TaqMan probes to differentiate wild-type and mutant alleles. Loss of heterozygosity (LOH) was detected in 81.8% (9/11) of end-stage lung adenocarcinomas and 71.4% (10/14) of macroscopic metastases (Table 4).

Since the $K\text{-}ras^{LA1}$ allele is a latent allele that is spontaneously activated in somatic cells, the expression of mutant *K-ras* was analysed in lung cancers and metastases at mRNA and protein levels (Figure 3). Mutant $K\text{-}ras^{G12D}$ having a glycine-to-aspartic acid substitution at codon 12 was expressed in lung adenocarcinomas isolated from both double mutant and $K\text{-}ras^{LA1/+}$ mice, and in metastases and mesotheliomas isolated from double mutant mice. Moreover, histologically normal lung tissue adjacent to lung adenocarcinoma isolated from double mutant mice and normal lung tissue isolated from wild-type mice did not show the expression of mutant *K-ras* by either protein or mRNA analysis. Thus, both *p53* (inherited) and *K-ras* (acquired) mutations were present in lung cancers and metastases.

Table 4 The status of wild-type p53 in tumors of K-ras$^{LA1/+}$ p53$^{R172H\Delta g/+}$ mice

Tumor[a]	$2^{-\Delta\Delta Ct}$	*LOH*[b]
Lung adenocarcinoma 1	0.18	–
Lung adenocarcinoma 2	0.08	+
Lung adenocarcinoma 3	0.11	+
Lung adenocarcinoma 4	0.03	+
Lung adenocarcinoma 5	0.01	+
Lung adenocarcinoma 6	0.12	+
Lung adenocarcinoma 7	0.55	–
Lung adenocarcinoma 8	0.05	+
Lung adenocarcinoma 9	0	+
Lung adenocarcinoma 10	0.03	+
Lung adenocarcinoma 11	0.14	+
Metastasis 1	0.25	–
Metastasis 2	0.25	–
Metastasis 3	0.01	+
Metastasis 4	0.35	–
Metastasis 5	0.01	+
Metastasis 6	0.06	+
Metastasis 7	0.15	+
Metastasis 8	0.22	–
Metastasis 9	0.02	+
Metastasis 10	0.04	+
Metastasis 11	0	+
Metastasis 12	0.01	+
Metastasis 13	0.11	+
Metastasis 14	0	+

Abbreviation: LOH, loss of heterozygosity. [a]Only the largest lung adenocarcinoma from each mouse and macroscopically visible metastases were analysed for LOH. All tumors were diagnosed microscopically. [b]The $2^{-\Delta\Delta Ct}$ values of $\leqslant 0.15$, 0.15–0.6 and >0.6 indicate 0, 1 or 2 copies of wild-type *p53* alleles, respectively (see Materials and methods for details).

Survival of p53$^{R172H\Delta g/+}$K-ras$^{LA1/+}$ *mice*

Mice of the various genotypes were monitored daily and killed if they showed signs of respiratory distress, lethargy, decreased body weight, or abdominal distension. Double mutant mice had significantly reduced survival when compared to other littermates ($P<0.0001$, Figure 4a). Double mutant mice developed much more aggressive lung cancers and higher tumor burden than *K-ras*$^{LA1/+}$ mice, leading to shorter lifespans. The median survival for double mutant mice was 266 days compared to 373 days for *K-ras*$^{LA1/+}$ mice. The *p53*$^{+/-}$ *K-ras*$^{LA1/+}$ mice showed a very similar survival curve to published data, and indicated no difference in survival as compared to *p53*$^{R172H\Delta g/+}$ *K-ras*$^{LA1/+}$ mice (Figure 4a). However, a significant difference in cumulative cancer-related death was observed between male and female double mutant mice ($P=0.0071$, Figure 4b). This gender difference in cancer-related death was not observed for *K-ras*$^{LA1/+}$ and *p53*$^{R172H\Delta g/+}$ littermates (Supplementary Figure 1A-B). The cumulative deaths for female and male wild-type littermates were also similar to each other (Supplementary Figure 1C).

Discussion

Current mouse models for lung cancer develop lung adenocarcinomas, but do not metastasize (Nikitin *et al*.,

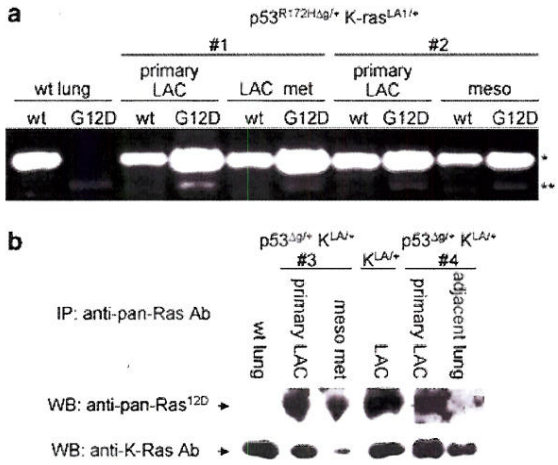


Figure 3 The expression of mutant *K-ras* in primary lung cancers and metastases. (**a**) Mutant *K-ras* was detected in primary lung cancers and metastases that were isolated from different double mutant mice, but not in normal lung tissue isolated from wild-type mice by RT–PCR. *Specific amplification; **nonspecific amplification. wt, wild-type; G12D, *K-ras*^{G12D}-specific primers to the missense mutation at codon 12; LAC, lung adenocarcinoma; met, metastasis; meso, mesothelioma. (**b**) Mutant K-ras was analysed in primary lung cancers, metastases and histologically normal lung tissues adjacent to lung adenocarcinoma by immunoprecipitation followed by western blots. Anti-pan-Ras^{12D} antibody specific for mutant Ras was probed first. The same membrane was stripped and probed with anti-K-Ras antibody. p53$^{\Delta g/+}$, p53$^{R172H\Delta g/+}$; K$^{LA/+}$, K-ras$^{LA1/+}$.

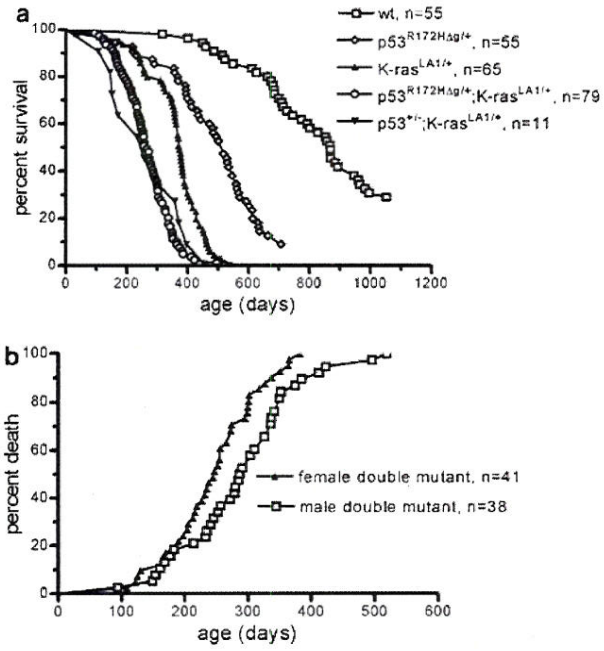


Figure 4 Kaplan–Meier survival of mice with different genotypes. (**a**) *p53*$^{R172H\Delta g/+}$ *K-ras*$^{LA1/+}$ mice had significantly reduced survival compared with *K-ras*$^{LA1/+}$, *p53*$^{R172H\Delta g/+}$ and wild-type littermates (logrank test, $P<0.0001$). No significant difference in survival was observed between *p53*$^{R172H\Delta g/+}$ *K-ras*$^{LA1/+}$ and *p53*$^{+/-}$ *K-ras*$^{LA1/+}$ mice. (**b**) Female double mutant mice had a significantly higher cancer-related death than male double mutant mice (logrank test, $P=0.0071$).

2004; Meuwissen and Berns, 2005). The deletion of a *p53* allele enhances lung tumorigenesis induced by mutant *K-ras*, but again does not promote the development of metastasis (Johnson *et al.*, 2001; Jackson *et al.*, 2005). In this study, we generated mice with both *p53* and *K-ras* missense mutations to test the suitability of such a model for metastatic lung adenocarcinoma.

In this model, primary lung cancer disseminated widely through both hematogenous and lymphatic pathways to multiple sites strikingly similar to those in human lung cancer (Tamura *et al.*, 1992; Quint *et al.*, 1996; Sadikot *et al.*, 1997). Surprisingly, no metastasis of lung cancer was found in bone and brain. Additional genetic changes may be needed to produce tumors that can metastasize to these organs.

Interestingly, a significant discrepancy in cumulative cancer death was observed between female and male $p53^{R172HΔg/+}$ $K\text{-}ras^{LA1/+}$ mice, but not in littermates with either single mutation. This gender difference in survival is supported by a study showing a higher number of pulmonary lesions induced by a tobacco-specific carcinogen NNK in A/J females as opposed to males (Belinsky *et al.*, 2003). In humans, the observation that female smokers are more susceptible to lung cancer than male smokers is supported by many case–control studies, but opposed by several prospective cohort studies (Zang and Wynder, 1996; Payne, 2001; Bach *et al.*, 2003; Bain *et al.*, 2004; Olak and Colson, 2004). Therefore, a gender difference in susceptibility to human lung cancer is still controversial. Nevertheless, the survival of female and male double mutant mice showed a statistically significant difference and will be an important model to probe this difference.

Pleural mesothelioma is an uncommon, but highly aggressive human malignancy that is invariably fatal because it is detected so late (Jaurand, 2005). In this study, 23% of $p53^{R172HΔg/+}$ $K\text{-}ras^{LA1/+}$ mice also developed pleural mesotheliomas. Four lines of evidence supported the diagnosis of this tumor in this model. The first is the restricted gross and microscopic localization to the pleural mesothelial lining and the distinct phenotypic differences from intra-pulmonary epithelial lesions. The second is positive staining of Calretinin and/or Cytokeratin 6, the two commonly used markers for human mesothelioma (Ordonez, 2003). Specifically, Calretinin was detected in 80% of murine mesotheliomas examined, corresponding to the frequency of 80% in human mesotheliomas (Abutaily *et al.*, 2002). An antibody against Cytokeratin 5 and 6 is positive in 63% of human mesotheliomas (Abutaily *et al.*, 2002). The cytokeratin 6 antibody detected staining in 40% of murine mesotheliomas (a murine-specific Cytokeratin 5 antibody is not available). Of note, these markers stain normal mesothelial cells and do not allow us to distinguish benign from malignant cells. None of lung adenocarcinomas examined in this study was positive for either marker. The third is negative PAS staining, which if positive, rules out mesothelioma. The fourth is that SPC staining was negative in mesothelioma, but positive in the adjacent lung adenocarcinoma. Taken together, histological features, immunohistochemical data, and PAS staining all support the diagnosis of mesothelioma in this study.

Thus, this new lung cancer model more faithfully simulates human metastatic lung cancer and promises to be invaluable in testing novel preventive or therapeutic modalities prior to clinical studies.

Materials and methods

Tumor samples and pathological analysis

The $K\text{-}ras^{LA1/+}$ mice were crossed with $p53^{R172HΔg/+}$ to generate $K\text{-}ras^{LA1/+}$, $p53^{R172HΔg/+}$, $p53^{R172HΔg/+}$ $K\text{-}ras^{LA1/+}$ and wild-type mice, and with $p53^{+/-}$ to generate $p53^{+/-}$ $K\text{-}ras^{LA1/+}$ mice. The background of these mice was greater than 90% 129Sv. Genotypes were determined as previously described (Liu *et al.*, 2000; Johnson *et al.*, 2001). Mice were housed in sterilized plastic cages with hardwood bedding and dust covers in a HEPA-filtered, specific pathogen-free room ($24\pm1^{\circ}C$, 45% humidity, 14/10 h light/dark cycle). The number of mice per cage was three to five. All mice were given sterilized NIH-31 mouse/rat diet (No. 7017, Harlan), and water *ad libitum*. Mice were monitored daily for signs of illness or obvious tumor burden and moribund mice were killed. Tumors and tissues were fixed with 10% buffered formalin, paraffin embedded, and sectioned at 4 μm. Sections (a single section for each tissue per mouse) were stained with hematoxylin and eosin (H&E) for histological evaluation. The diagnosis of a metastatic lesion was based on histological features and the gross finding that the lesion was not in direct contact with a lung tumor. A metastatic diagnosis of lung adenocarcinoma on parietal pleura was possible only if parietal and visceral pleurae were not adhering to each other.

Revese transcription–PCR and quantitative real-time TaqMan PCR

Total RNA was extracted from tumors or normal lung by using Trizol (Invitrogen, Carlsbad, CA, USA) and purified by an RNeasy kit (Qiagen, Gaithersburg, MD, USA). Reverse transcriptase reactions were performed using the First-Strand cDNA Synthesis Kit (Amersham Bioscience, Piscataway, NJ, USA). Primers for wild-type and mutant *K-ras* alleles were K-ras12G: TTGTGGTGGTTGGAGGTGG, K-ras12D: CTT GTGGTGGTTGGAGGTGA, and K-rasEx3R1: CTGTCTT GTCTTTGCTGAGGTC. Specific amplification was confirmed by sequencing PCR products.

Specific probes were used to differentiate mutant and wild-type *p53* alleles in tumors by real-time PCR. Primers and probes were p53 forward 5′-TCTACAAGAAGTCACAGCA CATGAC-3′, p53 reverse 5′-CCTTCCACCCGGATAAGA TGC-3′, wild-type probe 5′-TET-AGGTCGTGAGACACT GCC-3′, mutant probe 5′-FAM-TCGTGAGACGCTGCCC-3′. The GSC (goosecoid homeobox protein gene) forward 5′-CGGCACCGCACCATCT, GSC reverse 5′-TCGTCTCCT GGAAGAGGTTCC, and GSC probe 5′-VIC-CCGATGAGC AGCTCG-3′ were used for normalization. PCR reactions were performed in 384-well reaction plate using ABI PRISM 7900 Sequence Detection System (Applied Biosystems, Foster City, CA, USA). Each sample was measured in duplicate. The relative level of *p53* gene was determined by $\Delta\Delta C_t$ based on the formula $\Delta\Delta C_t$ = (sample C_t [*p53*]−sample C_t [GSC])−(control C_t [*p53*]−control C_t [GSC]). All tumor samples used the same reference sample for calculation, non-tumor DNA with wild-type *p53*. Analysis of diluted samples showed $2^{\Delta\Delta C_t}$ values of $\leqslant 0.15$, 0.15–0.6 or >0.6 indicating 0, 1, or 2 copies of wild-type *p53* alleles, respectively (Hill *et al.*, 2005).

Immunohistochemistry and PAS staining

Immunohistochemical analysis was performed on tissue sections using the Vectastain ABC kit (Vector, Burlingame, CA, USA). Antibodies used were Calretinin (Zymed, South San Francisco, CA, USA, 18-0291, 1:3000 dilution), SPC (Chemicon, Temecula, CA, USA, AB3786, 1:1000 dilution) and a murine-specific Cytokeratin 6 antibody (gift from Dennis R Roop). Sections were counterstained with nuclear fast red or hematoxylin (Vector). Immunoflourescence analysis was performed using a CC10 antibody (Santa Cruz SC-9772, Santa Cruz, CA, USA, 1:50 dilution).

Sections were also stained with PAS staining system (Sigma, St Louis, MO, USA). Normal mouse liver sections were used as positive controls. For a negative control, liver samples were treated with diastase (Sigma) to remove immunoreactivity.

Immunoprecipitation-western blot analysis

Tumor samples were homogenized in 50 mM Tris-Cl (pH 8.0), 150 mM NaCl, 0.5% NP40, and proteinase inhibitors (Roche, Mannheim, Germany). Agarose-conjugated anti-ras antibody Ab-1 (Calbiochem, San Diego, CA, USA, OP01A) was added according to the manufacturer's recommendation. Blots were probed with an anti-pan-Ras^{12D} antibody specific to mutant Ras with an aspartic acid at codon 12 (Oncogene, PC10). The same membrane was stripped and probed with an anti-K-Ras antibody (Santa Cruz, SC30, 1:150). The secondary antibody was horseradish peroxidase-conjugated and signals were detected with a chemiluminescence kit (Amersham Pharmacia, Piscataway, NJ, USA).

Statistics

Survival curves were plotted by the Kaplan–Meier method. The statistical significance between different survival data was determined by the logrank test (GraphPad Prism 4). Tabular data between groups were compared by the χ^2 test.

Acknowledgements

This study was supported by a grant from the Department of Defense, DAMD17-01-1-0689 and the Cancer Center Support Grant CA16672 from the NIH. We thank Tyler Jacks for the *K-ras*$^{LA1/+}$ mice.

References

Abutaily AS, Addis BJ, Roche WR. (2002). Immunohistochemistry in the distinction between malignant mesothelioma and pulmonary adenocarcinoma: a critical evaluation of new antibodies. *J Clin Pathol* **55**: 662–668.

Bach PB, Kattan MW, Thornquist MD, Kris MG, Tate RC, Barnett MJ *et al.* (2003). Variations in lung cancer risk among smokers. *J Natl Cancer Inst* **95**: 470–478.

Bain C, Feskanich D, Speizer FE, Thun M, Hertzmark E, Rosner BA *et al.* (2004). Lung cancer rates in men and women with comparable histories of smoking. *J Natl Cancer Inst* **96**: 826–834.

Becher OJ, Holland EC. (2006). Genetically engineered models have advantages over xenografts for preclinical studies. *Cancer Res* **66**: 3355–3358 discussion 3358–3359.

Belinsky SA, Klinge DM, Stidley CA, Issa JP, Herman JG, March TH *et al.* (2003). Inhibition of DNA methylation and histone deacetylation prevents murine lung cancer. *Cancer Res* **63**: 7089–7093.

Belinsky SA, Stefanski SA, Anderson MW. (1993). The A/J mouse lung as a model for developing new chemointervention strategies. *Cancer Res* **53**: 410–416.

Castonguay A, Pepin P, Stoner GD. (1991). Lung tumorigenicity of NNK given orally to A/J mice: its application to chemopreventive efficacy studies. *Exp Lung Res* **17**: 485–499.

Chiba I, Takahashi T, Nau MM, D'Amico D, Curiel DT, Mitsudomi T *et al.* (1990). Mutations in the p53 gene are frequent in primary, resected non-small cell lung cancer. Lung Cancer Study Group. *Oncogene* **5**: 1603–1610.

Greenblatt MS, Bennett WP, Hollstein M, Harris CC. (1994). Mutations in the p53 tumor suppressor gene: clues to cancer etiology and molecular pathogenesis. *Cancer Res* **54**: 4855–4878.

Hecht SS, Morse MA, Eklind KI, Chung FL. (1991). A/J mouse lung tumorigenesis by the tobacco-specific nitrosamine 4-(methylnitrosamino)-1-(3-pyridyl)-1-butanone and its inhibition by arylalkyl isothiocyanates. *Exp Lung Res* **17**: 501–511.

Hill R, Song Y, Cardiff RD, Van Dyke T. (2005). Selective evolution of stromal mesenchyme with p53 loss in response to epithelial tumorigenesis. *Cell* **123**: 1001–1011.

Jackson EL, Olive KP, Tuveson DA, Bronson R, Crowley D, Brown M *et al.* (2005). The differential effects of mutant p53 alleles on advanced murine lung cancer. *Cancer Res* **65**: 10280–10288.

Jaurand MC. (2005). Mesothelioma pathogenesis, facts and expectations. *Pathol Biol (Paris)* **53**: 41–44.

Johnson L, Mercer K, Greenbaum D, Bronson RT, Crowley D, Tuveson DA *et al.* (2001). Somatic activation of the K-ras oncogene causes early onset lung cancer in mice. *Nature* **410**: 1111–1116.

Kerr KM, Lamb D, Wathen CG, Walker WS, Douglas NJ. (1992). Pathological assessment of mediastinal lymph nodes in lung cancer: implications for non-invasive mediastinal staging. *Thorax* **47**: 337–341.

Kitamura H, Kameda Y, Ito T, Hayashi H. (1999). Atypical adenomatous hyperplasia of the lung. Implications for the pathogenesis of peripheral lung adenocarcinoma. *Am J Clin Pathol* **111**: 610–622.

Lang GA, Iwakuma T, Suh YA, Liu G, Rao VA, Parant JM *et al.* (2004). Gain of function of a p53 hot spot mutation in a mouse model of Li–Fraumeni syndrome. *Cell* **119**: 861–872.

Liu G, McDonnell TJ, Montes de Oca Luna R, Kapoor M, Mims B, El-Naggar AK *et al.* (2000). High metastatic potential in mice inheriting a targeted p53 missense mutation. *Proc Natl Acad Sci USA* **97**: 4174–4179.

Malkinson AM, You M. (1994). The intronic structure of cancer-related genes regulates susceptibility to cancer. *Mol Carcinog* **10**: 61–65.

Meuwissen R, Berns A. (2005). Mouse models for human lung cancer. *Genes Dev* **19**: 643–664.

Mitsudomi T, Steinberg SM, Nau MM, Carbone D, D'Amico D, Bodner S *et al.* (1992). p53 gene mutations in non-small-cell lung cancer cell lines and their correlation with the presence of ras mutations and clinical features. *Oncogene* **7**: 171–180.

Nikitin AY, Alcaraz A, Anver MR, Bronson RT, Cardiff RD, Dixon D *et al.* (2004). Classification of proliferative pulmonary lesions of the mouse: recommendations of the mouse models of human cancers consortium. *Cancer Res* **64**: 2307–2316.

Olak J, Colson Y. (2004). Gender differences in lung cancer: have we really come a long way, baby? *J Thorac Cardiovasc Surg* **128**: 346–351.

Olive KP, Tuveson DA, Ruhe ZC, Yin B, Willis NA, Bronson RT *et al.* (2004). Mutant p53 gain of function in two mouse models of Li–Fraumeni syndrome. *Cell* **119**: 847–860.

Ordonez NG. (2003). The immunohistochemical diagnosis of mesothelioma: a comparative study of epithelioid mesothelioma and lung adenocarcinoma. *Am J Surg Pathol* **27**: 1031–1051.

Payne S. (2001). 'Smoke like a man, die like a man'?: a review of the relationship between gender, sex and lung cancer. *Soc Sci Med* **53**: 1067–1080.

Quint LE, Tummala S, Brisson LJ, Francis IR, Krupnick AS, Kazerooni EA *et al.* (1996). Distribution of distant metastases from newly diagnosed non-small cell lung cancer. *Ann Thorac Surg* **62**: 246–250.

Rodenhuis S, Slebos RJ. (1992). Clinical significance of ras oncogene activation in human lung cancer. *Cancer Res* **52** (9 Suppl): 2665s–2669s.

Rodenhuis S, Slebos RJ, Boot AJ, Evers SG, Mooi WJ, Wagenaar SS *et al.* (1988). Incidence and possible clinical significance of K-ras oncogene activation in adenocarcinoma of the human lung. *Cancer Res* **48**: 5738–5741.

Sadikot RT, Renwick DS, DaCosta P, Chalmers AG, Pearson SB. (1997). Breast metastasis from non-small cell lung cancer. *South Med J* **90**: 1063–1064.

Salgia R, Skarin AT. (1998). Molecular abnormalities in lung cancer. *J Clin Oncol* **16**: 1207–1217.

Sausville EA, Burger AM. (2006). Contributions of human tumor xenografts to anticancer drug development. *Cancer Res* **66**: 3351–3354, discussion 3354.

Takahashi T, Nau MM, Chiba I, Birrer MJ, Rosenberg RK, Vinocour M *et al.* (1989). p53: a frequent target for genetic abnormalities in lung cancer. *Science* **246**: 491–494.

Tamura A, Matsubara O, Yoshimura N, Kasuga T, Akagawa S, Aoki N. (1992). Cardiac metastasis of lung cancer. A study of metastatic pathways and clinical manifestations. *Cancer* **70**: 437–442.

Toyooka S, Tsuda T, Gazdar AF. (2003). The Tp53 gene, tobacco exposure, and lung cancer. *Hum Mutat* **21**: 229–239.

Vahakangas KH, Bennett WP, Castren K, Welsh JA, Khan MA, Blomeke B *et al.* (2001). p53 and K-ras mutations in lung cancers from former and never smoking women. *Cancer Res* **61**: 4350–4356.

Wang Y, Zhang Z, Lubet RA, You M. (2006a). A mouse model for tumor progression of lung cancer in ras and p53 transgenic mice. *Oncogene* **25**: 1277–1280.

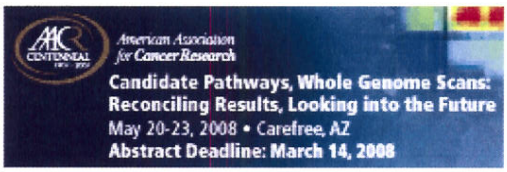
Wang Y, Zhang Z, Yao R, Jia D, Wang D, Lubet RA *et al.* (2006b). Prevention of lung cancer progression by bexarotene in mouse models. *Oncogene* **25**: 1320–1329.

You M, Wang Y, Stoner G, You L, Maronpot R, Reynolds SH *et al.* (1992). Parental bias of Ki-ras oncogenes detected in lung tumors from mouse hybrids. *Proc Natl Acad Sci USA* **89**: 5804–5808.

Zang EA, Wynder EL. (1996). Differences in lung cancer risk between men and women: examination of the evidence. *J Natl Cancer Inst* **88**: 183–192.

Supplementary Information accompanies the paper on the Oncogene website (http://www.nature.com/onc).

Cancer Research





HOME HELP FEEDBACK SUBSCRIPTIONS ARCHIVE SEARCH TABLE OF CONTENTS

Cancer Research | Clinical Cancer Research
Cancer Epidemiology Biomarkers & Prevention | Molecular Cancer Therapeutics
Molecular Cancer Research | Cell Growth & Differentiation

Institution: MD ANDERSON HOSPITAL | Sign In via User Name/Password

Cancer Research 67, 10647-10652, November 15, 2007. doi: 10.1158/0008-5472.CAN-07-1337
© 2007 American Association for Cancer Research

This Article

- Abstract FREE
- Full Text (PDF)
- Supplementary Data
- Alert me when this article is cited
- Alert me if a correction is posted

Services

- Similar articles in this journal
- Similar articles in PubMed
- Alert me to new issues of the journal
- Download to citation manager
- © Get Permissions

Google Scholar

- Articles by Wang, J.
- Articles by Mao, L.

PubMed

- PubMed Citation
- Articles by Wang, J.
- Articles by Mao, L.

Priority Reports

ΔDNMT3B Variants Regulate DNA Methylation in a Promoter-Specific Manner

Jie Wang[1,3], Manisha Bhutani[1], Ashutosh K. Pathak[1], Wenhua Lang[1], Hening Ren[1], Jaroslav Jelinek[2], Rong He[2], Lanlan Shen[2], Jean-Pierre Issa[2] and Li Mao[1]

Departments of [1] Thoracic/Head and Neck Medical Oncology and [2] Leukemia, The University of Texas M. D. Anderson Cancer Center, Houston, Texas and [3] Department of Oncology, Beijing Cancer Hospital, Beijing University School of Oncology, Beijing, China

Requests for reprints: Li Mao, Department of Thoracic/Head and Neck Medical Oncology, The University of Texas M. D. Anderson Cancer Center, Box 437, Unit 432, Room FC9.3065, 1515 Holcombe Boulevard, Houston, TX 77030. Phone: 713-792-6363; Fax: 713-792-1220; E-mail: lmao@mdanderson.org .

Abstract

DNA methyltransferase 3B (DNMT3B) is critical in *de novo* DNA methylation during development and tumorigenesis. We recently reported the identification of a DNMT3B subfamily, ΔDNMT3B, which contains at least seven variants, resulting from alternative pre-mRNA splicing. Δ*DNMT3B*s are the predominant expression forms of *DNMT3B* in human lung cancer. A

▲ Top
▪ Abstract
▼ Introduction
▼ Materials and Methods
▼ Results and Discussion
▼ References

strong correlation was observed between the promoter methylation of *RASSF1A* gene but not *p16* gene (both frequently inactivated by promoter methylation in lung cancer) and expression of Δ*DNMT3B4* in primary lung cancer, suggesting a role of ΔDNMT3B in regulating promoter-specific methylation of common tumor suppressor genes in tumorigenesis. In this report, we provide first experimental evidence showing a direct involvement of ΔDNMT3B4 in regulating *RASSF1A* promoter methylation in human lung cancer cells. Knockdown of Δ*DNMT3B4* expression by small interfering RNA resulted in a rapid demethylation of *RASSF1A* promoter and reexpression of *RASSF1A* mRNA but had no effect on p16 promoter in the lung cancer cells. Conversely, normal bronchial epithelial cells with stably transfected Δ*DNMT3B4* gained an increased DNA methylation in *RASSF1A* promoter but not *p16* promoter. We conclude that promoter DNA methylation can be differentially regulated and ΔDNMT3Bs are involved in regulation of such promoter-specific *de novo* DNA methylation. [Cancer Res 2007;67(22):10647–52]

Introduction

▲ Top
▲ Abstract
▪ Introduction
▼ Materials and Methods
▼ Results and Discussion
▼ References

DNA methylation plays an essential role in the normal development of the mammalian embryo by regulating gene transcription through genomic imprinting, X chromosome inactivation, and genomic stability (1). It is believed that DNA methylation patterns in somatic cells are established during gametogenesis and early embryonic development via consecutive waves of demethylation and *de novo* methylation (2). The *DNA methyltransferase 3* (*DNMT3*) gene consists of *DNMT3A* and *DNMT3B* and is the major *de novo* DNA methyltransferase that preferentially methylates cytosine in CpG sites (3). Methylation in CpG-rich promoter regions may result in transcriptional silencing of the corresponding genes, which is a major mechanism by which tumor suppressor genes are inactivated in tumorigenesis (4).

DNMT3B contains 24 exons spanning ~47 kb of genomic DNA. Two alternative 5' exons are used, but the same full-length DNMT3B protein (DNMT3B1 and DNMT3B2) is expected from both transcripts (5). Four additional transcriptional variants (*DNMT3B3, DNMT3B4, DNMT3B5*, and *DNMT3B6*) resulting from alternative pre-mRNA splicing have also been reported (5–7). Some of the variants may compete with each other, thereby resulting in even DNA hypomethylation (7). This possibility suggests a complex biological role of the *DNMT3B* variants. Increased expression of *DNMT3B* has been frequently observed in human cancer cell lines and primary tumors (3). However, an association between the expression level of *DNMT3B* and the promoter methylation status of tumor suppressor genes has not been established (8, 9). These data suggest that the regulation of DNA methylation of these promoters is complex.

Δ*DNMT3B*, a subfamily of *DNMT3B*, consists of at least seven transcriptional variants by alternative pre-mRNA splicing (10). In non–small cell lung cancer (NSCLC), Δ*DNMT3B* variants are the predominant forms of *DNMT3B* expression (10). We previously observed a strong and independent correlation between Δ*DNMT3B4* expression and DNA methylation of the *RASSF1A* promoter but not the *p16* promoter (11). This finding suggested that Δ*DNMT3B* variants are involved in the regulation of

promoter methylation, possibly in a promoter-specific manner.

Materials and Methods

▲ Top
▲ Abstract
▲ Introduction
▪ Materials and Methods
▼ Results and Discussion
▼ References

Cell lines. Human NSCLC lines H1299 and H358 were purchased from the American Type Culture Collection. The HBE1 cell line was a gift from Dr. John Minna (The University of Texas Southwest Medical Center, Dallas, TX).

RNA extraction and reverse transcription-PCR. We isolated total RNA from cells by using Tri-Reagent (Molecular Research Center) according to the manufacturer's instruction. The primers used for reverse transcription-PCR (RT-PCR) were described previously (10).

Methylation-specific PCR. One microgram of genomic DNA was used for bisulfite treatment to modify unmethylated cytosine residues, and the modified DNA was used for methylation-specific PCR (MSP) using methylation-specific and unmethylation-specific primers as described previously (10, 11). Unmodified DNA was used to test all the primer sets and we failed to observe any amplified DNA fragment in our experimental conditions.

Small interfering RNA and antisense RNA transfection. Small interfering RNA (siRNA) specifically targeted to the junction of exons 5 and 7 of *ΔDNMT3B* was designed and synthesized chemically (Ambion). Both annealed siRNA and corresponding oligonucleotides of single strands were used. The sequences were 5'-CACGCAACCAGAGAACAAGUU-3' (sense) and 5'-CUUGUUCUCUGGUUGCGUGUU-3' (antisense) for the target sequence 5'-AACACGCAACCAGAGAACAAG-3'. siRNA specifically targeting glyceraldehyde-3-phosphate dehydrogenase (*GAPDH*) or scramble siRNA was also obtained from Ambion to serve as controls.

Bisulfite sequencing of the *RASSF1A* promoter. MSP products were derived from H1299 cells treated with 40 nmol/L siRNA targeting *ΔDNMT3B4/2* or *GAPDH* for 24 h and were recovered by gel purification. The DNA fragments were cloned into a TA cloning vector (Invitrogen) according to the manufacturer's protocol. Plasmid DNA from each clone was then extracted, and inserts in individual clones were sequenced (T3 or T7 primer) using an ABI PRISM 377 DNA sequencer (Perkin-Elmer).

Western blot analysis. Cell lysates were obtained and equal amounts of protein from each sample were diluted with loading buffer, boiled, and loaded onto 7.5% SDS-polyacrylamide gel to be separated by electrophoresis followed by protein transfer to polyvinylidene fluoride membranes (Amersham). Proteins were detected by incubation with corresponding antibodies specific to either DNMT1 or V5 tag (Sigma) followed by blotting with horseradish peroxidase–conjugated secondary antibody (Sigma). The blots were then exposed to chemiluminescent substrate (Amersham) for detection.

Cell growth and cell cycle analyses. The ACEA RT-CES microelectronic cell sensor system (ACEA Biosciences) was used to confirm the number of living cells. The electronic sensors provided a

continuous and quantitative measurement of the cell index (which depends on the number of attached cells and the shape of the cells) in each well. The cell cycle distribution of the cells was determined using a BD FACSCalibur flow cytometer and CellQuest software (Becton Dickinson).

Stable transfection. pcDNA6/V5-His (Invitrogen) was used to construct plasmids containing full-length Δ*DNMT3B2* or Δ*DNMT3B4*. Empty vector or plasmids containing Δ*DNMT3B2* or Δ*DNMT3B4* were used to transfect HBE1 cells and establish clones with stable expression of the corresponding proteins. Several clones were selected from each transfectant, and passages 5 and 10 were subsequently used for promoter methylation analysis.

Bisulfite pyrosequencing. Pyrosequencing was used to quantitatively measure the levels of cytosine methylation of CpG sites of promoters as described previously (12). The primers used in this study are listed in Supplementary Table S1 and their locations in the CpG islands are presented in Supplementary Fig. S1. Assays were repeated thrice and the means of all experimental results were used with SEs. The quantification of cytosine methylation was performed using Pyro Q-CpG software (Biotage).

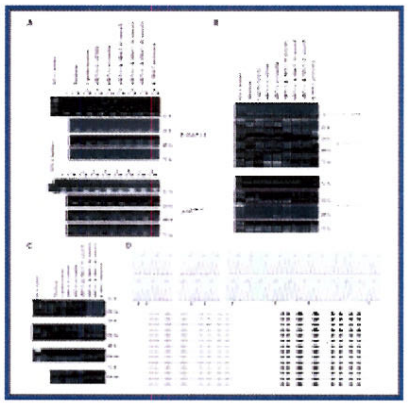
Results and Discussion

▲ Top
▲ Abstract
▲ Introduction
▲ Materials and Methods
▪ Results and Discussion
▼ References

To test the role of Δ*DNMT3B4* in the promoter-specific methylation of *RASSF1A*, we designed a siRNA that specifically targeted the junction of exons 5 and 7 of Δ*DNMT3B*. Because both Δ*DNMT3B4* and Δ*DNMT3B2* lack exon 6, this siRNA is expected to trigger the degradation of both these transcripts. We used NSCLC cell line H1299 because it carries promoter methylation of both *p16* and *RASSF1A* and expresses a high level of Δ*DNMT3B4* but no detectable *DNMT3B* (10).

We found that down-regulation of Δ*DNMT3B4/2* resulted in *RASSF1A* promoter demethylation in H1299 cells (Fig. 1). In the cells treated with 20 nmol/L or a higher concentration of the siRNA targeting Δ*DNMT3B4/2*, a near complete *RASSF1A* promoter demethylation was observed as early as 12 h after treatment (Fig. 1*A*). This effect was maintained up to 72 h after treatment. The results are consistent with the dose-dependent reduction of Δ*DNMT3B4* expression by the siRNA or antisense treatment (Fig. 1*B*). In contrast, the promoter methylation status of *p16* was not affected (Fig. 1*A*). These results provide the first direct evidence of a causal relationship between ΔDNMT3B4 and the promoter methylation of *RASSF1A* in lung cancer cells.

Figure 1. Down-regulation of Δ*DNMT3B4/2* expression and demethylation of *RASSF1A* promoter. *A,* promoter methylation status of *p16* and *RASSF1A* at different time points following treatment as measured by MSP. –, negative control; +, positive control. *U,* unmethylated DNA; *M,* methylated DNA. *B,* expression of Δ*DNMT3Bs* in H1299 cells treated with siRNAs at various time points using RT-



View larger version (55K):
[in this window]
[in a new window]

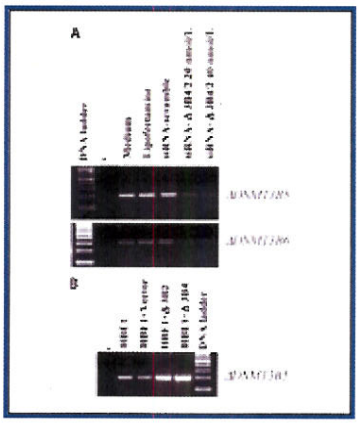
PCR. *C,* expression of *RASSF1A* mRNA (234 bp) of the corresponding samples measured by RT-PCR. *D,* methylation status in the *RASS1A* promoter according to bisulfate sequencing analysis. *Arrowheads,* cytosines not converted to thymidines in the CpG sites (*bottom panel of the sequences*) because of the resistance of the methylated cytosines to bisulfate treatment. Line in the figure below the sequences represents a clone. *Open dot,* a CpG site not methylated; *solid dot,* a methylated CpG site. The left set of lines represents clones from cells treated with control, and the right set of lines represents clones from cells treated with siRNA targeting Δ*DNMT3B4/2*.

Consistent with the *RASSF1A* promoter demethylation, *RASSF1A* mRNA expression was restored in the cells also in a dose-dependent manner (Fig. 1*C*). Because MSP is a qualitative assay and cannot reveal the methylation status of each CpG site, we performed bisulfite sequencing of the MSP products from cells with or without Δ*DNMT3B4/2* knockdown. The MSP fragment is a part of the *RASSF1A* promoter and contains 10 CpG sites, excluding the primer sequences. None of the cytosine residues at the 10 CpG sites of the *RASSF1A* promoter fragment were converted to thymidine by bisulfite treatment (an indication of a methylated status) in the 14 individual clones derived from cells without Δ*DNMT3B4/2* knockdown, whereas the cytosine residues at all the 10 CpG sites were converted to thymidine (an indication of an unmethylated status) in all 14 clones derived from cells with Δ*DNMT3B4/2* knockdown (Fig. 1*D*).

In a separate experiment, we used pyrosequencing method to analyze DNA from H1299 cells treated with either 20 nmol/L scramble siRNA control or 20 nmol/L siRNA targeting Δ*DNMT3B4/2* 24 h after treatment. The primers used in this experiment were designed to avoid amplification bias (Supplementary Table S1). We observed that that promoter methylation of *RASSF1A* was decreased from 94% in the control-treated to 33% in the siRNA-treated DNA, whereas no difference was observed in the *p16* promoter between control-treated and the siRNA-treated DNA (Supplementary Fig. S2). These results indicate that knockdown of Δ*DNMT3B4/2* can reverse the methylated CpG sites in the *RASSF1A* promoter region. Our finding is unlikely due to the inhibition of DNMT1 because the protein expression level was not reduced in the H1299 cells treated with the siRNA (data not shown). To determine whether the *RASSF1A* promoter demethylation due to knockdown of Δ*DNMT3B4/2* is limited to H1299 cells, we performed the same experiments with NSCLC cell line H358. Similar to our results with the H1299 cells, the *RASSF1A* promoter became unmethylated after the siRNA treatment but no effect was observed on the methylated *p16* promoter (data not shown).

To address the issue whether some of the observed results are due to a shift in balance between Δ*DNMT3B4* and other Δ*DNMT3B* isoforms, we also analyzed mRNA expression of Δ*DNMT3B5* and

Δ*DNMT3B6* that are expressed in the H1299 cells beside Δ*DNMT3B1* that did not show change in expression levels after siRNA treatment (Fig. 1*A*). Interestingly, the expression of Δ*DNMT3B5* and Δ*DNMT3B6* was reduced in the siRNA-treated samples compared with the controls (Fig. 2*A*). To ensure that the result was not due to nonspecific knockdown by the siRNA, we analyzed the expression of Δ*DNMT3B5* (Δ*DNMT3B6* was not expressed in the cell line) in HBE1 cells transfected with either Δ*DNMT3B2* or Δ*DNMT3B4*. The expression of Δ*DNMT3B5* was increased in the cells transfected with either Δ*DNMT3B2* or Δ*DNMT3B4* compared with controls (Fig. 2*B*). The result indicates that the expression of either Δ*DNMT3B2* or Δ*DNMT3B4* may affect expression levels of Δ*DNMT3B5* and Δ*DNMT3B6*.

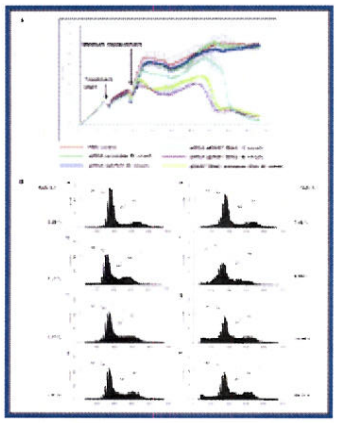


View larger version (38K):
[in this window]
[in a new window]

Figure 2. Expression of Δ*DNMT3B5* and Δ*DNMT3B6* following change of Δ*DNMT3B4/2* expression levels. *A,* expression of Δ*DNMT3B5* and Δ*DNMT3B6* in H1299 cells treated with siRNAs measured by RT-PCR. *B,* expression of Δ*DNMT3B5* and Δ*DNMT3B6* in HBE1 cells transfected with Δ*DNMT3B2* or Δ*DNMT3B4*.

We used RT-CES System to determine the dynamic change in cell growth affected by the Δ*DNMT3B4/2* knockout (measured every 30 min). In the H1299 cells, growth was inhibited at ~10 h after treatment with the siRNA-Δ*DNMT3B4/2* in a dose-dependent manner or with the antisense RNA (Fig. 3*A*). Because the RT-CES System works by measuring the electronic impedance of sensor electrodes integrated on the bottom of microtiter E-plates, factors besides cell numbers, such as morphology and tightness of the cells attached to the culture surface, can affect the reading. The major drop observed 36 h after treatment with the siRNA might reflect to a reduced ability of the cells detaching to the plastic surface. To determine the mechanism by which the growth of the Δ*DNMT3B4/2* knockout is inhibited, we used flow cytometry to examine the cell cycle distribution of the H1299 cells 24 h after treatment. We observed an increase in the sub-G_1 fraction of cells treated with the siRNA-Δ*DNMT3B4/2* in a dose-dependent manner or with the antisense RNA (Fig. 3*B*). These results suggest that treatment with siRNA-Δ*DNMT3B4/2* increased apoptosis.

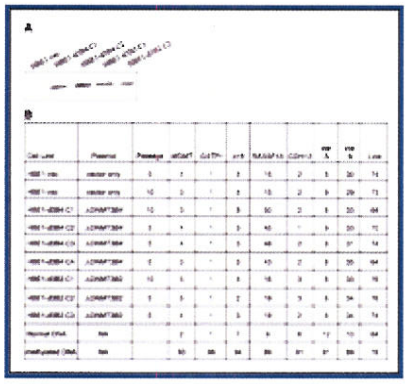
Figure 3. Biological effects of Δ*DNMT3B4/2* down-regulation. *A,* growth of H1299 cells transfected with siRNAs as measured using



View larger version (42K):
[in this window]
[in a new window]

a microelectronic cell sensor system every 30 min. The representation of individual color lines is indicated and described in the figure. *B,* cell cycle distributions of H1299 cells 24 h after treatment with siRNAs as measured with a flow cytometer (*a*, cells treated with culture medium; *b*, Lipofectamine only; *c*, siRNA targeting *GAPDH; d*, scramble siRNA; *e–g*, 10, 20, and 40 siRNA, respectively; *h*, 40 nmol/L antisense RNA targeting Δ*DNMT3B4/2*). Percentages of sub-G_1 cells were labeled inside each panel.

To provide direct evidence to support the possibility that Δ*DNMT3B4* but not Δ*DNMT3B2* contributed to the differential regulation of *RASSF1A* promoter methylation, we constructed mammalian expression plasmids containing Δ*DNMT3B2* or Δ*DNMT3B4* and used HBE1 cells (immortalized, normal-appearing bronchial epithelial cells from a patient with NSCLC; ref. 13). Stable clones expressing Δ*DNMT3B2* or Δ*DNMT3B4* were established (Fig. 4*A*). At passages 5 and 10, we used the quantitative pyrosequencing method to analyze the promoter methylation status of the genes *MGMT, GSTP1, p16, RASSF1A, CDH13*, and *PR* (two regions) in the HBE1 cells transfected with empty vector only, Δ*DNMT3B2*, or Δ*DNMT3B4*. Consistent with our hypothesis that Δ*DNMT3B4* but not Δ*DNMT3B2* contributed to the differential regulation of *RASSF1A* promoter methylation, cells transfected with Δ*DNMT3B4*, but not cells transfected with the empty vector or Δ*DNMT3B2*, showed substantially increased DNA methylation in the *RASSF1A* promoter compared with vector control ($P < 0.001$, Kruskal-Wallis test; Fig. 4*B*). No change in methylation status was observed in any of the other promoters for any of the transfectants (Fig. 4*B*).



View larger version (25K):
[in this window]
[in a new window]

Figure 4. Overexpression of Δ*DNMT3B4* resulted in *RASSF1A* promoter hypermethylation. *A,* expression of recombinant ΔDNMT3B4 and ΔDNMT3B2 in HBE1 clones recognized on Western blots using antibody against V5 tag. *HBE1-vec,* vector only–transfected HBE1 cells. *B,* CpG methylation in promoter regions of six genes and in line sequences. Clones d3B4.C1, d3B4.C2, d3B4.C3, and d3B4.C4 expressed ΔDNMT3B4, and clones d3B2.C1, d3B2.C2, and d3B2.C3 expressed ΔDNMT3B2. The values for the genes represent the approximate percentages of the CpG sites that were methylated as measured by pyrosequencing analysis.

Our findings suggest a mechanism for the development of "tissue-specific DNA methylation." This term refers to different promoters being methylated in different cell types or organs during development and tumorigenesis (14). In somatic cells, most of the CpG sites in genomic DNA are methylated except in CpG-enriched promoter regions (CpG islands) of the transcriptionally active genes. The maintenance of established DNA methylation patterns is largely performed by DNMT1, which is constitutively expressed in somatic tissues. The expression of DNMT3B is low or absent in somatic tissues but significantly increased in transformed cancer cells and is thought to be critical to *de novo* promoter methylation (15). During tumorigenesis, *de novo* DNA methylation occurs in the promoters of selected genes and contributes to their functional inactivation by suppressing the expression of those genes. Global analysis of promoter methylation has revealed several abnormally methylated promoters found in tumors but not in normal tissue counterparts (16). However, each tumor exhibits a unique pattern of methylated promoters, although some promoters are commonly methylated in certain tumor types. These observations indicate the presence of cellular mechanisms, which result in differential promoter methylation that is maintainable during tumor development and progression.

In a previous study, we found a statistically significant correlation between *RASSF1A* promoter methylation and Δ*DNMT3B4* expression in a large number of primary NSCLC tumors (11). That result provided *in vivo* evidence of a role for Δ*DNMT3B4* in regulating the methylation of CpG islands in a promoter-specific manner. The results presented in the current report provide enough direct evidence to establish the causal relationship between Δ*DNMT3B4* and *RASSF1A* promoter methylation but not between several other commonly methylated promoters we examined. In the siRNA-based experiment, the down-regulation of Δ*DNMT3B4* resulted in demethylation of the *RASSF1A* promoter but not the *p16* promoter in two NSCLC cell lines. Because the siRNA used also knocked down Δ*DNMT3B2* (because of the shared exon-exon junction between Δ*DNMT3B2* and Δ*DNMT3B4*), a role for Δ*DNMT3B2* in that process cannot be excluded. The experiments using HBE1 cells that express specific Δ*DNMT3B* variants (Δ*DNMT3B2* or Δ*DNMT3B4*) provided conclusive evidence that Δ*DNMT3B4* but not Δ*DNMT3B2* contributes to *RASSF1A*-specific promoter methylation. Although expression levels of Δ*DNMT3B4* may affect expression levels of Δ*DNMT3B5* and Δ*DNMT3B6*, the expression of the later isoforms is unlikely contributed to *RASSF1A* promoter methylation because overexpressing Δ*DNMT3B2* also caused an increased expression of Δ*DNMT3B5* (Fig. 3*B*) but did not affect the methylation status of *RASSF1A* promoter (Fig. 4*B*).

Although our study results firmly establish the importance of ΔDNMT3Bs in promoter-specific methylation, the detailed mechanisms are unknown. DNMT1 is the predominant cellular DNA methyltransferase, but it requires the participation of DNMT3B to achieve promoter methylation (17, 18). Because DNMT3Bs contain a PWWP domain, which has direct DNA-binding capability (19), the fact that there are ΔDNMT3Bs with structural differences at and around the PWWP domain suggests that the ΔDNMT3B variants interact with a class of promoters with a similar consensus sequence and are responsible for the methylation of the promoters. The recent finding that tumor-specific methylated

genes have common sequence motifs in their promoters (20) supports this notion. It should be noted that, in our study, overexpression of ΔDNMT3B4 in the HBE1 cells resulted in only partial methylation of the *RASSF1A* promoter; this observation indicates that an additional component or components are needed for the stable and complete methylation of the promoter. Alternatively, the peptide tags fused with ΔDNMT3B4 may cause changes in protein folding and result in reduced efficiency of the protein.

Our findings place ΔDNMT3Bs at the center of *de novo* promoter methylation, particularly in lung tumorigenesis. The promoter-specific demethylation we observed is particularly interesting for cancer therapy because it raises the possibility of inhibiting specific variants of ΔDNMT3B to selectively activate critical tumor suppressor genes whose expression is down-regulated due to promoter methylation. Such an approach may lead to the development of novel therapeutic strategies tailored to individual tumors with particular epigenetic abnormalities. These strategies would cause limited adverse effects because normal tissue would be spared most of the effects of less targeted treatment on the promoters methylated.

Acknowledgments

Grant support: Department of Defense grants DAMD17-01-1-01689-1 and W81XWH-05-2-0027.

The costs of publication of this article were defrayed in part by the payment of page charges. This article must therefore be hereby marked *advertisement* in accordance with 18 U.S.C. Section 1734 solely to indicate this fact.

We thank Elizabeth L. Hess for scientific editing of the manuscript.

Footnotes

Note: Supplementary data for this article are available at Cancer Research Online (http://cancerres.aacrjournals.org/).

J. Wang, M. Bhutani, and A.K. Pathak contributed equally to this work.

Received 4/11/07. Revised 8/30/07. Accepted 10/ 5/07.

References

▲ Top
▲ Abstract
▲ Introduction
▲ Materials and Methods
▲ Results and Discussion
▪ References

1. Surani MA. Imprinting and the initiation of gene silencing in the germline. Cell 1998;93:309–12.[CrossRef][Medline]
2. Monk M, Boubelik M, Lehnert S. Temporal and regional changes in DNA methylation in the embryonic, extra-embryonic, and germ cell

lineages during mouse embryo development. Development 1987;99:371–82.[Abstract]
3. Okano M, Xie S, Li E. Cloning and characterization of a family of novel mammalian DNA (cytosine-5) methyltransferases. Nat Genet 1998;19:219–20.[CrossRef][Medline]
4. Jones PA, Baylin SB. The fundamental role of epigenetic events in cancer. Nat Rev Genet 2002;3:415–28.[Medline]
5. Okano M, Bell DW, Haber DA, Li E. DNA methyltransferases Dnmt3a and Dnmt3b are essential for *de novo* methylation and mammalian development. Cell 1999;99:247–57.[CrossRef][Medline]
6. Robertson KD, Uzvolgyi E, Liang G, et al. The human DNA methyltransferases (DNMTs) 1, 3a and 3b: coordinate mRNA expression in normal tissues and overexpression in tumors. Nucleic Acids Res 1999;27:2291–8.[Abstract/Free Full Text]
7. Saito Y, Kanai Y, Sakamoto M, Saito H, Ishii H, Hirohashi S. Overexpression of a splice variant of DNA methyltransferase 3b, DNMT3b4, associated with DNA hypomethylation on pericentromeric satellite regions during human hepatocarcinogenesis. Proc Natl Acad Sci U S A 2002;99:10060–5.[Abstract/Free Full Text]
8. Yakushiji T, Uzawa K, Shibahara T, Noma H, Tanzawa H. Over-expression of DNA methyltransferases and CDKN2A gene methylation status in squamous cell carcinoma of the oral cavity. Int J Oncol 2003;22:1201–7.[Medline]
9. Sato M, Horio Y, Sekido Y, Minna JD, Shimokata K, Hasegawa Y. The expression of DNA methyltransferases and methyl-CpG-binding proteins is not associated with the methylation status of p14(ARF), p16(INK4a) and RASSF1A in human lung cancer cell lines. Oncogene 2002;21:4822–9.[CrossRef][Medline]
10. Wang L, Wang J, Sun S, et al. A novel DNMT3B subfamily, ΔDNMT3B, is the predominant form of DNMT3B in non-small cell lung cancer. Int J Oncol 2006;29:201–7.[Medline]
11. Wang J, Walsh G, Liu DD, Lee JJ, Mao L. Expression of ΔDNMT3B variants and its association with promoter methylation of p16 and RASSF1A in primary non-small cell lung cancer. Cancer Res 2006;66:8361–6.[Abstract/Free Full Text]
12. Issa JP, Gharibyan V, Cortes J, et al. Phase II study of low-dose decitabine in patients with chronic myelogenous leukemia resistant to imatinib mesylate. J Clin Oncol 2005;23:3948–56. [Abstract/Free Full Text]
13. Ramirez RD, Sheridan S, Girard L, et al. Immortalization of human bronchial epithelial cells in the absence of viral oncoproteins. Cancer Res 2004;64:9027–34.[Abstract/Free Full Text]
14. Kitamura E, Igarashi J, Morohashi A, et al. Analysis of tissue-specific differentially methylated regions (TDMs) in humans. Genomics 2006;89:326–37.[CrossRef][Medline]
15. Liu K, Wang YF, Cantemir C, Muller MT. Endogenous assays of DNA methyltransferases: evidence for differential activities of DNMT1, DNMT2, and DNMT3 in mammalian cells *in vivo*. Mol Cell Biol 2003;23:2709–19.[Abstract/Free Full Text]
16. Hatada I, Fukasawa M, Kimura M, et al. Genome-wide profiling of promoter methylation in human. Oncogene 2006;25:3059–64.[CrossRef][Medline]
17. Rhee I, Bachman KE, Park BH, et al. DNMT1 and DNMT3b cooperate to silence genes in human cancer cells. Nature 2002;416:552–6.[CrossRef][Medline]
18. Kim GD, Ni J, Kelesoghu N, Roberts RJ, Prodham S. Co-operation and communication between the human maintenance and *de novo* DNA methyltransferases. EMBO J 2002;21:4183–95. [CrossRef][Medline]
19. Qiu C, Sawada K, Zhang X, Cheng X. The PWWP domain of mammalian DNA methyltransferase Dnmt3b defines a new family of DNA-binding folds. Nat Struct Biol 2002;9:217–24.[Medline]
20. Keshet I, Schlesinger Y, Farkash S, et al. Evidence for an instructive mechanism of *de novo* methylation in cancer cells. Nat Genet 2006;38:149–53.[CrossRef][Medline]

This Article

- **Abstract** FREE
- **Full Text (PDF)**
- **Supplementary Data**
- **Alert me when this article is cited**
- **Alert me if a correction is posted**

Services

- **Similar articles in this journal**
- **Similar articles in PubMed**
- **Alert me to new issues of the journal**
- **Download to citation manager**
- © Get Permissions

Google Scholar

- **Articles by Wang, J.**
- **Articles by Mao, L.**

PubMed

- **PubMed Citation**
- **Articles by Wang, J.**
- **Articles by Mao, L.**

HOME HELP FEEDBACK SUBSCRIPTIONS ARCHIVE SEARCH TABLE OF CONTENTS

Cancer Research | Clinical Cancer Research
Cancer Epidemiology Biomarkers & Prevention | Molecular Cancer Therapeutics
Molecular Cancer Research | Cell Growth & Differentiation